

ISTANBUL TECHNICAL UNIVERSITY ★ GRADUATE SCHOOL OF SCIENCE
ENGINEERING AND TECHNOLOGY

**A NUMERICAL STUDY ON THE IMPACT BEHAVIOR OF
THERMOPLASTIC PLATES**

M.Sc. THESIS

Fehmi MULLAOĞLU

Department of Aeronautical and Astronautical Engineering

Aeronautical and Astronautical Engineering Programme

MAY 2015

ISTANBUL TECHNICAL UNIVERSITY ★ GRADUATE SCHOOL OF SCIENCE
ENGINEERING AND TECHNOLOGY

**A NUMERICAL STUDY ON THE IMPACT BEHAVIOR OF
THERMOPLASTIC PLATES**

M.Sc. THESIS

Fehmi MULLAOĞLU
(511121166)

Department of Aeronautical and Astronautical Engineering

Aeronautical and Astronautical Engineering Programme

Thesis Advisor: Prof. Dr. Halit Süleyman Türkmen

MAY 2015

İSTANBUL TEKNİK ÜNİVERSİTESİ ★ FEN BİLİMLERİ ENSTİTÜSÜ

**TERMOPLASTİK LEVHALARIN DARBE DAVRANIŞININ NÜMERİK
OLARAK İNCELENMESİ**

YÜKSEK LİSANS TEZİ

**Fehmi MULLAOĞLU
(511121166)**

Uçak ve Uzay Mühendisliği Anabilim Dalı

Uçak ve Uzay Mühendisliği Programı

Tez Danışmanı: Prof. Dr. Halit Süleyman Türkmen

MAYIS 2015

Fehmi MULLAOĞLU, a **M.Sc.** student of **ITU Graduate School of Science Engineering and Technology** student ID 511121166, successfully defended the thesis entitled “**A Numerical Study On The Impact Behavior of Thermoplastic Plates**”, which he/she prepared after fulfilling the requirements specified in the associated legislations, before the jury whose signatures are below.

Thesis Advisor : **Prof. Dr. Halit Süleyman Türkmen**
Istanbul Technical University

Jury Members : **Prof. Dr. Zahit Mecitoğlu**
Istanbul Technical University

Assoc. Prof. Dr. Zafer Kazancı
Turkish Air Force Academy

Date of Submission : 30 April 2015
Date of Defense : 26 May 2015

FOREWORD

I would first like to thank my advisor, Prof. Dr. Halit Süleyman Türkmen, for giving me valuable advice and support always when needed. Also, I am so grateful to Burcu Eskiocak who has supported and encouraged in my efforts towards receiving a masters degree.

May 2015

Fehmi MULLAOĞLU
Mechanical Engineer

TABLE OF CONTENTS

	<u>Page</u>
FOREWORD	vii
TABLE OF CONTENTS	ix
ABBREVIATIONS	xi
LIST OF TABLES	xiii
LIST OF FIGURES	xv
SUMMARY	xix
ÖZET	xxi
1. INTRODUCTION	1
1.1 Purpose of Thesis	1
1.2 The Importance of Engineering Thermoplastics in Aerospace Industry	1
1.3 Literature Review	2
2. GENERAL INFORMATION OF THERMOPLASTICS	5
2.1 Material Production and Properties of Polycarbonates	6
2.2 Production and Properties of Polymethylmethacrylate (PMMA)	8
2.3 Key Characteristics / Differences of Acrylic and Polycarbonate	11
2.3.1 Acrylic compared to polycarbonate	11
2.3.2 Polycarbonate compared to acrylic	11
3. FINITE ELEMENT ANALYSIS	13
3.1 Introduction	13
3.2 Numerical Methods	14
3.3 Basic Steps In The Finite Element Method	14
3.4 Numerical Analysis Methods	15
3.4.1 Methods of space discretization	15
3.4.1.1 Lagrange method	16
3.4.1.2 Euler method	16
3.4.1.3 ALE (Arbitrary Lagrange Euler) method	17
3.4.2 Meshfree lagrangian method – SPH (Smooth particles hydrodynamics) ..	18
3.5 Elastic-Plastic Model Theory	20
3.5.1 Introduction	20
3.5.2 Elastic plastic behavior	22
3.5.3 Elasticity	24
3.5.4 Viscoelastic behavior	25
3.5.5 Plasticity	25
3.5.5.1 Yield criteria for polymers	27
3.5.5.2 Modified criteria for polymers	30
3.5.5.3 Hardening	31
4. IMPACT ANALYSIS SETUP	35
4.1 Target Model	35
4.1.1 Geometry	35
4.1.2 Material properties	36

4.2 Projectile.....	37
4.2.1 Geometry.....	37
4.2.2 Material properties of spherical steel projectile	38
4.3 Numerical Analysis	38
4.3.1 Material models.....	38
4.3.2 Failure criterias.....	40
5. RESULTS AND DISCUSSIONS	43
5.1 Introduction	43
5.2 Verification Study	43
5.3 Behavior of polycarbonate plates during impact.....	47
5.4 Behavior of PMMA plates during impact	56
5.5 Comparison of Behavior of Polycarbonate and PMMA Plates Under Impact.	63
5.6 Determine Strain Rates of Polycarbonate Plates in 1.9 mm Thick At Plate Center.....	69
5.7 Determine Strain Rates of PMMA Plates in 1.9 mm Thick At Plate Center ...	69
5.8 Comparison of Polycarbonate Plates For Shell and Solid Elements.....	69
6. CONCLUSIONS.....	77
REFERENCES	81
CURRICULUM VITAE.....	87

ABBREVIATIONS

ALE	: Arbitrary Lagrange Euler
FEA	: Finite Element Analysis
Fig	: Figure
g	: Gram
GPa	: Gigapascal
J	: Joule
kg	: Kilogram
m	: Meter
mJ	: MiliJoule
mm	: Milimeter
MPa	: Megapascal
nm	: Nanometer
PC	: Polycarbonate
PMMA	: Polymethyl methacrylate
s	: Second
SPH	: Smooth Particles Hydrodynamics
UV	: Ultraviolet

LIST OF TABLES

	<u>Page</u>
Table 4.1 : Material Property of PC	36
Table 4.2 : Material Property of PMMA	37
Table 4.3 : Material Properties	38
Table 4.4 : Ductile damage initiation properties for PMMA	42
Table 5.1 : Material Properties of PC	44
Table 5.2 : Material Properties of Projectile	44
Table 5.3 : Von Mises stresses for polycarbonate plates.	48
Table 5.4 : Maximum deformation values.	52
Table 5.5 : Maximum shear stress values.	52
Table 5.6 : Maximum plastic strain values.	53
Table 5.7 : Maximum energy absorption values.	55
Table 5.8 : Maximum von Mises stress values.	56
Table 5.9 : Maximum shear stress values for PMMA plates.	57
Table 5.10 : Maximum deformation values.	59
Table 5.11 : Maximum plastic strain values for PMMA plates.	60
Table 5.12 : Maximum energy absorption values for PMMA plates.....	62
Table 5.13 : Von Mises Stress for PC and PMMA plates.....	64
Table 5.14 : Maximum shear stress for PC and PMMA plates.....	64
Table 5.15 : Maximum Deformation of PC and PMMA plates.....	65
Table 5.16 : Maximum plastic strain for PC and PMMA plates.....	66
Table 5.17 : The maximum energy absorption for PC and PMMA plates.	67
Table 5.18 : Strain Rates at Different Velocity.....	69
Table 5.19 : Strain Rates at Different Velocity.....	69
Table 5.20 : All conclusions for shell and solid elements.....	75

LIST OF FIGURES

	<u>Page</u>
Figure 2.1 : Bird strike damage to a cockpit window	6
Figure 2.2 : Hail damage to a cockpit window.	6
Figure 2.3 : The main type of polycarbonate	7
Figure 2.4 : F-22 Raptor jet fighter canopy.	8
Figure 2.5 : The main type of PMMA	9
Figure 2.6 : Rear lights.....	10
Figure 2.7 : Lamp covers	11
Figure 3.1 : Lagrangian Mesh.....	16
Figure 3.2 : Eulerian Mesh.....	17
Figure 3.3 : Examples of Lagrange, Euler, ALE, and SPH Methods on an impact problem	19
Figure 3.4 : Example of Lagrange/Lagrange Interaction and Euler/Lagrange Coupling in the impact simulations	19
Figure 3.5 : True stress-strain curve from tensile test.....	20
Figure 3.6 : The stress-strain graph for polymer materials	22
Figure 3.7 : Elastic behavior	24
Figure 3.8 : Strain rate dependence	24
Figure 3.9 : Plastic loading	26
Figure 3.10 : Plastic unloading	26
Figure 3.11 : Tresca and von Mises yield criteria for plane stress.....	29
Figure 3.12 : Yield criteria fitted to data for PS.....	31
Figure 3.13 : Kinematic hardening of the von Mises criterion	32
Figure 3.14 : Bauschinger effect	32
Figure 4.1 : The exposed area of the plates with impact locations on the horizontal paths.	35
Figure 4.2 : Target model.....	36
Figure 4.3 : The spherical steel projectile.....	37
Figure 4.4 : A portion of the target plate and rigid projectile mesh for finite-element simulation.....	38
Figure 4.5 : The hardening properties of PMMA for rates $= 0.0001; 1; 2000; 4000$ and $40,000 \text{ s}^{-1}$	40
Figure 4.6 : Test specimen of polycarbonate with a gage length of 50 mm, a thickness of 1.91mm and a width of 9.74 mm.....	41
Figure 5.1 : Impact Points	44
Figure 5.2 : History of Energy Absorption with LSDYNA.....	45
Figure 5.3 : History of Energy Absorption with AUTODYN.	45
Figure 5.4 : Plastic strain at the point of impact with LSDYNA	46
Figure 5.5 : Plastic strain at the point of impact with AUTODYN.	46
Figure 5.6 : Numerical simulations.....	47

Figure 5.7 : Von Mises stress at the center of polycarbonate plate and 1.9 mm thick.....	47
Figure 5.8 : Von Mises Stress at the side profile of plate at 1.9 mm thickness.	48
Figure 5.9 : Von Mises stress distribution and perforated at 40 mm distance and 1.9 mm thick.....	49
Figure 5.10 : Von Mises stress distribution at 40 mm distance and 2.4 mm thick (in front of plate).....	49
Figure 5.11 : Von Mises stress distribution at 40 mm distance and 2.4 mm thick (back of plate).....	50
Figure 5.12 : Von Mises stress distribution at 40 mm distance and 2.4 mm thick. ..	50
Figure 5.13 : Von Mises stress and fragmentation at plate center and 1.4 mm thick.....	51
Figure 5.14 : Maximum deformation at plate center and 2.4 mm thickness.....	51
Figure 5.15 : Maximum deformation at plate center and 1.4 mm thickness.....	52
Figure 5.16 : Maximum shear stress distribution at 1.9 mm thickness.....	53
Figure 5.17 : Plastic strain values at plate center.	54
Figure 5.18 : Max. plastic strain simulation at 40 m distance and 1.9 mm thick.....	54
Figure 5.19 : Energy absorption distribution at 2.4 mm thickness.	55
Figure 5.20 : Energy absorption distribution at 40 mm distance.	56
Figure 5.21 : Von Mises stress distribution at plate center.	57
Figure 5.22 : Maximum shear stress in front of plate.	58
Figure 5.23 : Maximum shear stress at back of plate.....	58
Figure 5.24 : Maximum shear stress graph at plate center.....	59
Figure 5.25 : Max. shear stress simulation at 40 mm distance and 1.9 mm thick. ...	59
Figure 5.26 : Maximum deformation simulation at 20 distance and 1.9 mm thick. .	60
Figure 5.27 : Maximum plastic strain values at 1.4 mm thickness.....	61
Figure 5.28 : Max. plastic strain simulation at 40 mm distance and 1.4 mm thick. .	61
Figure 5.29 : Energy absorption distribution at 2.4 mm thickness.	62
Figure 5.30 : Energy absorption distribution at plate center.	63
Figure 5.31 : At plate center and 1.9 mm thickness.....	63
Figure 5.32 : Max. shear stress for PC and PMMA at middle of plate and 1.4 mm thick.....	65
Figure 5.33 : Maximum plastic strain for PC and PMMA plates.	66
Figure 5.34 : Energy absorption for PC and PMMA plates at 1.4 mm thick.....	67
Figure 5.35 : Energy absorption for PC and PMMA plates at 2.4 mm thick and at center of plate.....	68
Figure 5.36 : Energy absorption for PC and PMMA plates at 2.4 mm thick and 40 mm distance from center of plate.....	68
Figure 5.37 : Von Mises stress simulation at plate center and 1.9 mm thick for shell element.	70
Figure 5.38 : Von Mises stress simulation at side profile of plate and 1.9 mm thick for shell element.....	70
Figure 5.39 : Von Mises stress simulation at plate center and 1.9 mm thick for solid element.....	71
Figure 5.40 : Von Mises stress at 40 mm distance and 1.9 mm thick for solid and shell element.	71
Figure 5.41 : Maximum shear stress simulation at plate center and 1.9 mm thick for shell element.	72
Figure 5.42 : Maximum shear stress at plate center and 1.9 mm thick for solid and shell element.	72

Figure 5.43 : Deformation simulation at plate center and 1.9 mm thick for shell element.....	73
Figure 5.44 : Plastic strain simulation at plate center and 1.9 mm thick for shell element.....	73
Figure 5.45 : Plastic strain at plate center and 1.9 mm thick for solid and shell element.....	74
Figure 5.46 : Energy absorption distribution at plate center for solid and shell element.....	74

A NUMERICAL STUDY ON THE IMPACT BEHAVIOR OF THERMOPLASTIC PLATES

SUMMARY

In this thesis, dynamic response of exposure to a certain velocity impact of polycarbonate and polymethylmethacrylate plates were investigated depending on increasing thickness of plates and impacts at locations center of the plate, 20 and 40 mm were carried out by a spherical steel projectile using finite element and compare to each target plate behavior. First of all, it was investigated that impact events for polycarbonate and polymethylmethacrylate armor plates. It was conducted that explicit analyses later in this way. Analysis methods for impact problem are searched Lagrangian formulation is chosen for this study. Also, von Mises criteria is used for pc plates in this thesis. PMMA was assumed to obey the Drucker – Prager material model in the present study. Polycarbonate and PMMA materials are shown elastic-plastic behavior. Further, these polymer types are also shown viscoelastic behavior. However, it is realized that at extremely high strain rates, the strength of the material does not increase indefinitely. For these reasons, a reasonable choice was made to preserve the measured ductility while neglecting viscous effects at very high strain rates. That is, it was ignored viscoelastic behavior in this thesis. Thus, polymers like pc and PMMA are only modeled with elastic-plastic properties when it is used analysis program which Abaqus, Autodyn etc.

Three different thickness of plate and three different impact locations are taken consideration in this study. Plate thickness was selected as 1.4, 1.9 and 2.4 mm. In addition, the plates were modeled using 90×90 mm. Thin square polycarbonate and PMMA plates was subjected to a spherical projectile impact at a velocity of 140 m/s. Subsequent impacts were made at plate center, 20 and 40 mm of the plate depending on changing plate thickness. The target plate outer edge was constrained for all degrees of freedom. A spherical steel projectile of 6.98 mm diameter was launched against the square plate and also the mass of projectile was calculated as 0.00139 kg. According to this information, kinetic energy of the projectile was computed as 13.693 joule. The distance between target plate and projectile doesn't have any effect on the results, because gravitational force is neglected. When setting the material properties, "Bilinear Kinematic Hardening" model is used from the Ansys Library. Since polycarbonate is a ductile material, it is selected that plastic strain failure criteria for pc. PMMA is shown brittle fracture and ductile deformation at room temperature. Therefore, two failure criteria are combined which tensile failure and ductile failure during numerical modeling.

Plastic strain, von Mises stresses, maximum shear stresses, deformation of plate and energy absorption histories were recorded in this study. As increasing plate thickness, energy absorption quantity is increased as predicted for both polycarbonate and PMMA plates. At 1.9 and 2.4 mm thick, there was no

fragmentation for pc plates. However, it was observed that perforated event at all plate thickness for PMMA. It is expected that this phenomenon because PMMA has less impact resistance than pc material. Also, all energy absorption values are seen to be higher for pc than PMMA material at all plate thickness. That is, kinetic energy was not completely transformed into internal energy and therefore it was occurred that perforated event during impact loading for PMMA target plate. Furthermore, maximum plastic strain values were decreased while thickness of plate was increased. This situation was expected as well because resistance of plate is increased when the plate thickness is higher. On the other hand, it is occurred that higher stress values at close to fixed edge than other impact locations for both target material since square plate edges are constraint, as expected. It is observed that plastic deformation and fragmentation events with different plate thickness and impact points in this thesis. Furthermore, it was conducted that a validation analysis before thesis study. It can be said that this verification study is similar with thesis thesis. It was used that a circular polycarbonate plate. Once it was accomplished the validation analysis, it was implemented thesis study.

TERMOPLASTİK LEVHALARIN DARBE DAVRANIŞININ NÜMERİK OLARAK İNCELENMESİ

ÖZET

Bu tez kapsamında, sabit bir hıza sahip olan vurucu cismin, polikarbonat ve akrilikten yapılmış levhalara çarpıtılarak; levhaların dinamik yükler altındaki davranışı incelenmek istenmiştir. Bu darbe yükü altındaki levhaların davranışları, farklı kalınlıkta ve değişen darbe yerlerine bağlı olarak incelenmiştir. Levha kalınlıkları 1.4, 1.9 ve 2.4 mm olarak seçilmiştir. Ayrıca darbe yerleri levhanın merkezinden başlayarak 20 mm aralıklarla dış kenara doğru yapılmıştır. Yani vurucu cisim levhanın merkezine, merkezden 20 mm mesafeye ve aynı şekilde 40 mm merkezden uzaklığa olmak üzere darbe analizi gerçekleştirilmiştir. Bu çalışmada, farklı kalınlıklardaki levhalarda ve farklı darbe noktalarındaki davranışlar birbirleriyle kıyaslanmıştır.

Vurucu eleman olarak 7850 kg/m^3 yoğunluğa sahip olan çelik bilye kullanılmıştır ve bu malzemenin özellikleri Ansys kütüphanesinden alınmıştır. Analize başlamadan önce, ilk olarak polikarbonat ve PMMA malzemeleri ile yapılmış olan darbe çalışmaları incelenmiştir ve bu yönde malzemeleri modelleyip çalışma yapılmıştır. Bu çarpışma çalışması için “Lagrange” methodunu kullanarak analiz yapılması uygun görülmüştür. Ayrıca sünek malzemeler için daha çok kullanılan von Mises akma kriterine göre polikarbonat modellenmiştir. Fakat PMMA sünek deformasyonun yanı sıra oda koşullarında gevrek kopma gibi bir özellik gösterdiğinden Ansys kütüphanesinde malzemenin failure kriterlerini atarken bu gevreklik özelliğine uyum gösteren ‘the Drucker – Prager’ malzeme modeli seçilmiştir. Polikarbonat ve PMMA hem elastik hem de plastik davranış gösteren malzeme tipleridir. Ancak bu özelliklerinin dışında ayrıca viskoelastik özelliğe de sahiptirler.

Deneysel yapılan çalışmalarda anlaşılmış ki yüksek gerinim oranlarında malzemenin mukavemeti sonsuz biçimde artma göstermez. Bu sebepten ötürü, viskoz özellik ihmal edilirken yüksek gerinim oranlarında makul bir seçim yapılarak malzemenin sünekliliğini koruyacak şekilde plastisite ve diğer failure kriterleri atanmıştır. Bu yüzden polikarbonat ve PMMA gibi polimerler bilgisayar üzerinde analiz programı kullanırken, örneğin Abaqus, Autodyn gibi, yalnızca elasto-plastik davranışlarına bağlı olarak malzeme modellemesi yapıldığı literatürde görülmüştür. Aynı şekilde bu çalışmada da viskoz özellik ihmal edilmiştir.

Polikarbonat ve PMMA’dan yapılmış levhalar 90x90 mm boyutlarında kare plaka olarak tasarlanmıştır. Farklı kalınlıklarda üretilmiş bu levhalara çelik bilye 140 m/s hızla fırlatılmıştır. Polikarbonat ve PMMA malzemelerinden yapılmış olan tüm farklı kalınlıktaki levhalarda ve aynı zamanda üç farklı darbe noktasında yalnızca 140 m/s hızında çelik bilye fırlatılmıştır. Yani bu hız değeri tüm analizlerde sabit kalmıştır.

Darbe noktaları levhanın merkezi, 20 ve 40 mm merkezden uzaklıkta olacak şekilde ayarlanmıştır. Kullanılan levhalar dört kenardan ankastre olarak mesnetlenmiştir. Fırlatılan çelik bilyenin çapı 6.98 mm kadardır. Çeliğin yoğunluk değerinden faydalanılarak kütlesi 0.00139 kg olarak bulunmuştur. Bu bilgiler ışığında cismimizin kinetik enerjisi 13.693 joule olarak hesaplanmıştır. Yerçekimi dikkate alınmadığından, levhalarla ve çarpan çelik bilye arasındaki ilk mesafe sonuca etki etmeyeceği düşünülmüştür. Malzeme özellikleri atanırken polikarbonat için “Bilinear Kinematic Hardening” plastisite özelliği seçilmiştir. Buna ilaveten polikarbonat sünek bir malzeme olduğundan dolayı failure kriteri olarak “plastic strain failure” seçilmiştir. PMMA malzemesini modellerken ise, bu malzeme oda koşullarında gevrek kopma ve sünek deformasyon gösterdiği için iki farklı failure kriteri kombin yapılarak modellenmiştir. Bu kriterler “tensile failure” ve “ductile failure” şeklindedir.

Bu tez çalışmasında, maksimum von Mises gerilimi, soğurulan enerji, maksimum deformasyon, maksimum plastik gerinim ve maksimum shear gerilmeleri bulunmuştur. Daha sonra bu sonuçlar farklı kalınlıklarda ve değişen darbe yerlerinde birbiriyle kıyas edilmiştir. Hem polikarbonat hem de PMMA malzemelerinden yapılmış levhalarda, levha kalınlığı arttıkça beklenildiği üzere soğurulan enerjinin de arttığı görülmüştür. 1.9 ve 2.4 mm kalınlıktaki polikarbonat levhalarda parçalanmanın görülmeyeceği, yalnızca plastik deformasyonun meydana geldiği ancak PMMA ile yapılan çalışmalarda tüm kalınlıklarda çelik bilyenin levhayı parçalayıp geçtiği görüldü. Bu sonuç beklenen bir durumdu çünkü PMMA’nın darbe dayanımı polikarbonata göre daha düşüktür. Bu yüzden polikarbonat levhaların birçoğunda parçalanmanın meydana gelmemesi daha muhtemeldir. Aynı şekilde birçok farklı kalınlıktaki polikarbonat levhaların hemen hemen hiçbirinde parçalanma olayı meydana gelmediği analizler sonucunda kolaylıkla görülmüştür. Bu yüzden ki soğurulan enerji tüm kalınlıklarda polikarbonat levhalarda daha yüksek mertebelerdedir. Bu durumdan da anlaşılıyor ki, PMMA levhalarda kinetik enerji iç enerjiye tam olarak dönüşmemiş olduğu anlaşılmıştır. Bu yüzden de parçalanma olayı meydana gelmektedir. Bunun haricinde her iki malzeme tipindeki levhalarda plastik gerinim değeri levha kalınlığı arttıkça azalmıştır. Bu durum beklenen bir olaydır. Çünkü levhanın kalınlığı arttıkça daha mukavemetli bir hal alacaktır ve deforme olması daha zor olacaktır. Diğer yandan ankastre kenara yaklaştıkça her iki levhada gerilme değerleri yüksek çıkmıştır ki bu da beklenen bir durumdur. Bu çalışmada sonuç olarak, genel olarak farklı kalınlık ve darbe yerlerine bağlı olarak plastik deformasyon ve parçalanma olayları gözlemlenmiştir. Yapılan tüm çalışmalarda gözlemlenildiği üzere polikarbonat malzemesinin PMMA malzemesine göre çok daha yüksek darbe dayanımı olduğu tespit edilmiştir.

Aynı şekilde literatürde de yapılmış olan benzer çalışmalarda çıkan sonuçlara paralel sonuçların elde edildiği bulunmuştur. Kullanılmış olan bu iki farklı malzemenin kimyasal yapıları da incelenmiş olup, beklenen bir sonucun alındığı gözlemlenmiştir. Malzemelerin kimyasal yapıları incelenmiş ve polikarbonat malzemesinin kimyasal bağ yapısı çok daha yüksek mertebede olduğu görülmüştür. Elde edilen sonuçlarda yine bu duruma paralel olarak çıkmıştır. Ayrıca tez çalışmasından önce, tez kapsamında kullanılan polikarbonat malzemesi ile yapılmış olan akademik bir çalışmanın doğrulama analizi yapılmıştır. Bu doğrulama çalışması başarıyla yapıldıktan sonra tez çalışmasına geçilmiştir.

1. INTRODUCTION

1.1 Purpose of Thesis

In this thesis, canopy structure was investigated to see the results of fragmentation. For this situation, polycarbonate and PMMA materials were utilized to composed plates for structure. These materials were chosen in order to contribute in the literature due to lacking of the studies. In this study, dynamic provision of exposure to a fixed velocity impact of polycarbonate and polymethylemethacrylate plates were investigated depending on increasing thickness of plates and impacts at locations center of the plate, 20 and 40 mm were carried out by a spherical steel projectile using finite element and compare to each target plate attitude. Ansys workbench software program, which is commanly preferred for explicit dynamics, was used by developing and analysis in Autodyn. Here the most significant point in this study, polycarbonate and PMMA materials have ideal physical and chemical properties for situations of impact in comparison with the materials used for canopy structures.

1.2 The Importance of Engineering Thermoplastics in Aerospace Industry

Engineering thermoplastics have a combination of perfect thermal, mechanical, electrical and chemical properties compared to basic material resins. These plastics can be composed into parts that can bear loads and high stresses, perform at high rise temperatures and be modified to come close to the properties of metal, glass, and wood. It is widely known that engineering thermoplastics can be amorphous. It can be given that amorphous engineering thermoplastic types include acrylics, polycarbonates (PCs) and polyurethanes. Polycarbonate and acrylic materials were used in this study. This thesis study will describe their production, properties and impact behavior.

Optically crystalline multi-layered polymer layers was used in military defense applications like transparent shield for personnel guard and air/ground vehicle windows.

The general requirements for see-through shield are to hinder incoming threats, withstand multiple impacts and maintain optical clarity with minimal disintegration and optical distortion for the user [1-3]. A characteristic format of transparent shield consists of multiple rigid thermoplastic polymer external layers with rubbery interlayer sticks. The transparency, toughness and rate dependence of Polycarbonate and acrylic materials are the primary reasons they are excellent choices for use in see-through shield to withstand projectile impact.

Significant implementation of polymers is as an adhesive for joining airplane components. It is possible to manufacture quite high strength, durable joints using polymer adhesives without the need for bonders such as rivets and screws [4-5].

Polycarbonate windscreens are also invulnerable to damage by large hailstones. Damage induced to aircraft windows by bird strike or hail. Even though the polycarbonate windows are damaged, they were impacted under heavy conditions that would have caused most other polymer materials to break leading to cabin depressurisation. PMMA is one of the polymers that is most resistant to straight sunlight exposure. This property of acrylic makes it appropriate for products intended for long open-air operation. PMMA has less impact resistance than Polycarbonate. However, it has 10-24 times more resistant than glass.

In present study, these materials which polycarbonate and PMMA are investigated and then their impact behaviors are compared in engineering scope.

1.3 Literature Review

Owing to its good impact resistance specialties, the polycarbonate material is used in and bulletproof armored vehicles [1]. Polycarbonate (PC) is also under exploration for the progress and manufacture of sandwiched panels for bullet-proof waistcoats and armored systems where alternate layers of polymethylemethacrylate acrylic (PMMA) and polycarbonate are used to diminish the damage caused by high-velocity projectiles [2]. Polycarbonate is a in the extreme ductile matter at room temperature. Also, it undergoes major plastic deformation when loaded statically and dynamically. The deformation in a static loading case is larger than on the dynamic loading condition

cause under dynamic loading the failure might happen at a smaller plastic strain. Back plane spall and breakup might not show a difficulty to the polycarbonate armor plate. As a general practice most of the armored plates are tested by subjecting them to a plate mid-point impact however there are very few studies where the defense talent has been investigated based upon the impact position on a particular shaped shield plate [3, 4]. In [4] it was seen that for annular polycarbonate armor sheet the thickness close to the fixed edge reduced by 53% and then impact matched to its original thickness before hit. Additionally, 10% scale down in thickness was enlisted when matched to the thickness at the plate center after hit. A rather affecting investigation respecting the Multiple- Hit- Criterion evaluation way for a patterned armor consisting of ceramic quarries has been negotiated in [5]. It has been explained that due to the performance requirements none of the armor can beat the threat of a continuous gun fire. Thus, an armor should be drafted which can continue the automatic gun fire that can land at least 10 rounds at a single point or in its vicinity. Multiple impact wreckage to the airplane fuselage lap joints and their reparation procedure has been mentioned in [6]. On account of their light weight, economical, even simple manufacturing processes, the usage of polymers is on the uptrend in a lot of industries. Experimental studies noticed on the attitude of polymers are not as numberless as on metals and numerical studies are even rare because of the absent of convenient material models [7–13]. The response of rectangular sheets subjected to explode loading was noticed where the authors research the response of quadrangular stiffened steel sheets [14-15]. In this study, target model is selected a square model. Similarly, impact event was started from plate center to clamped edge. The influences of large and close range explosions on circular shield plates have been investigated very lately where [16]. Numerical studies on the reaction of shield systems made up of PC and PMMA were studied [8] where perfect particle hydrodynamics was used to simulate the response of PC and acrylic layers. Furthermore, numerical results based upon the tests [17] have been reported in [18] where the effect of varying support forms have been investigated on the plastic failure of the annular steel plates. Annular plates subjected to intensive fragment cluster impact [19-20] research the failure process of shield plates subjected to a fragment cluster consisting of plenty projectiles impacting the plate at the same time. It was studied that the ballistic resistance of fixed very thin

PC sheets to single [21, 22]. It was concluded that reinforcements have to be provided close to the fixed edges. A study was made on sloped impact of polymethylmethacrylate (PMMA) thick sheets [23, 24].

Glazed polymers such as polymethylmethacrylate (PMMA) are an desirable choice for shield related applications owing to their material properties for instance pressure sensitivity, strain rate dependent strength, transparency, low density and very high durability [25]. For this purpose, it was seen that on punch experiments [26], PMMA fractures in a brittle format in the absence of external limitation. The mechanical features of glazed polymers at high strain rates and limitation were studied: PMMA [27]. Impact and puncture of acrylic plates have been studied [28]. In their simulations the real mechanical properties of acrylic were not handled, however were systematically varied till a convincing resemblance between the experiments and the simulations was obtained. Their primary result was that spalling is the primary responsible agent for the formation of the ricochet [29]. According to these works, analyses were implemented properly on Autodyn.

2. GENERAL INFORMATION OF THERMOPLASTICS

It was predicted to be given a general information about thermoplastics for this study. It was given some information about polymers since polycarbonate and PMMA are used during analysis. The use of thermoplastics in aircraft is small compared with the much greater use of thermosets. Some sectors of the aerospace industry are prying to increase the use of thermoplastics in composite materials, and the number of applications is gradually increasing. It is widely known that thermoplastics ensure many significant advantages over thermosets when used in composite materials, most considerably better hit damage resistance, higher fracture toughness, even higher operating temperatures. However, thermoplastics have to be processed at high temperature that makes them sumptuous to fabricate into aircraft composite supplementaries. Many types of thermoplastics are transparent, even tough impact durable which makes them well conformed for airplane windows and canopies. The thermoplastics most frequently handled in airplane windows are PMMA and polycarbonates. Acrylic plastics are any polymer and copolymer of acrylic acid. A model of acrylic plastic used in airplane windows is polymethyl- methacrylate (PMMA). PMMA plastics have different names such as Plexiglas and Perspex. Acrylic plastics are lighter, stronger and tougher than glass. Polycarbonates are stronger and tougher than acrylic plastics and are used when high-impact resistance is needed, such as cockpit windows and canopies. In polycarbonate applications, the material must have high impact strength due to the risk of clash with birds. Even though bird strikes do not occur at cruise heights, they present a considerable risk at low heights, specially during take-off and landing [30].

Polycarbonate windscreens are also invulnerable to damage by large hailstones. It is given that Figs 2.1 and 2.2 examples of damage caused to aircraft windows by bird strike or hail, respectively. Even though the polycarbonate windows are damaged, they were impacted under heavy conditions that would have caused most other polymer materials to break leading to cabin depressurisation. A large bird hit the window shown

in Fig. 2.1 when the aircraft was flying at several hundred kilometres per hour and hailstones larger than golf balls caused the damage shown in Fig. 2.2. Had these windows been made with glazing the bird and hailstones would almost definitely have holed through and entered the cockpit. Polycarbonate windows help to rather good safety to the flight crew against intense impact events [31].

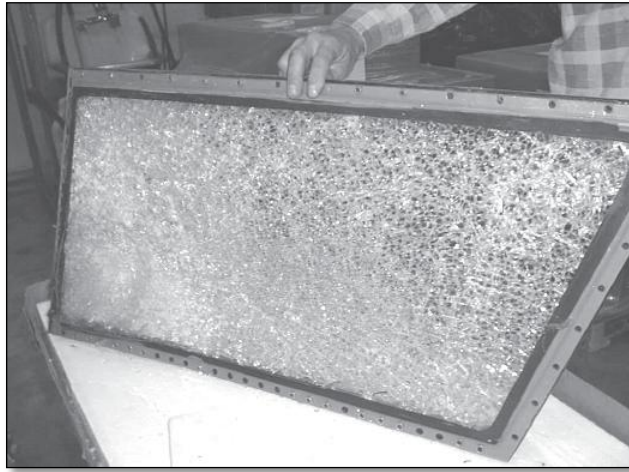


Figure 2.1: Bird strike damage to a cockpit window [31].



Figure 2.2: Hail damage to a cockpit window [31].

2.1 Material Production and Properties of Polycarbonates

Polycarbonate is a quite tough material. Even though polycarbonate has high impact resistance, it has weak scratch strength and so a hard coating is implemented to

polycarbonate eyewear lenses and polycarbonate outer automotive components. The typical properties of polycarbonate are quite like those of polymethylmethacrylate (PMMA, acrylic). However, polycarbonate is stronger and useable over a greater temperature range. Polycarbonate is highly see-through to appearing light, with better light conduction than many types of glazing. The main type of polycarbonate used in airplane is given in Fig. 2.3.

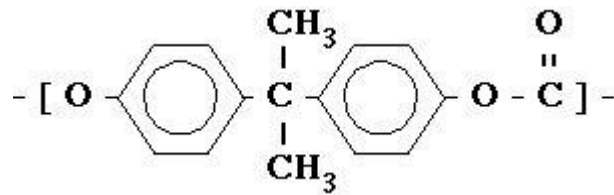


Figure 2.3: The main type of polycarbonate.

Polycarbonate has a glass transition temperature of about 147 °C (297 °F), so it softens by stages above this point and flows above about 155 °C (311 °F). Low molecular mass categories are easier to give shape than higher grades. However, their strength is lower.

Unlike most thermoplastics, polycarbonate could undergo major plastic deformations without cracking or rupturing. Consequently, it can be operated and created at room temperature using plate metal techniques, like bending on a brake. Inasmuch that for sharp angle bends with a strict radius, heating might not be imperative. This provides it precious in prototyping applications where see-through and electrically non-conductive parts are required, which cannot be made from sheet metal.

- Polycarbonate applications

The high clearness and perfect impact resistance of polycarbonates provide them appropriate for applications like high-pressure injectors, disposable dental instruments, surgical face shields, blood oxygenators, blood collection reservoirs, blood separation devices, surgical devices, kidney dialysis equipment and centrifuge bowls. The toughness of PC is required in the medicinal environment to prevent from rupture when

apparatus are struck by trays or carts. A great deal other medical applications for polycarbonate include medicinal equipment parts, such as housings, connectors and stopcocks, tubing, surgical skin stapler housings, syringe assemblies for labs. Polycarbonate is used for particular medical packing applications as well [32]. Other applications of polycarbonates include automotive, traffic lights, cash dispenser, drinking bottle, mobile phone, Riot shields. Furthermore, significant application area which the cockpit canopy of the F-22 Raptor jet fighter is made from a piece of high optic standard polycarbonate and is the largest part of its type formed all around the world (Figure 2.4) Url-3.



Figure 2.4: F-22 Raptor jet fighter canopy Url-3.

2.2 Production and Properties of Polymethylmethacrylate (PMMA)

General Polymethacrylates are polymers of the esters of methacrylic acids. The most usually used among them is PMMA. PMMA is a linear thermoplastic polymer [33]. The main type of PMMA is shown Fig. 2.5.

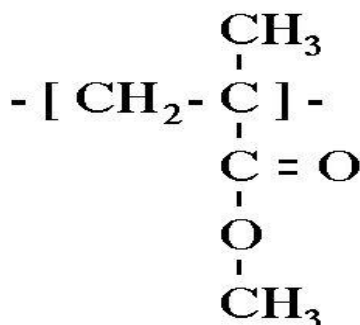


Figure 2.5: The main type of PMMA Url-4.

Its strength features during injection cast differ significantly in longitudinal and transversal direction as a result of the orientation influence. The mechanical specialties of PMMA change as the warmth replaces as in the case with other thermoplastics. This material tends to creep. It is not much appropriate for process under multiple dynamic loads.

PMMA is one of the polymers that the most resistant to straight sunlight exposure. Its resistance characteristics indicate quite small changes under the influence of UV-radiation, as well as in the being of ozone. These features of acrylic provide it appropriate for products purposed for long time open-air operation.

PMMA depicts very well optic features it conveys more light (up to 93% of visible light) than glass.. Unlike glass, PMMA does not drain ultraviolet light. PMMA conveys UV light down to 300 nm and permits infrared light of up to 2800 nm to pass.

Acrylics are uninfluenced by watery solutions of most laboratory chemicals, by detergents, cleaners, dilute inorganic acids, alkalis however, acrylics are not recommended for use with chlorinated, esters and ketone. It dissolves completely in chloroform, di- and tri-chlorethane, which is used for procurement of glues. The chemical resistance will change with stress level, temperature, reagents and duration of exposure [34].

PMMA are physiologically innocuous. Owing to their low rise humidity adsorption capacity they are not attacked by moldiness and enzymes.

It can be said that PMMA is appropriate for injection moulding, pressing, extrusion blow moulding (impact modified acrylics only), casting. Acrylics are easily holed, milled, engraved and finished with sharp carbide-tipped tools. They are with ease bent at low rise temperature and solvent linking of agreeably fitting parts produces a strong, out of sight joint as well. PMMA can be welded by all the plastics welding treatments such as hot-blade, hot-gas, ultrasonic and spin welding [35].

- Polymethyl methacrylate applications

PMMA has very quite high optic clearness and UV transmittance. The high optic clearness of PMMA provides it a very appropriate material in diagnostic applications like diagnostic test packs and optical sensor view ports [36]. Diverse types of acrylics are used in a extensive variety of areas and applications, including [37].

- **Optics:** Dust covers for hi-fi equipment, , watch glasses, lenses, sunglasses;
- **Vehicles:** Rear lights (Fig. 2.6) Url-5, indicators, warning triangles, tachometer covers;
- **Electrical engineering:** Lamp covers (Fig. 2.7) Url-6, switch parts, control, buttons dials;
- **Office equipment:** Writing and drawing instruments, pens;
- **Others:** Leaflet dispensers, shatter-resistant glazing, shower cubicles, transparent pipelines, toy, artificial fingernails are sometimes made of acrylic.



Figure 2.6: Rear lights Url-5.



Figure 2.7: Lamp covers Url-6.

2.3 Key Characteristics / Differences of Acrylic and Polycarbonate

2.3.1 Acrylic compared to polycarbonate

- More likely to chip, less impact resistance than Polycarbonate. (still 10-24 times more resistant than glass)
- Less likely to scratch.
- More of a consumer (household) level and is easier to find at hardware stores.
- Does not yellow after time.
- Better clarity and can be restored to optical clarity Url-7.

2.3.2 Polycarbonate compared to acrylic

- Impact/chip resistance is much higher with Polycarbonate. (about 30 times more resistant than glass)
- More likely to scratch.
- Substantially more expensive. (roughly 2 to 3 times)
- Used for more industry applications.
- Bulletproof when thick enough.
- More bendable.

- More formable.
- Yellows over time due to ultraviolet rays.
- Easier to work with (cut, less likely to break).
- Poorer clarity, diffuses light, can lighten (could be positive) Url-7.

3. FINITE ELEMENT ANALYSIS

3.1 Introduction

It can be said that finite element analysis (FEA) has become ordinary in recent years and is now the basis of a multibillion dollar per year industry. Numerical solutions to even very complicated stress problems can now be obtained routinely using FEA, and the method is so important that even introductory treatments of Mechanics of Materials - such as these modules - should outline its principal features.

In spite of the great power of FEA, the disadvantages of computer solutions must be kept in mind when using this and similar methods: they do not necessarily reveal how the stresses are influenced by important problem variables such as materials properties and geometrical features, and errors in input data can produce wildly incorrect results that may be overlooked by the analyst. It might be the most important function of theoretical modeling is that of sharpening the designer's intuition; users of finite element codes should plan their strategy toward this end, supplementing the computer simulation with as much closed-form and experimental analysis as possible [38].

Finite element codes are less complicated than many of the word processing and spreadsheet packages found on modern microcomputers. Nevertheless, they are complex enough that most users do not find it effective to program their own code. A number of prewritten commercial codes are available, representing a broad price range and compatible with machines from microcomputers to supercomputers [38]. However, users with specialized needs should not necessarily shy away from code development, and may find the code sources available in such texts as that by Zienkiewicz [39] to be a useful starting point. Most finite element software is written in Fortran, but some newer codes such as felt are in C or other more modern programming languages.

3.2 Numerical Methods

There are many practical engineering problems for which we cannot obtain exact solutions. This inability to obtain an exact solution may be attributed to either the complex nature of governing differential equations or the difficulties that arise from dealing with the boundary and initial conditions. To deal with such problems, we resort to numerical approximations. In contrast to analytical solutions, which show the exact behavior of a system at any point within the system, numerical solutions approximate exact solutions only at discrete points, called nodes the first step of any numerical procedure is discretization. This process divides the medium of interest into a number of small subregions and nodes .There are two common classes of numerical methods: (1) finite difference methods and (2) finite element methods. With finite difference methods, the differential equation is written for each node, and the derivatives are replaced by difference equations. This approach results in a set of simultaneous linear equations .Although finite difference methods are easy to understand and employ in simple problems: they become difficult to apply to problems with complex geometry or complex boundary conditions. This situation is also true for problems with nonisotropic material properties.

In contrast, the finite element method uses integral formulations rather than difference equations to create a system of algebraic equations. Moreover, an approximate continuous function is assumed to represent the solution for each element. The complete solution is then generated by connecting or assembling the individual solutions, allowing for continuity at the interelemental boundaries [40].

3.3 Basic Steps In The Finite Element Method

The basic steps involved in any finite element analysis consist of the following:

Preprocessing phase

1. Create and discretize the solution domain into finite elements; that is, subdivide the problem into nodes and elements.

2. Assume a shape function to represent the physical behavior of an element; that is, an approximate continuous function is assumed to represent the solution of an element.
3. Develop equations for an element.
4. Assemble the elements to present the entire problem. Construct the global stiffness matrix.
5. Apply boundary conditions, initial conditions, and loading.

Solution phase

6. Solve a set of linear or nonlinear algebraic equations simultaneously to obtain nodal results such as displacement values at different nodes or temperature values at different nodes in a heat transfer problem.

Postprocessing phase

7. Obtain other important information. At this point, you may be interested in values of principal stresses, heat fluxes, etc.

In general, there are several approaches to formulating finite element problems: (1) Direct Formulation, (2) The Minimum Total Potential Energy Formulation and (3) Weighted Residual Formulations Again. It is important to note that the basic steps involved in any finite element analysis regardless of how we generate the finite element model will be the same as those listed above [41].

3.4 Numerical Analysis Methods

3.4.1 Methods of space discretization

The spatial discretization is performed by representing the fields and structures of the problem using computational points in space, usually connected with each other through computational grids. Usually, the finer the grid is, more accurate the solution. The most commonly used spatial discretizations are Lagrange, Euler, ALE (Arbitrary Lagrange Euler - a mixture of Lagrange and Euler), and meshfree methods such as SPH (Smooth Particles Hydrodynamics) [41].

3.4.1.1 Lagrange method

The Lagrange method of space discretization, as described in [42], where the numerical grid moves and deforms with the material, is ideal for following the material motion and deformation in regions of relatively low distortion, and possibly large displacement. Conservation of mass is automatically satisfied and material boundaries are clearly defined. The Lagrange method is most appropriate for representing solids like structures and projectiles. The advantages of the Lagrange method are computational performance and ease of incorporating complex material models. The disadvantage of Lagrange is that the numerical grid can become severely distorted or tangled in an extremely deformed region, which can lead to adverse effects on the integration time step and accuracy. However, these problems can be overcome to a certain extent by applying numerical techniques such as erosion and rezoning. In this thesis, it has been conducted with Lagrange Method in Autodyn .

The Lagrangian description can be visualized in terms of the corresponding meshes (Figure 3.1) Url-9.

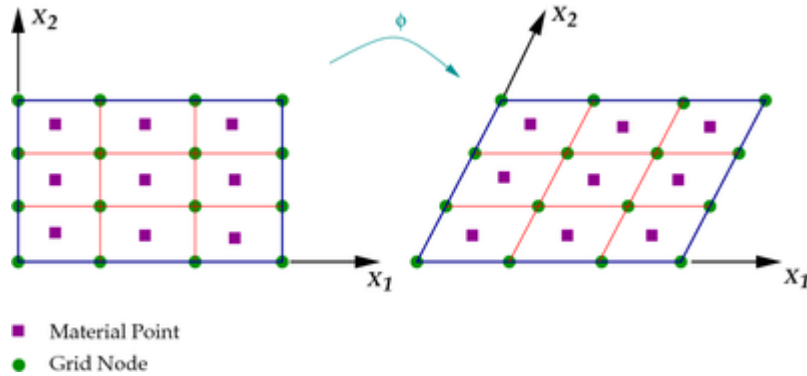


Figure 3.1: Lagrangian Mesh Url-9.

3.4.1.2 Euler method

The Euler method of space discretization, as described in [43], where the numerical grid is fixed in space while the physical material flows through the grid, is typically well suited for the description of the material behavior of severe deformations. The Euler

method is generally used for representing fluids and gases, for example, the gas product of high explosives after detonation. To describe solid behavior, additional calculations are required to transport the solid stress tensor and the history of the material through the grid. The advantage of the Euler method is that large deformations or flow situations, by definition, do not result in grid distortions due to the fixed grid. The tradeoff is the extra computational work required to maintain material interfaces and to reduce numerical diffusion [43].

The Eulerian description can be visualized in terms of the corresponding meshes (Fig. 3.2) Url-9.

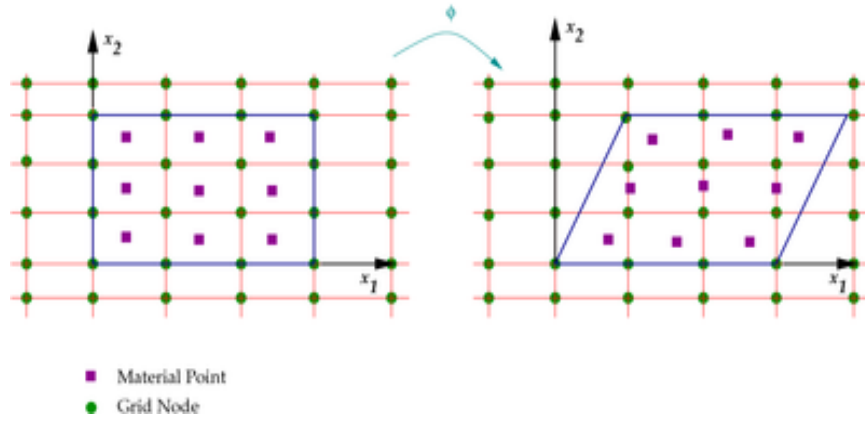


Figure 3.2: Eulerian Mesh Url-9.

3.4.1.3 ALE (Arbitrary Lagrange Euler) method

The ALE (Arbitrary Lagrange Euler) method of space discretization is a hybrid of the Lagrange and Euler methods. It allows redefining the grid continuously in arbitrary and predefined ways as the calculation proceeds, which effectively provides a continuous rezoning facility. Various predefined grid motions can be specified such as free (Lagrange), fixed (Euler), equipotential, equal spacing, and others. The ALE method can model solids as well as liquids. The advantage of ALE is the ability to reduce and sometimes eliminate difficulties caused by severe mesh distortions encountered by the Lagrange method and allows a calculation to continue efficiently. However, compared

with Lagrange, an additional computational step of rezoning is employed, as described in [42, 43], to move the grid and remap the solution onto a new grid.

3.4.2 Meshfree lagrangian method – SPH (Smooth particles hydrodynamics)

The meshfree Lagrangian method of space discretization - SPH (Smooth Particles Hydrodynamics), initially was used in astro-physics [44]. It was implemented in AUTODYN in 1995 [44]. The SPH particles are not only interacting mass points but also interpolation points used to calculate the value of physical variables based on the data from neighboring SPH particles, scaled by a weighting function. Because there is no grid defined, the SPH method does not suffer from grid tangling in large deformation problems. Compared with the Euler method, material boundaries and interfaces in the SPH are rather well defined and material separation is naturally handled. Therefore, the SPH method is very useful to simulate material behavior subject to severe deformation and distortion, for example, in hyper-velocity impact and for the cracking of brittle materials. However, the SPH method requires a sort of the particles in order to locate current neighboring particles, which makes the computational time per cycle more expensive than mesh based Lagrangian techniques – this can make meshfree methods less efficient than mesh based Lagrangian methods with comparable resolution.

It is given an example of Lagrange, Euler, ALE, and SPH Methods below.

To demonstrate the use of Lagrange, Euler, ALE, and SPH methods, a numerical simulation of an impact problem shown in Fig. 3.3 is conducted. The steel projectile has a diameter of 7.5mm and weighs about 2.9g. It impacts 22.5 mm thick aluminium plate at a velocity of 1000 m/s. An erosion mechanism is applied to the Lagrange as well as ALE grids to eliminate the elements that become highly distorted.

All of these methods display similar impact damage on both the projectile and the target. The Euler method needs extra cells around the materials representing a void region into which deformed materials may flow. The ALE grid distorts less than the Lagrange grid because of equipotential rezoning where a node is re-positioned relative to its nearest

neighbors. Compared with the Lagrange and the ALE, the SPH method maintains a well-defined material interface without the need to use erosion [44].

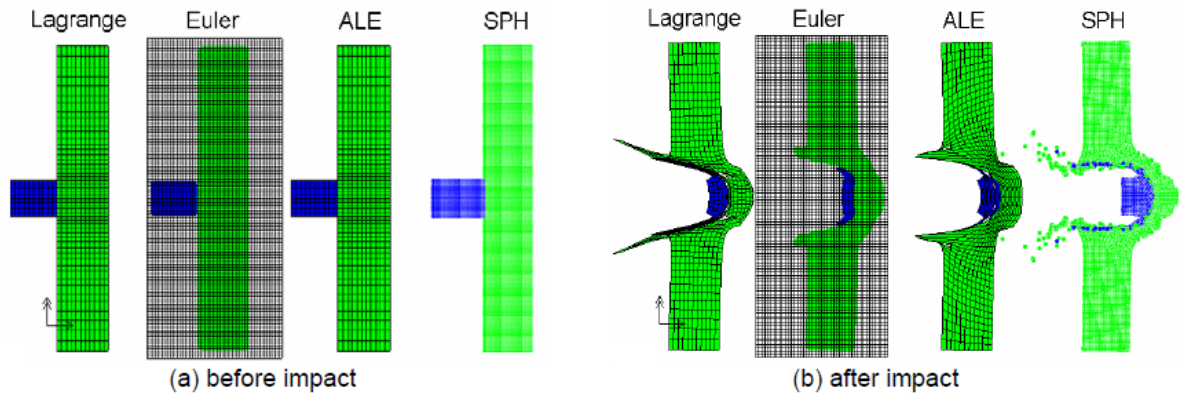


Figure 3.3: Examples of Lagrange, Euler, ALE, and SPH Methods on an impact problem [44].

It can be also seen that an example of lagrange/lagrange interaction and euler/lagrange coupling in the impact simulations in Fig. 3.5.

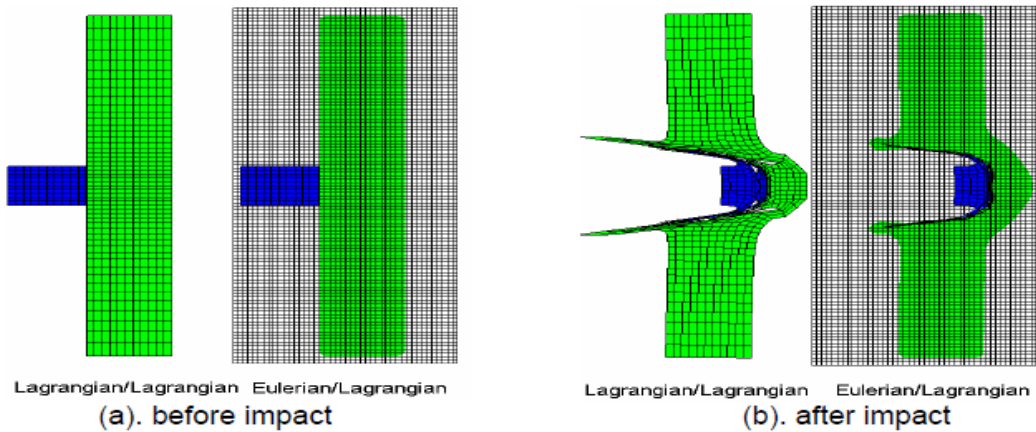


Figure 3.4: Example of Lagrange/Lagrange Interaction and Euler/Lagrange Coupling in the impact simulations [44].

3.5 Elastic-Plastic Model Theory

3.5.1 Introduction

The theory of linear elasticity is useful for modeling materials which undergo small deformations and which return to their original configuration upon removal of load. Almost all real materials will undergo some permanent deformation, which remains after removal of load. With metals, significant permanent deformations will usually occur when the stress reaches some critical value, called the yield stress, a material property. Elastic deformations are termed reversible; the energy expended in deformation is stored as elastic strain energy and is completely recovered upon load removal. Permanent deformations involve the dissipation of energy; such processes are termed irreversible, in the sense that the original state can be achieved only by the expenditure of more energy. The characteristic look of the stress-strain curve of a plastic material is shown in Fig. 3.5 Url-10.

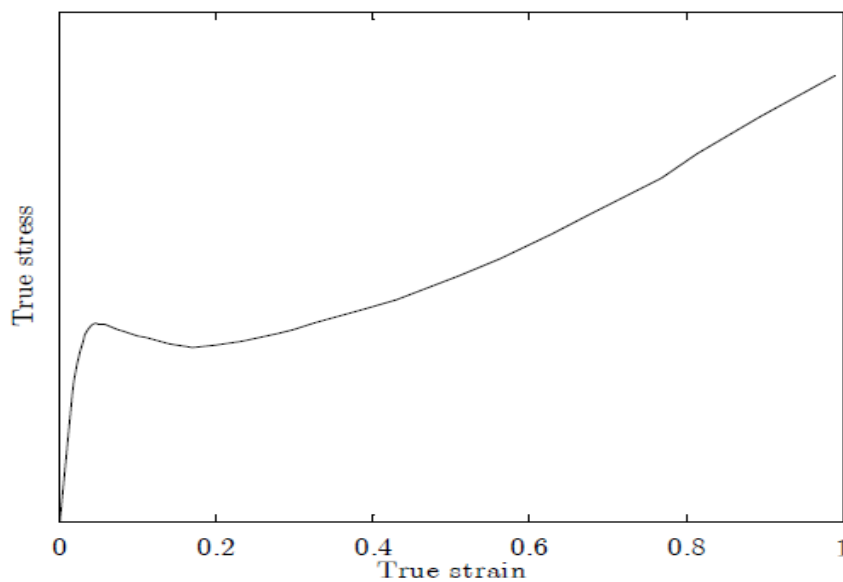


Figure 3.5: True stress-strain curve from tensile test Url-10.

The classical theory of plasticity grew out of the study of metals in the late nineteenth century. It is concerned with materials which initially deform elastically, but which deform plastically upon reaching a yield stress. In metals and other crystalline materials the occurrence of plastic deformations at the micro-scale level is due to the motion of dislocations and the migration of grain boundaries on the micro-level. A good part of the discussion in what follows is concerned with the plasticity of metals; this is the ‘simplest’ type of plasticity and it serves as a good background and introduction to the modeling of plasticity in other material-types. There are two broad groups of metal plasticity problem which are of interest to the engineer and analyst. The first involves relatively small plastic strains, often of the same order as the elastic strains which occur. Analysis of problems involving small plastic strains allows one to design structures optimally, so that they will not fail when in service, but at the same time are not stronger than they really need to be. In this sense, plasticity is seen as a material failure (two other types of failure, brittle fracture, due to dynamic crack growth, and the buckling of some structural components, can be modeled reasonably accurately using elasticity theory). The second type of problem involves very large strains and deformations, so large that the elastic strains can be disregarded. These problems occur in the analysis of metals manufacturing and forming processes, which can involve extrusion, drawing, forging, rolling and so on. In these latter-type problems, a simplified model known as perfect plasticity is usually employed, and use is made of special limit theorems which hold for such models. Plastic deformations are normally rate independent, that is, the stresses induced are independent of the rate of deformation (or rate of loading). This is in marked contrast to classical Newtonian fluids for example, where the stress levels are governed by the rate of deformation through the viscosity of the fluid. Materials commonly known as “plastics” are not plastic in the sense described here. They, like other polymeric materials, exhibit viscoelastic behavior where, as the name suggests, the material response has both elastic and viscous components. Due to their viscosity, their response is, unlike the plastic materials, rate-dependent. Further, although the viscoelastic materials can suffer irrecoverable deformation, they do not have any critical yield or threshold stress, which is the characteristic property of plastic behavior. When a material undergoes plastic deformations, i.e. irrecoverable and at a critical yield stress

and these effects are rate dependent, the material is referred to as being viscoplastic Url-10.

In this thesis, it was only used with elasto-plastic stress analysis for both polycarbonate and PMMA materials, although polymers have elastic, plastic and viscoelastic properties. It will be explained that why viscoelasticity property not used later.

3.5.2 Elastic plastic behavior

With elastic-plastic models, calculations of stress and strain distributions at low strains are based on linear elasticity. The onset of non-linearity is attributed to plastic deformation and occurs at a stress level regarded as the first yield stress. The subsequent increase in stress with strain is associated with the effects of strain hardening, and increases to a maximum corresponding to the flow region. In this non-linear region, the total strain is considered to be the sum of a recoverable elastic component and a plastic component, which is non-recoverable. Stress analysis calculations then involve the use of multiaxial yield criteria and a flow law. The yield criterion relates components of applied stress field to material parameters after the onset of yielding (Fig. 3.6). The material parameters will depend upon the plastic strain for a strain hardening material Url-11.

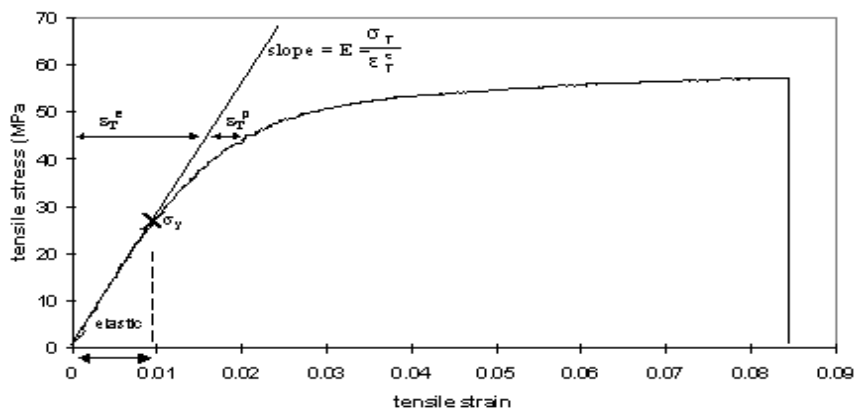


Figure 3.6: The stress-strain graph for polymer materials Url-11.

The calculation of plastic strain components is achieved in plasticity theory using a flow rule, which relates increments of plastic strain to a plastic flow potential. If the flow behavior for a particular material is such that the flow potential can be identified with the yield function then this is termed associated flow. In general, this will be an approximation and extra information is needed to characterise non-associated flow. In order to calculate some of the parameters in elastic-plastic models, it is necessary to select stress values from different tests under the same state of yielding. This requires the definition of an effective plastic strain, and equivalent stresses are then a set of stresses that characterise stress states having the same effective plastic strain.

The formulation of elasto-plastic relation for a complex problem under multiaxial stresses can be achieved by assuming a reasonable mathematical model to correlate between the uniaxial test results and the multiaxial cases. The general relation between stress and strain can be obtained in terms of the uniaxial behavior, by specifying the following rules and conditions [45].

- (i) The elastic stress–strain relations,
- (ii) An initial yield condition,
- (iii) A flow rule which relates the plastic strain increments to the stresses and stress increments,
- (iv) A hardening rule for establishing the conditions for subsequent yield from a plastic state.

It is necessary to have an initial yield condition which characterize the transition of a material from the elastic state to the state of yielding under any possible combination of stresses. One of the most widely used yield criteria for metallic materials is the von Mises criterion. The von Mises criterion is based on the assumption that the hydrostatic stress has no effect on yielding of metallic materials, i.e the only effective component is the deviatoric stress [46].

3.5.3 Elasticity

The characteristic of elastic strain is that the response is independent of the load history. After removing the load, the material returns to its initial condition and the unloading stress-strain curve retraces the loading curve, cf. Fig. 3.7 [47].

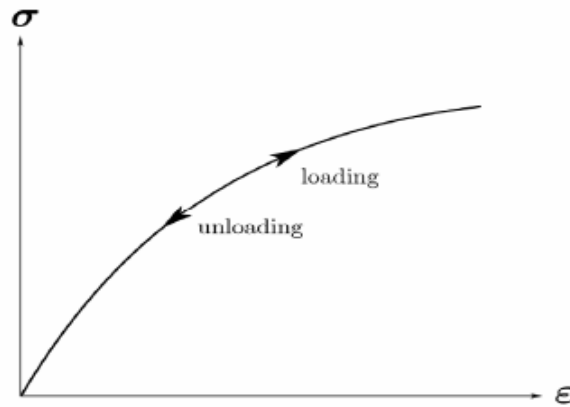


Figure 3.7: Elastic behavior [47].

The elastic part of the stress-strain curve of most metals is linear. The stress is related to the strain by an elastic modulus which is constant through the elastic region. However, the elasticity of materials such as plastics and rubber shows a non-linear elastic behavior. Not only is the stress-strain curve non-linear, but the stress level is also dependent of the strain rate, cf. Figure 3.8 [47].

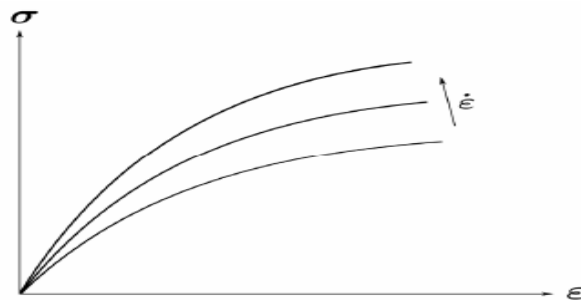


Figure 3.8: Strain rate dependence [47].

3.5.4 Viscoelastic behavior

Viscoelasticity is the property of materials that exhibit both viscous and elastic characteristics when undergoing deformation. Viscous materials, like honey, resist shear flow and strain linearly with time when a stress is applied. Elastic materials strain when stretched and quickly return to their original state once the stress is removed. Viscoelastic materials have elements of both of these properties and, as such, exhibit time-dependent strain. Whereas elasticity is usually the result of bond stretching along crystallographic planes in an ordered solid, viscosity is the result of the diffusion of atoms or molecules inside an amorphous material [48].

So some plastics like polystyrene yield, but others fracture in a brittle manner like polystyrene. Rubbers do not yield, but at high strains some of them crystallise and hence stiffen. When the stresses are removed from a polymeric material before fracture, the strain recovery path is not necessarily identical to that of the loading part of the deformation cycle. So energy must have been dissipated during the deformation of such materials – another indication of deviation from perfect elasticity. Both the deformation and the subsequent recovery are time-dependent, suggesting that some part of their behavior is viscous. In fact solid polymers show a combination of elastic and viscous behavior known as viscoelasticity. The degree of viscoelasticity is strongly dependent upon the temperature of test and the rate at which the polymer is deformed, as well as such structural variables as degree of crystallinity, crosslinking and molecular mass [12].

3.5.5 Plasticity

At sufficiently high strain levels, most materials exhibit a non-linear behavior. This is often an irreversible process known as plasticity. Fig. 3.9 shows a typical stress-strain relation from a tensile test on a metal bar for small deformations [47].

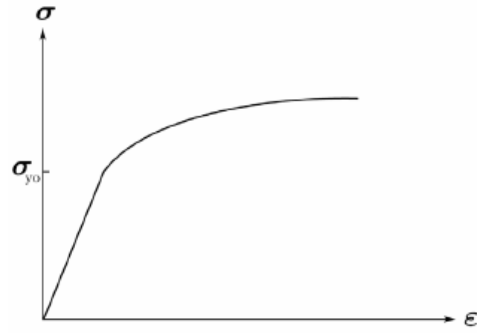


Figure 3.9: Plastic loading [47].

The elastic limit is defined by a yield criterion and the plastic curve is governed by laws of hardening and a flow rule. The strains can be divided into an elastic part and a plastic part.

$$\varepsilon = \varepsilon^e + \varepsilon^p \quad (3.1)$$

When unloading in the plastic region, the behavior is again elastic. After complete unloading, the remaining strain is the plastic strain ε^p or damage in the material, cf. Fig. 3.10. The stress level is not uniquely determined from the strain though it is dependent of the strain history.

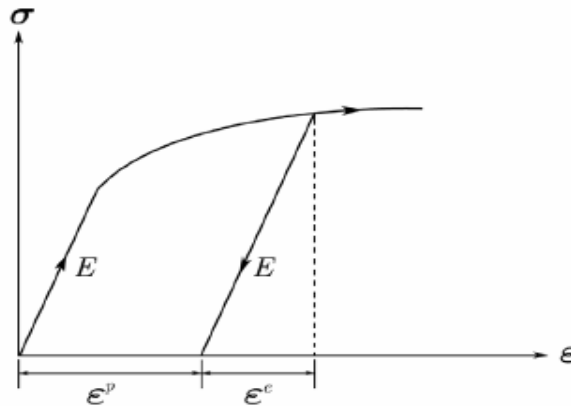


Figure 3.10: Plastic unloading [47].

3.5.5.1 Yield criteria for polymers

- Traditional criteria

A tensile test alone cannot give a full description of the yield behavior for design and it is important to obtain a general yield criteria, ie a function of the stress or strain components which reaches a critical value for all forms of test and combinations of stress components.

Although many yield criteria have been suggested, with varying experimental support, the two main criteria adopted for metals are those of Tresca (1864) and von Mises (1913). With some modification these criteria can also be applicable to polymers. The criteria for isotropic materials are normally given in terms of the stress components of the stress tensor, σ_{ij} .

$$\sigma_{ij} = \begin{bmatrix} \sigma_{11} & \sigma_{12} & \sigma_{13} \\ \sigma_{21} & \sigma_{22} & \sigma_{23} \\ \sigma_{31} & \sigma_{32} & \sigma_{33} \end{bmatrix} \quad (3.2)$$

By choosing axes parallel to the principal stress directions, ie where the shear stresses are all zero, the stress tensor becomes:

$$\sigma_{ij} = \begin{bmatrix} \sigma_1 & 0 & 0 \\ 0 & \sigma_2 & 0 \\ 0 & 0 & \sigma_3 \end{bmatrix} \quad (3.3)$$

and the criteria can be written in terms of the three principal stresses, σ_1 , σ_2 and σ_3 . For isotropic materials the yield criteria must be invariant with respect to coordinate transformation [49].

- Tresca yield criterion

This criterion proposes that yield occurs when the maximum shear stress, σ_s , reaches a critical value. For $\sigma_1 > \sigma_2 > \sigma_3$

$$\sigma_s = \frac{\sigma_1 - \sigma_3}{2} = \text{constant} \quad (3.4)$$

In a tensile test $\sigma_1 =$ applied stress and $\sigma_2 = \sigma_3 = 0$

$$\sigma_s = \frac{\sigma_1}{2} = \frac{\sigma_y}{2} \quad (3.5)$$

where $\sigma_y =$ tensile yield stress.

The Tresca criterion is therefore:

$$\frac{\sigma_1 - \sigma_3}{2} = \frac{\sigma_y}{2} \quad (3.6)$$

von Mises yield criterion

This criterion is based on the condition that yield occurs when the strain energy of shear reaches a critical value. It can be expressed as follows:

$$(\sigma_1 - \sigma_2)^2 + (\sigma_2 - \sigma_3)^2 + (\sigma_3 - \sigma_1)^2 = \text{constant} \quad (3.7)$$

In a tensile test this reduces to:

$$2 \sigma_1^2 = \text{constant} \quad (3.8)$$

The critical value for the constant is $2 \sigma_y^2$ where $\sigma_y =$ tensile yield stress. Von Mises criterion is therefore:

$$(\sigma_1 - \sigma_2)^2 + (\sigma_2 - \sigma_3)^2 + (\sigma_3 - \sigma_1)^2 = 2 \sigma_y^2 \quad (3.9)$$

In pure shear $\sigma_1 = -\sigma_2$ and $\sigma_3 = 0$ and the criterion gives:

$$\sigma_1 = \frac{\sigma_y}{\sqrt{3}} \quad (3.10)$$

The shear yield stress is predicted to be 1/3 times the tensile yield stress compared with $\sigma_y / 2$ for the Tresca condition [49].

- Graphical presentation of Tresca and von Mises criterion in plane stress

Consider initially the case of plane stress, $\sigma_3 = 0$. Von Mises criterion reduces to:

$$2\sigma_1^2 + 2\sigma_2^2 - 2\sigma_1\sigma_2 = 2\sigma_y^2 \quad (3.11)$$

$$\left(\frac{\sigma_1}{\sigma_y}\right)^2 + \left(\frac{\sigma_2}{\sigma_y}\right)^2 - \left(\frac{\sigma_1}{\sigma_y}\right)\left(\frac{\sigma_2}{\sigma_y}\right) = 1 \quad (3.12)$$

which describes an ellipse in principal stress space as shown in Fig. 3.11.

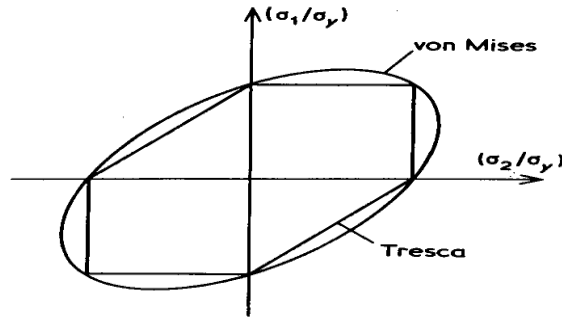


Figure 3.11: Tresca and von Mises yield criteria for plane stress [49].

The Tresca criterion in plane stress depends on the sign of the applied stress components. For σ_1 and σ_2 with the same sign (both either tensile or compressive):

$$\sigma_1 = \sigma_y \text{ or } \sigma_2 = \sigma_y \quad (3.13)$$

For σ_1 and σ_2 with opposite signs (one tensile and the other compressive):

$$\sigma_1 - \sigma_2 = \sigma_y \text{ or } \sigma_2 - \sigma_1 = \sigma_y \quad (3.14)$$

It can be seen from Fig. 8 that the Tresca criterion inscribes the von Mises ellipse. Von Mises predicts the possibility of an applied stress larger than the tensile yield stress in some stress states. This is not the case for Tresca [50].

3.5.5.2 Modified criteria for polymers

The applicability of either of the above criteria can be tested by performing experiments with different states of stress, eg plane stress, pure shear, biaxial tension etc. Modifications of the criteria have been found necessary for polymers. Firstly, it was found that compressive strengths are greater than tensile strengths, having the effect of shifting the yield ellipse or hexagon to the more compressive values. Hydrostatic pressure has also been shown to have a pronounced effect on the yield behavior, a fact clearly related to the increased compressive strengths. Von Mises and Tresca criteria have therefore been modified to take into account the effect of hydrostatic stress. In most cases polymers tend to follow a pressure dependent von Mises criterion. The effect of hydrostatic stress can be introduced into von Mises criterion through an additional hydrostatic term:

$$A(\sigma_1 + \sigma_2 + \sigma_3) + B[(\sigma_1 - \sigma_2)^2 + (\sigma_2 - \sigma_3)^2 + (\sigma_3 - \sigma_1)^2] = 1 \quad (3.15)$$

A and B can be defined in terms of the tensile and compressive yield stresses, σ_{YT} and σ_{YC} , since in these cases $\sigma_2 = \sigma_3 = 0$. Thus:

$$A = \frac{(\sigma_{YC} - \sigma_{YT})}{\sigma_{YC} * \sigma_{YT}} \quad (3.16)$$

and

$$B = \frac{1}{2\sigma_{YC} * \sigma_{YT}} \quad (3.17)$$

Fig. 3.12 shows the modified von Mises criterion fitted to polystyrene data. That is same criterion has been found acceptable where glassy amorphous are used makes it seem unnecessary to use different yield criteria for polymers of varying structural conditions [51]. In addition, a modified Tresca helix based on Coulomb's work on failure in soils is shown.

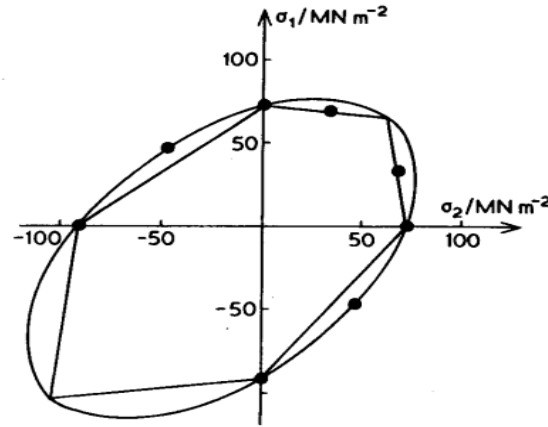


Figure 3.12: Yield criteria fitted to data [51].

3.5.5.3 Hardening

- Bilinear kinematic hardening

Bilinear Kinematic Hardening model was chosen in this study for polycarbonate model. This option assumes the total stress range is equal to twice the yield stress, so that the Bauschinger effect is included. Bilinear Kinematic Hardening may be used for materials that obey von Mises yield criteria (which includes most metals). The material behavior is described by a bilinear total stress-total strain curve starting at the origin and with positive stress and strain values. The initial slope of the curve is taken as the elastic modulus of the material. At the specified yield stress, the curve continues along the second slope defined by the tangent modulus, (having the same units as the elastic modulus). The tangent modulus cannot be less than zero nor greater than the elastic modulus [52]. Kinematic hardening of the von Mises criterion is illustrated in Figure 3.13 [53].

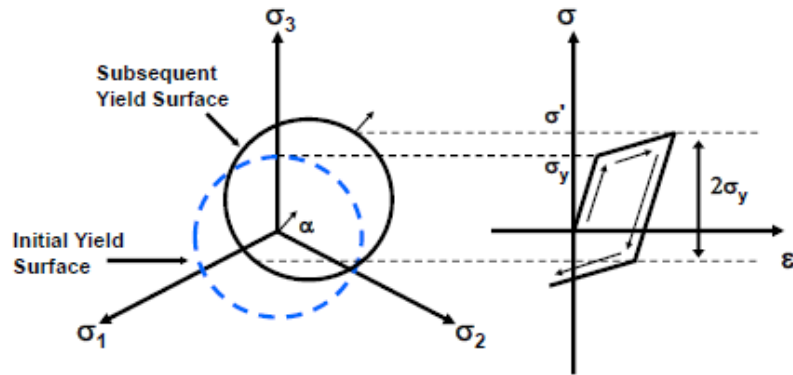


Figure 3.13: Kinematic hardening of the von Mises criterion [53].

Figure 3.13 shows subsequent yield in compression is decreased by the amount that the yield stress in tension increased, so that a $2\sigma_y$ difference between the yields is always maintained. This phenomenon is called the Bauschinger effect and is illustrated in Figure 3.14 [53].

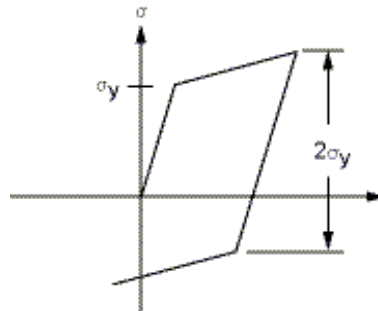


Figure 3.14: Bauschinger effect [53].

- The Drucker – Prager yield criterion

The Drucker–Prager yield criterion is a pressure-dependent model for determining whether a material has failed or undergone plastic yielding. The criterion was introduced to deal with the plastic deformation of soils. It and its many variants have been applied to rock, concrete, polymers, foams and other pressure-dependent materials [54]. When

the Drucker–Prager yield criterion is used, it is occurred that plasticity property is deactivate. This situation is expected because The Drucker–Prager yield criterion is used for brittle materials. It is known that PMMA behaviors brittle manner at room temperature. The Drucker–Prager model has been used to model for PMMA in this study.

4. IMPACT ANALYSIS SETUP

4.1 Target Model

4.1.1 Geometry

The plates were modeled using 90×90 mm size and 1.4 mm, 1.9 mm and 2.4 mm thickness. Subsequent impacts were made at the center, 20 and 40 mm of the plate depending on increasing thickness of plates. The exposed area of the polycarbonate and PMMA armor plates with impact locations on the horizontal paths as shown in Fig. 4.1.

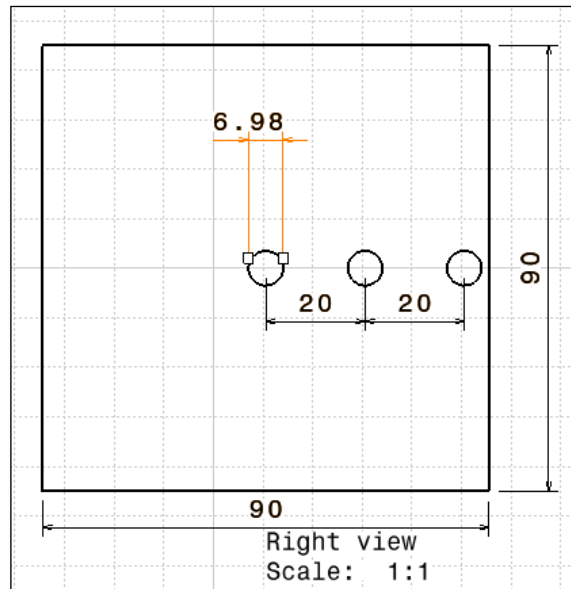


Figure 4.1: The exposed area of the plates with impact locations on the horizontal paths.

Also, target plate model was given as CAD model in Fig. 4.2 below.

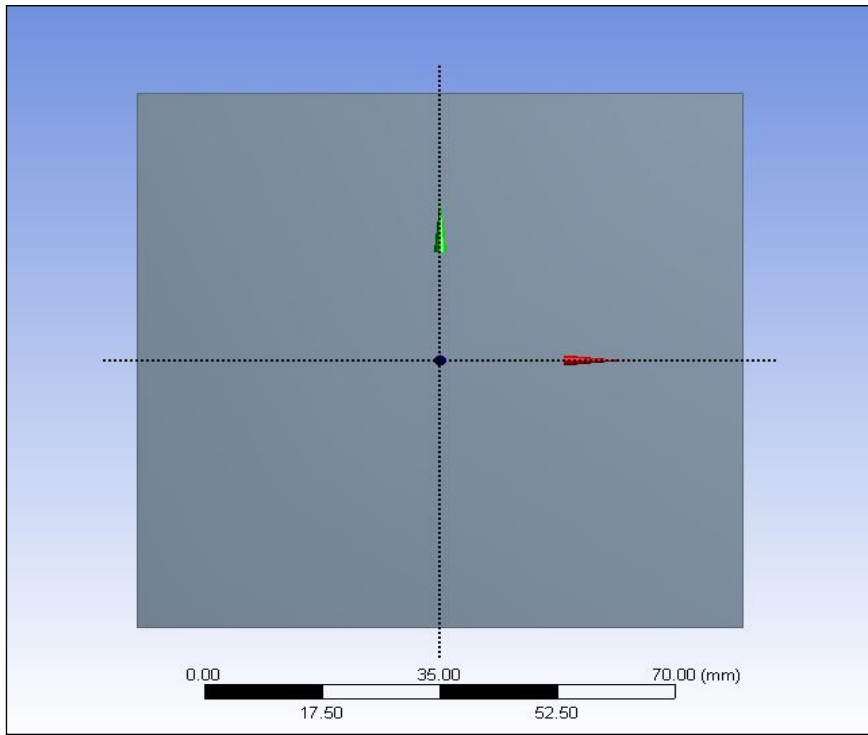


Figure 4.2: Target model.

4.1.2 Material properties

In this study, the impact performances of thin polycarbonate and acrylic plates were investigated in detail. These material properties were given as Table 4.1 and Table 4.2 [55].

Table 4.1: Material Property of PC [55].

Density (kg/m³)	1200
Elastic Modulus (MPa)	1530
Poisson ratio	0.38
Yield Strength (MPa)	63
Tangent Modulus (MPa)	35

Table 4.2: Material Property of PMMA [56].

Density (kg/m³)	1190
Elastic Modulus (GPa)	5.76
Poisson's ratio	0.42
Yield Strength (MPa)	44
Frictional Drucker–Prager angle (β)	20°

Bilinear Kinematic Hardening was selected for polycarbonate material model and PMMA was assumed to obey the Drucker–Prager material model in the present study.

4.2 Projectile

4.2.1 Geometry

A spherical steel projectile of 6.98 mm diameter was launched against the square plate. The spherical steel projectile was selected from ANSYS menu as rigid model in this study. The mass of projectile was calculated as 0.00139 kg from the density of steel projectile. Also, projectile velocity of 140 m/s was determined. According to this information, kinetic energy of the projectile was computed as 13.693 joule. The spherical steel projectile was shown in Fig. 4.3.

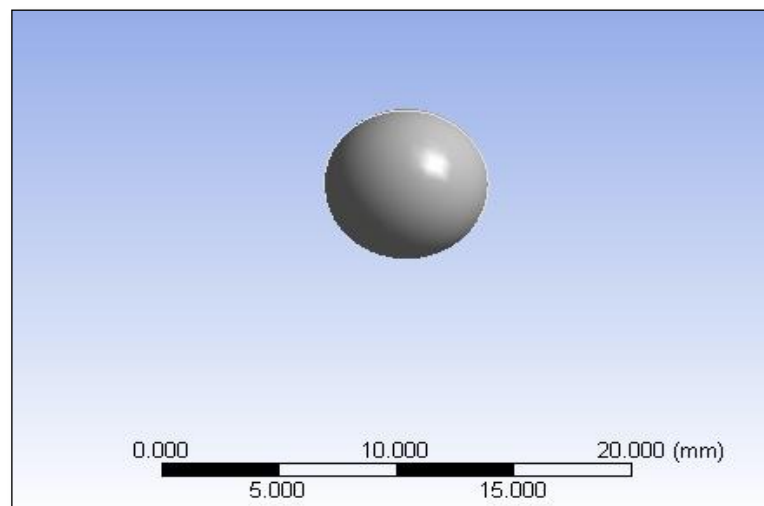


Figure 4.3: The spherical steel projectile.

4.2.2 Material properties of spherical steel projectile

The properties of spherical steel projectile were given Table 4.3.

Table 4. 3: Material Properties [57].

Density (kg/m³)	7850
Elastic Modulus (GPa)	200
Poisson's ratio	0.3

4.3 Numerical Analysis

4.3.1 Material models

The polycarbonate and PMMA plates were modeled into ANSYS/ Workbench/ Autodyn with approximately 94000 solid elements. Further, the polycarbonate target was modeled with approximately 67000 shell elements. One portion of finite-element mesh is shown in Fig. 4.4. The target plate outer edge was constrained for all degrees of freedom. Projectile was launched against the target plate with an initial velocity of 140 m/s. Plastic strain, von Mises stresses, maximum shear stresses, deformation of plate and energy absorption histories were recorded. Further, impacts at locations center of the plate, 20 and 40 mm were carried out by a spherical steel projectile of 6.98 mm by 20 mm towards the boundary of the plate depending on changing plate thickness.



Figure 4.4: A portion of the target plate and rigid projectile mesh for finite-element simulation.

Firstly, the material model used for the polycarbonate target plate was Kinematic Hardening with a bi-linear trend with an elastic modulus of 1530 MPa and a Poisson's ratio of 0.38. A tangent modulus of 35 MPa was used to incorporate the plastic deformation until the material failure under a plastic failure strain. The

polycarbonate material density used was 1200 kg/ m^3 . The yield strength for polycarbonate was considered to be 63 MPa. These material properties were shown as Table 4.1 [55]. The steel ball projectile was modeled as a rigid material with a density of 7850 kg/ m^3 with an elastic modulus of 200 GPa and a Poisson's ratio of 0.30. The properties of spherical steel projectile were given Table 4.3 [57].

Secondly, the material properties of commercial PMMA were previously investigated by Rittel and Brill [2]. PMMA is assumed to obey the Drucker–Prager material model, with dynamic elastic properties (from [55]) (E , ν), density (ρ) and pressure sensitivity (β) all listed in Table 4.2 [56]. Experimentally uniaxial determined stress–plastic strain curves at different strain rates ($\dot{\epsilon}=0.0001$; 1; 2000 and 4000 s^{-1}) are shown in Fig. 4.5. In the absence of experimental data at significantly higher strain rates, we assumed that the behavior of the material is that measured at 4000 s^{-1} . Yet, it should be kept in mind that at high strain rates, under confined compression, PMMA was shown to fail by adiabatic shear banding, which is the main characteristic to be preserved in the simulation, as opposed to pure brittleness (shattering). In parallel, it is realized that at extremely high strain rates, the strength of the material does not increase indefinitely. For these reasons, a reasonable choice was made to preserve the measured ductility while neglecting viscous effects at very high strain rates. In this study, it is taken consideration only elastic-plastic behavior.

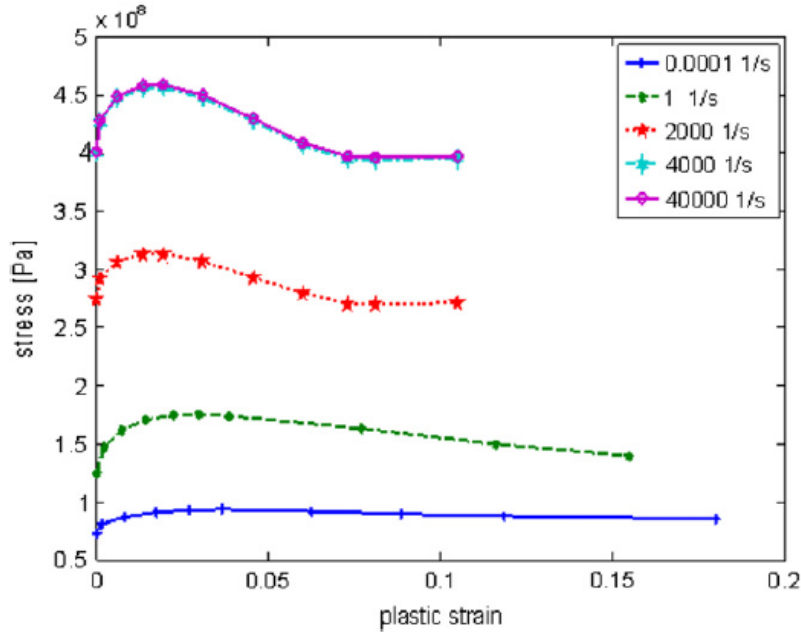


Figure 4.5: The hardening properties of PMMA for rates $\dot{\epsilon} = 0.0001; 1; 2000; 4000$ and 40000 s^{-1} [56].

4.3.2 Failure criterias

The material properties available for polycarbonate material at high strain rate found in the literature were very scarce and material models in most cases were incomplete or lacked precision [58–60]. Polycarbonate tensile tests were therefore performed on the test coupon shown in Fig.4.6 Stress–strain curve obtained from the tension test at various strain rates. Failure strain was found to be 150%. A low capacity polymer testing machine was used to conduct the tensile tests. At low loading rate the strain to failure is observed to be large but for dynamic loads the strain to failure is smaller. As is evident from the stress–strain curves the elastic modulus at higher strain rates increases significantly unlike most metals. The curve with the largest failure strain was obtained from the static tensile test. The rest of the curves were obtained for higher strain rates. As the strain rate increases the yield strength increases but for polymers it remain constant after a certain strain rate. Although the material properties used were obtained at lower strain rates than the actual material properties that are required to be conducted at higher strain rates [61] that are encountered in bullet impacts, the results still closely agree with the experimental investigations.

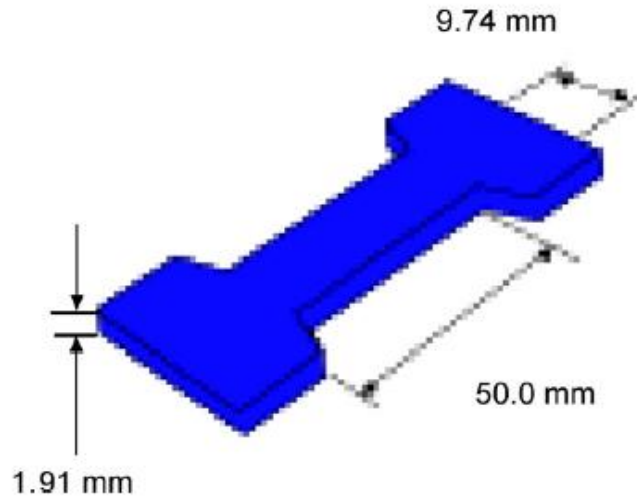


Figure 4. 6: Test specimen of polycarbonate with a gage length of 50 mm, a thickness of 1.91mm and a width of 9.74 mm [61].

The influence of the confinement on the mechanical response of these materials was determined. A simple dynamic pressure-sensitive constitutive equation was identified, and it was also observed [27] that under a suitable confinement level and strain rate, PMMA can undergo a brittle–ductile transition resulting in the formation of an adiabatic shear band. It is therefore evident that aside from a brittle (spalling) failure mechanism, PMMA can also undergo ductile deformations (including localized). The extent to which plasticity plays a role in the slant impact/perforation process remains to be investigated. Consequently, this study addresses the impact and perforation of PMMA plates under the combined effects of brittle spalling and ductile deformations. The investigation is done essentially by numerical simulations into which the ductile and the brittle responses of this material are included. Two failure criteria which are used on Autodyn explicit [62] were used for PMMA: tensile failure and ductile failure. The failure criteria can be applied combined without any need of user subroutine.

The “tensile failure” uses the hydrostatic pressure as a measure of the failure stress to model dynamic spall, or a pressure cutoff. It is designed for high-strain-rate deformation and offers a number of choices to model failure. Five failure choices are offered for the failed material points: the default choice, which includes element removal, and four different spall models (the crumbling of a material). It is used the

default choice in which when the tensile failure criterion is met at an element integration point, the material point fails and the element is removed. This criterion can be used in conjunction with other failure criteria. It means that in each material point each failure criteria is tested separately. Polymethylmethacrylate is known to be extremely brittle at high strain rates, with a typical spall strength of 100–150 MPa [63]. A representative value of 133 MPa is used throughout this work.

The “ductile failure” criterion is used to predict the onset of damage due to nucleation, growth and coalescence of voids. The model assumes that the equivalent plastic strain at the onset of damage is a function of the stress triaxiality and plastic strain rate. Maximum plastic strains at which failure initiates as a function of strain rate and triaxiality are listed in Table 4.4 [27]. The data is taken from Table 4.4. Note that the higher strain-rate response is assumed to be similar to that measured at 4000 s^{-1} .

Table 4.4: Ductile damage initiation properties for PMMA [27].

Strain rate (s^{-1})	ϵ_p^{\max}	Triaxiality
Quasi-static	0.30	all
1	0.20	all
2000	0.12	all
4000	0.10	all
40000	0.10	all

5. RESULTS AND DISCUSSIONS

5.1 Introduction

In this thesis study, dynamic response of exposure to a constant velocity impact of polycarbonate and polymethylmethacrylate plates were investigated depending on increasing thickness of plates and impacts at locations center of the plate, 20 and 40 mm were carried out by a spherical steel projectile using finite element analysis program which AUTODYN modul. The velocity of spherical steel projectile was selected as 140 m/s and also impacted approximately 21 mm distance from the center of plate. The contact time of projectile was calculated as 0.000153 s. Thus, analysis time which means end time was given as 2.5 times of contact time. That is, end time is 0.000338 s. Analyses were studied for polycarbonate and PMMA plates at different thickness of plates and impact locations. Furthermore, all results with respect to comments of graphs and tables will be explained in conclusions section.

It is getting started this chapter, it was conducted that a validation study before thesis study. This validation study is similar to thesis study. It was used circular polycarbonate plate and it was impacted by a spherical steel projectile in academic study.

5.2 Verification Study

A 1.91-mm thick circular polycarbonate plate of 115mm diameter was impacted by a spherical steel projectile of 6.98mm diameter at its center. Subsequent impacts were made at 10, 20, 30, 40, and 50 mm radii of the plate. For a constant projectile velocity of 138 m/s which was below the perforation limit of the plate under investigation, a maximum thickness reduction close to the edge support was observed. This study was modeled into explicit finite-element analysis program LSDYNA for simulations. The polycarbonate plate was modeled into LSDYNA with 41,751 shell elements. Additionally, the polycarbonate plate was modeled into ANSYS/ Workbench/ AUTODYN with approximately 40000 shell elements.

Maximum energy absorption and plastic strain values were recorded. Stress–strain curve obtained from the tension test at various strain rates. Failure strain was found to be 150% [21]. It can be shown material properties in Tables 5.1 and 5.2 below [21].

Table 5.1: Material Properties of PC [21].

Density	1200 kg/m ³
Elastic Modulus	1530 MPa
Poisson ratio	0.38
Yield Strength	63 MPa
Tangent Modulus	35 MPa

Table 5.2: Material Properties of Projectile [21].

Density	7850 kg/m ³
Elastic Modulus	200 GPa
Poisson's ratio	0.3

It can be also seen that impact points Figure 5.1 [21].

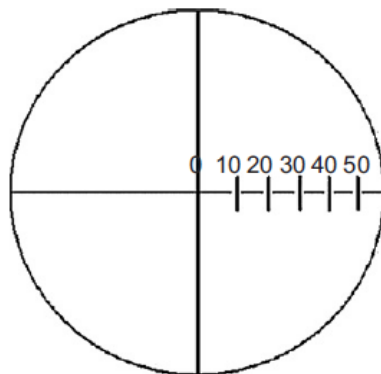


Figure 5.1: Impact Points [21].

- Results and validation

It is given that energy absorption distribution with LSDYNA and Autodyn.

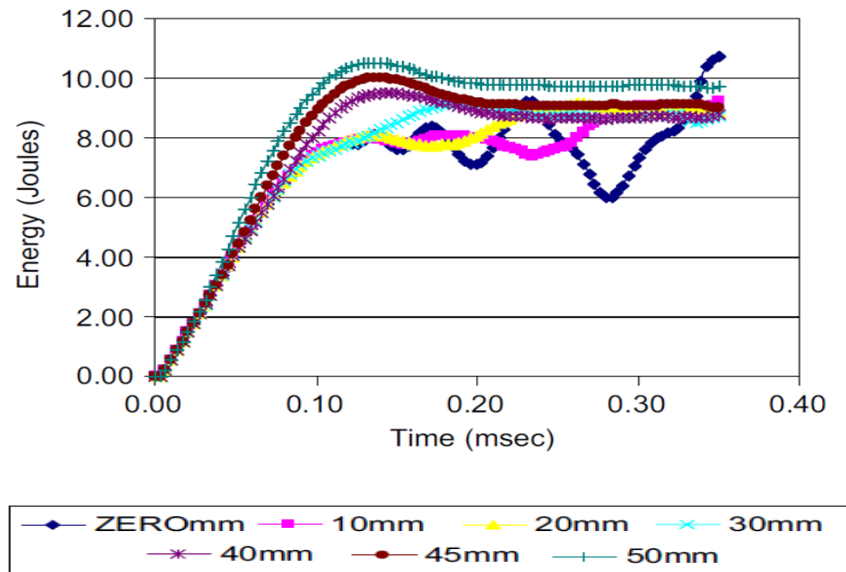


Figure 5.2: History of Energy Absorption with LSDYNA [21].

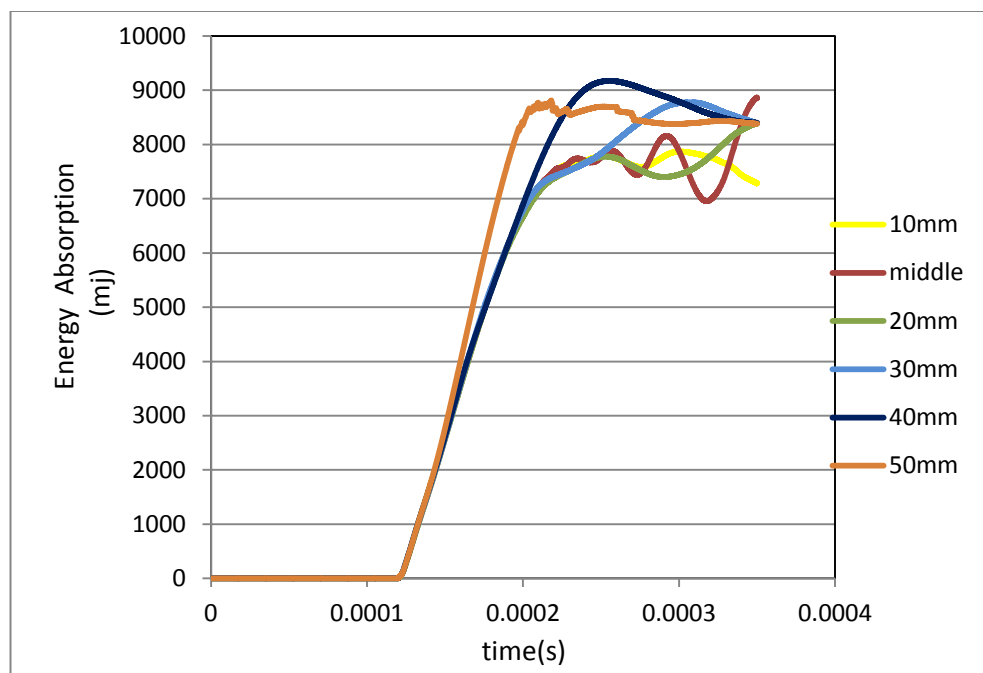


Figure 5.3: History of Energy Absorption with AUTODYN.

It was also compared that plastic strain values at each impact point. It is given that graphs below.

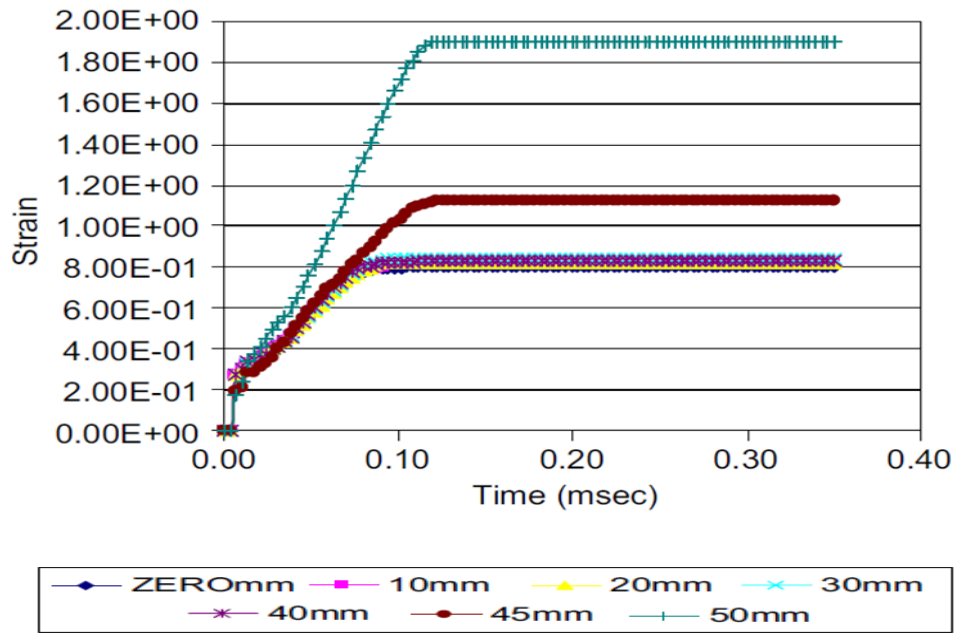


Figure 5.4: Plastic strain at the point of impact with LSDYNA [21].

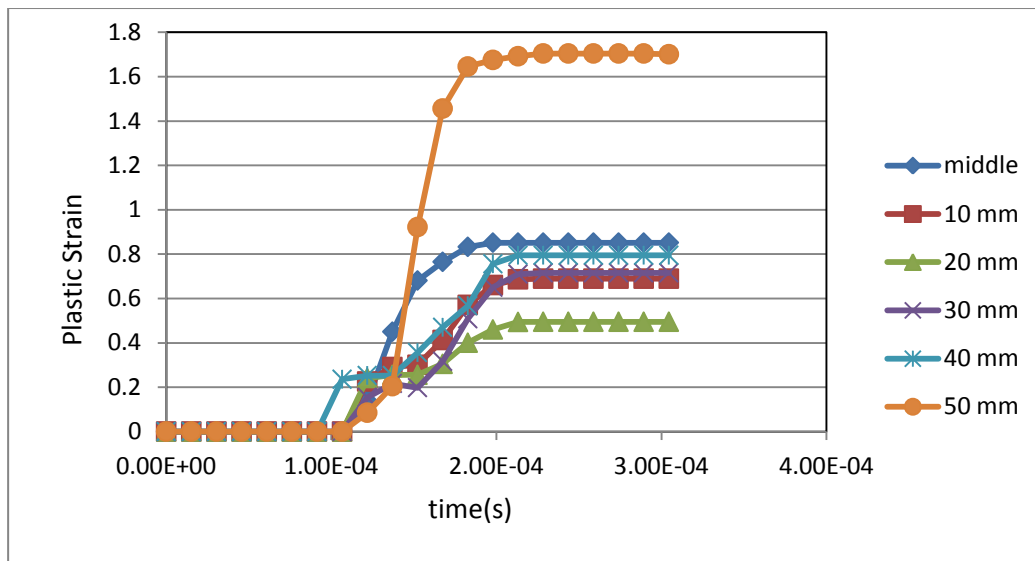


Figure 5.5: Plastic strain at the point of impact with AUTODYN.

It can be understood that both energy absorption and plastic strain values are close to quite each other. It is concluded that under a constant projectile velocity that is unable to cause any material separation in the plate center region, the plate perforation may be possible near the clamped edge of an armor plate. In order to prevent such failure close to the fixed edge it is suggested to incorporate an additional annular plate to cover the near edge zone. In this way, it can be said that verification study has been implemented successfully.

5.3 Behavior of polycarbonate plates during impact

Numerical simulations were performed as shown in Fig. 5.6 below.

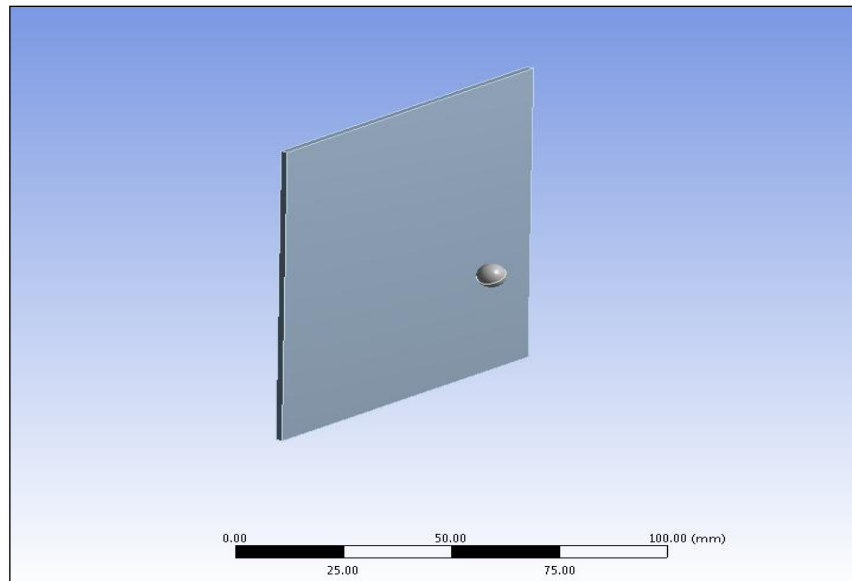


Figure 5.6: Numerical simulations.

Von Mises stress at the center of polycarbonate plate and 1.9 mm thickness is shown in Fig. 5.7. The yield stress of polycarbonate is 63 MPa and it was obtained that the yield stress was 88.759 MPa after analysis. Thus, it was occurred plastic deformation as expected.

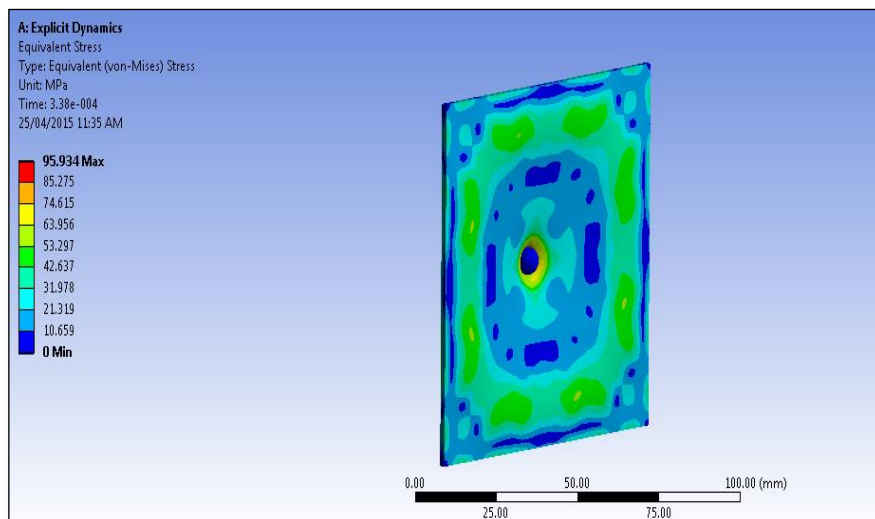


Figure 5.7: Von Mises stress at the center of polycarbonate plate and 1.9 mm thick.

The side profile of plate is shown that penetration and partially perforated in Fig. 5.8.

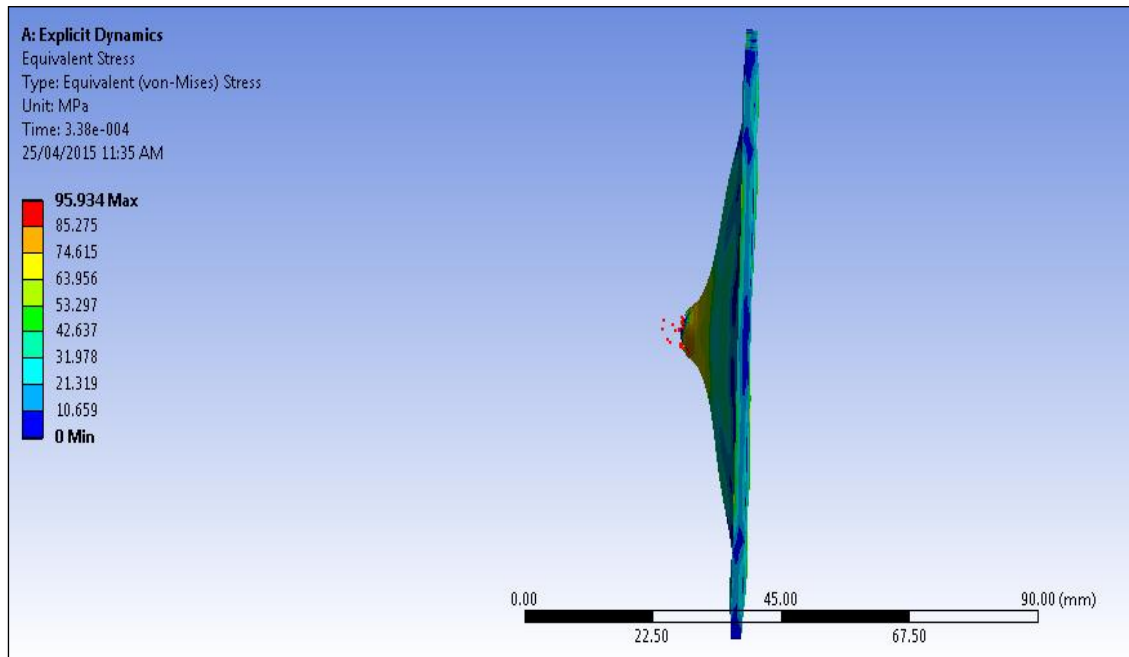


Figure 5.8: Von Mises Stress at the side profile of plate at 1.9 mm thick.

It is shown that von Mises stresses at different thickness and different impact locations for polycarbonate plates in table 5.3.

Table 5.3: Von Mises stresses for polycarbonate plates.

	1.4 mm thickness	1.9 mm thickness	2.4 mm thickness
Plate Center (MPa)	100.5	101.7	88.8
At 20 mm (MPa)	100.7	99.1	89.3
At 40 mm (MPa)	97.9	102.8	102.7

It was also seen that perforated at 40 mm distance from plate center in 1.9 mm thickness in Fig. 5.9 and other impact locations were shown partially perforated.

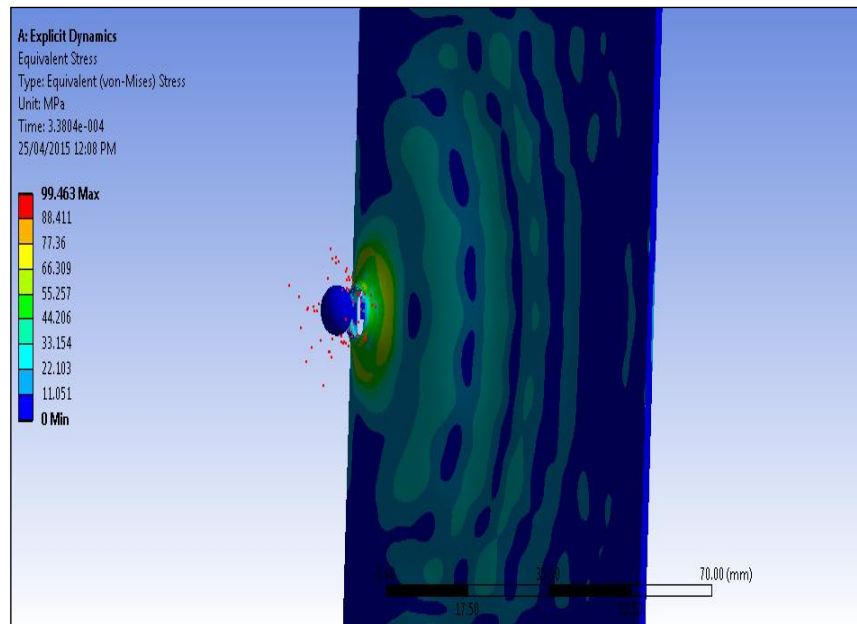


Figure 5.9: Von Mises stress distribution and perforated at 40 mm distance and 1.9 mm thick.

It is seen that von Mises stress was increased from plate center to fixed edge for 2.4 mm thickness. At the same thickness of plate, it was shown that it was occurred plastic deformation at plate center and 40 m distance. Further, there was seen a diminutive fragmentation at 40 mm distance in Figs. 5.10 and 5.11 at different perspective.

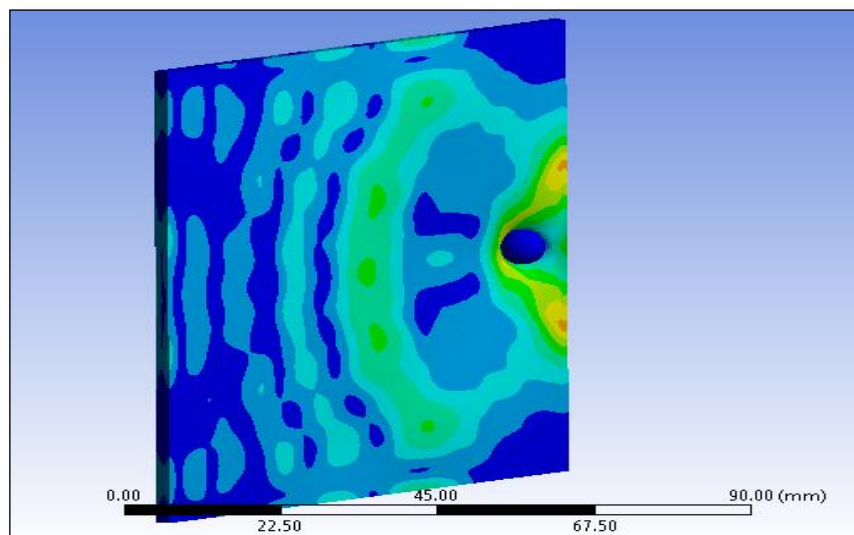


Figure 5.10: Von Mises stress distribution at 40 mm distance and 2.4 mm thickness (in front of plate).

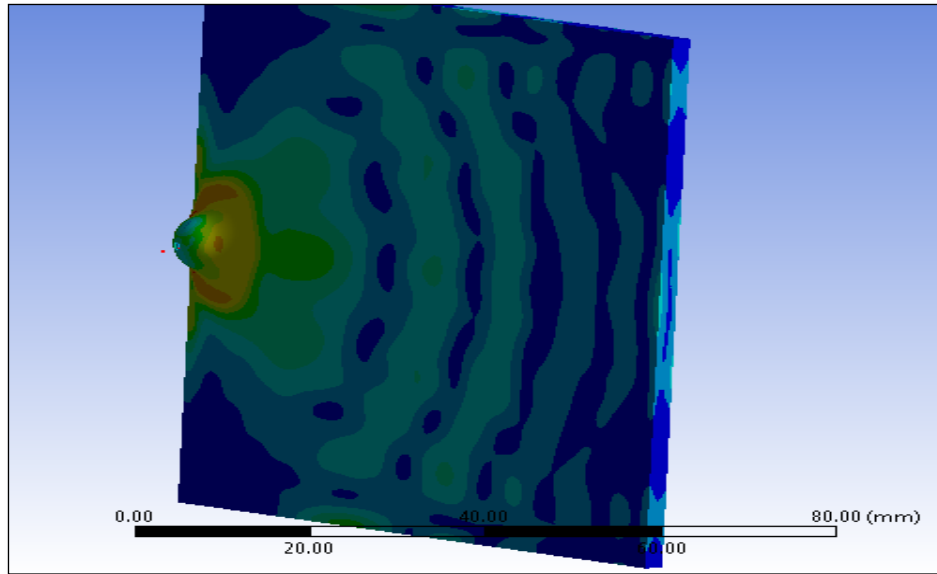


Figure 5.11: Von Mises stress distribution at 40 mm distance and 2.4 mm thickness (back of plate).

It is given that von Mises stress distribution at 40 mm distance and 2.4 mm thickness in Fig. 5.12.

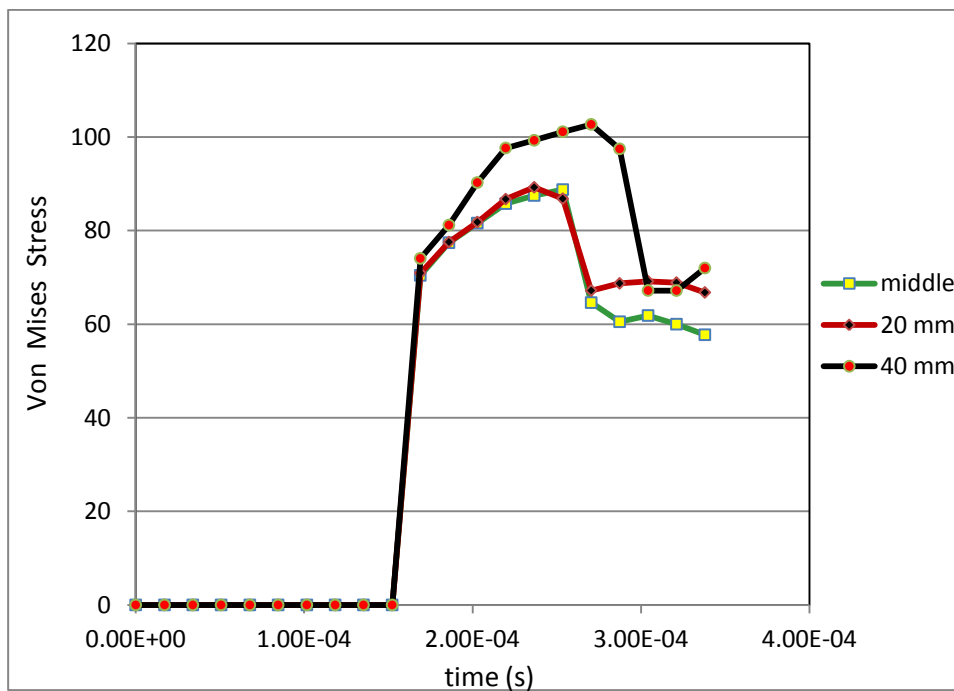


Figure 5.12: Von Mises stress distribution at 40 mm distance and 2.4 mm thickness.

It was observed that all impact points were showed that perforated at 1.4 mm thickness of polycarbonate plate. The fragmentation simulation was given in Fig. 5.13 below.

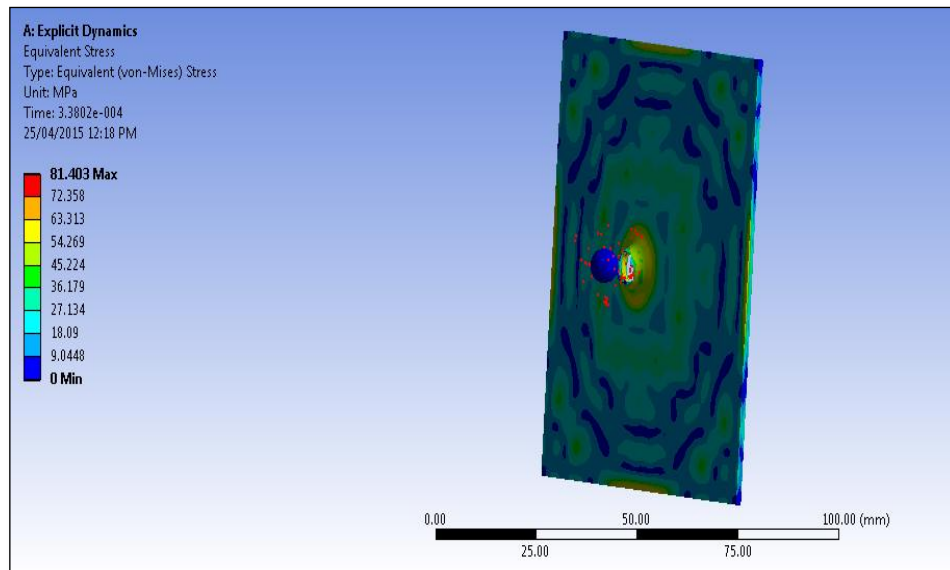


Figure 5.13: Von Mises stress and fragmentation at plate center and 1.4 mm thickness of plate.

After impacts, maximum deformation was 9.0131 mm at plate center and 2.4 mm thickness of plate in Fig. 5.14. Similarly, it was found that maximum deformation at 20 mm distance was 9.20 mm and maximum deformation at 40 mm was 9.011 mm.

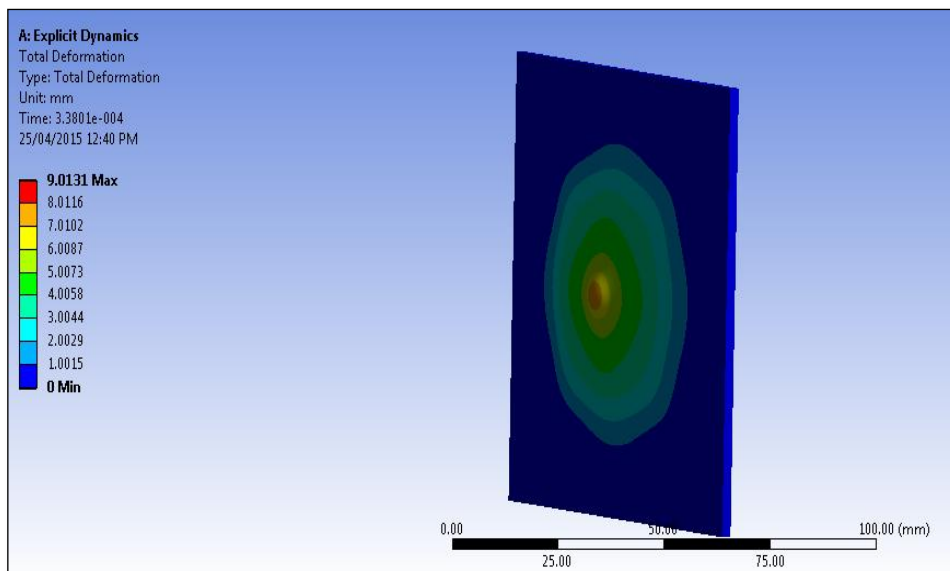


Figure 5.14: Maximum deformation at plate center and 2.4 mm thickness.

Maximum deformation is also shown at plate center and 1.4 mm thickness of plate in Fig. 5.15.

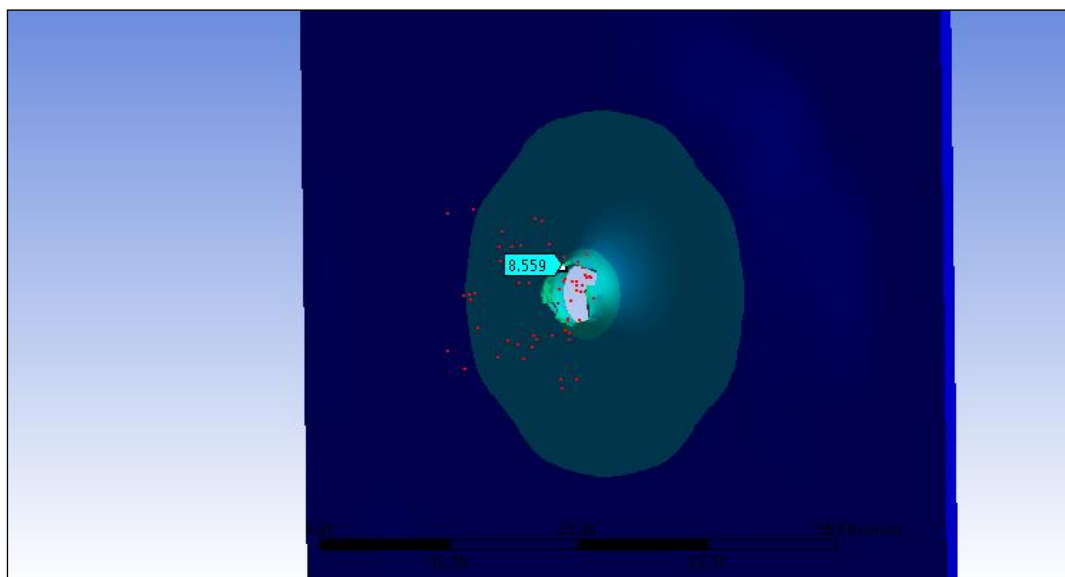


Figure 5.15: Maximum deformation at plate center and 1.4 mm thickness of plate.

It is given that max. deformation values at different thicknesses in 0.000338 s as table 5.4 below.

Table 5.4: Maximum deformation values.

	1.4 mm thickness	1.9 mm thickness	2.4 mm thickness
Plate Center (mm)	8.6	10.5	9,1
At 20 mm (mm)	8.6	10.6	9.2
At 40 mm (mm)	7.3	7.1	9.1

It is seen that maximum shear stress values at different thicknesses and different impact locations in table 5.5.

Table 5.5: Maximum shear stress values.

	1.4 mm thickness	1.9 mm thickness	2.4 mm thickness
Plate Center (MPa)	57.1	56.8	45.4
At 20 mm (MPa)	57.4	56.1	46.1
At 40 mm (MPa)	55.1	58.4	57.9

Maximum shear stress increased toward clamped edge as table 5.5. Maximum shear stress distribution is given for plate of 1.9 mm thickness as Fig. 5.16 below.

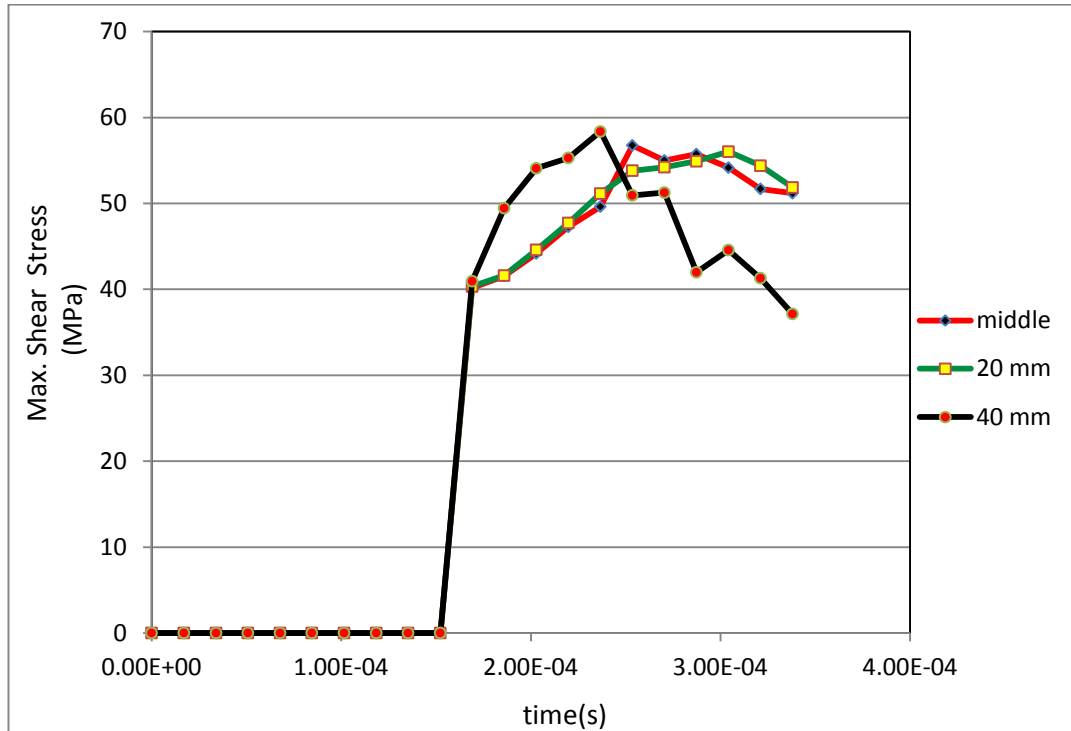


Figure 5. 16: Maximum shear stress distribution at 1.9 mm thickness.

It is given that maximum plastic strain values at different thicknesses and different impact locations in table 5.6.

Table 5.6: Maximum plastic strain values.

	1.4 mm thickness	1.9 mm thickness	2.4 mm thickness
Plate Center	1.2	1.1	0.8
At 20 mm	1.3	1.1	0.9
At 40 mm	1.3	1.3	1.2

For all different thickness of plate, plastic strain values increased from plate center to fixed edge. It is shown that plastic strain distribution at plate center in Fig. 5.17. It is also shown that plastic strain values decreased while thickness of polycarbonate plate increased in Fig. 5.17.

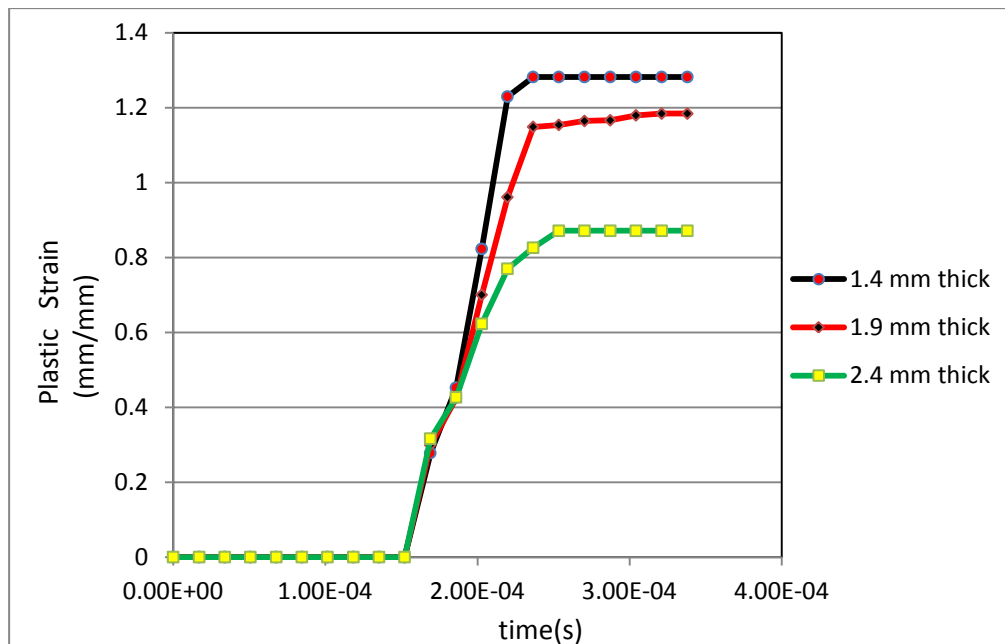


Figure 5.17: Plastic strain values at plate center.

It is given that maximum plastic strain simulation at 40 m distance and plate of 1.9 mm thickness in Fig. 5.18.

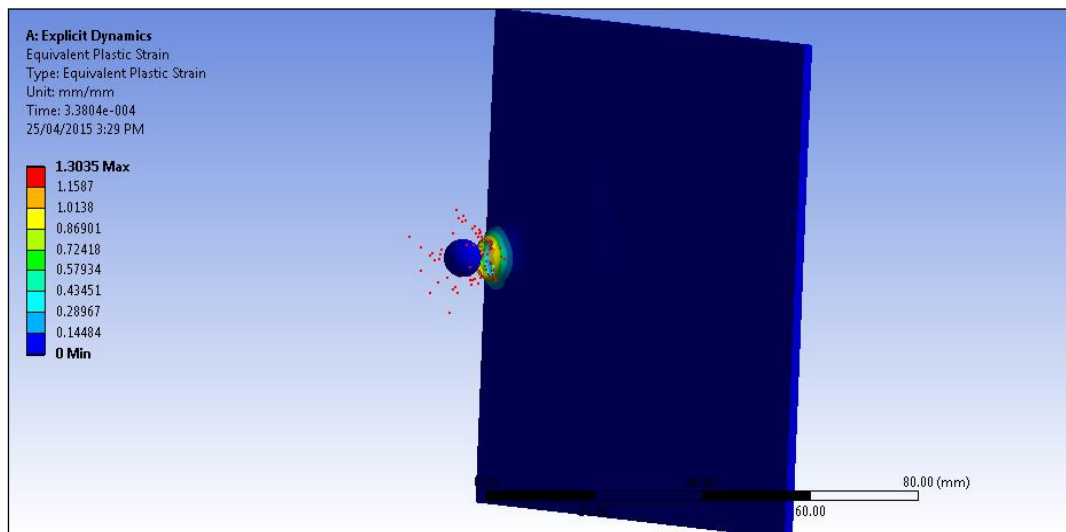


Figure 5.18: Maximum plastic strain simulation at 40 m distance and 1.9 mm thickness.

It is given that maximum energy absorption values at different thicknesses in Table 5.7. The energy absorption increased from 1.4 mm thickness to 2.4 mm thickness.

Table 5.7: Maximum energy absorption values.

	1.4 mm thickness	1.9 mm thickness	2.4 mm thickness
Plate Center (J)	5.2	8.8	9.4
At 20 mm (J)	5.2	9.7	10.2
At 40 mm (J)	5.1	7.9	11.7

It is given that energy absorption distribution for plate of 2.4 mm thickness in Fig. 5.19. Maximum energy absorption was found at close to the clamped edge which is at 40 mm distance.

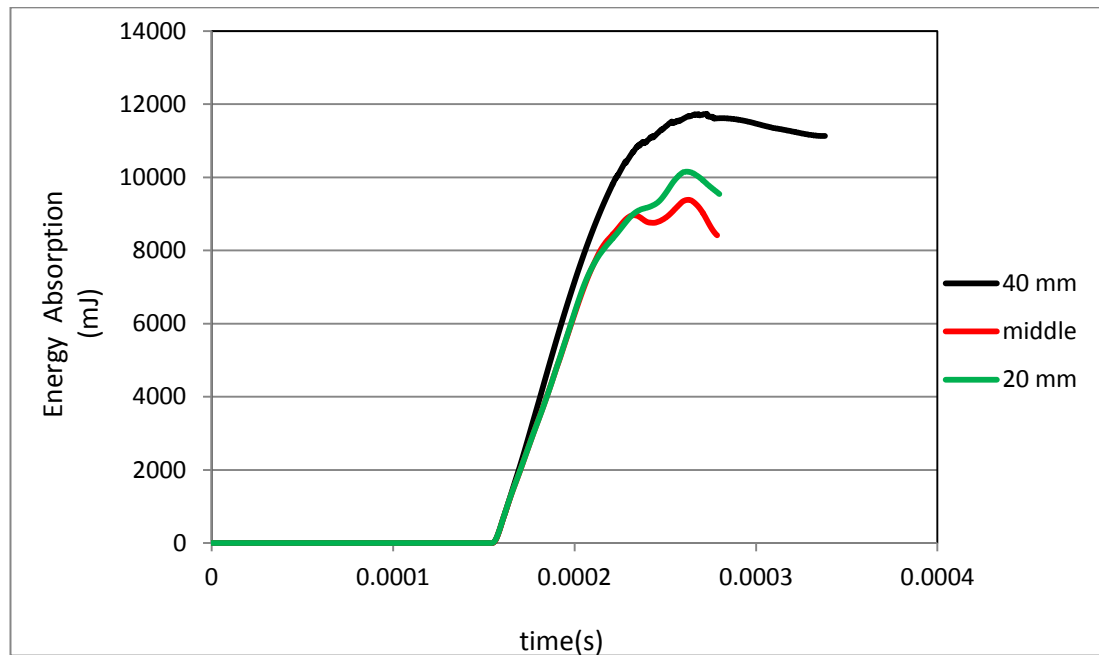


Figure 5.19: Energy absorption distribution for 2.4 mm thickness.

It is also given that energy absorption distribution at different thickness and 40 mm distance in Fig.5.20. Maximum energy absorption was found for 2.4 mm thickness of polycarbonate plate.

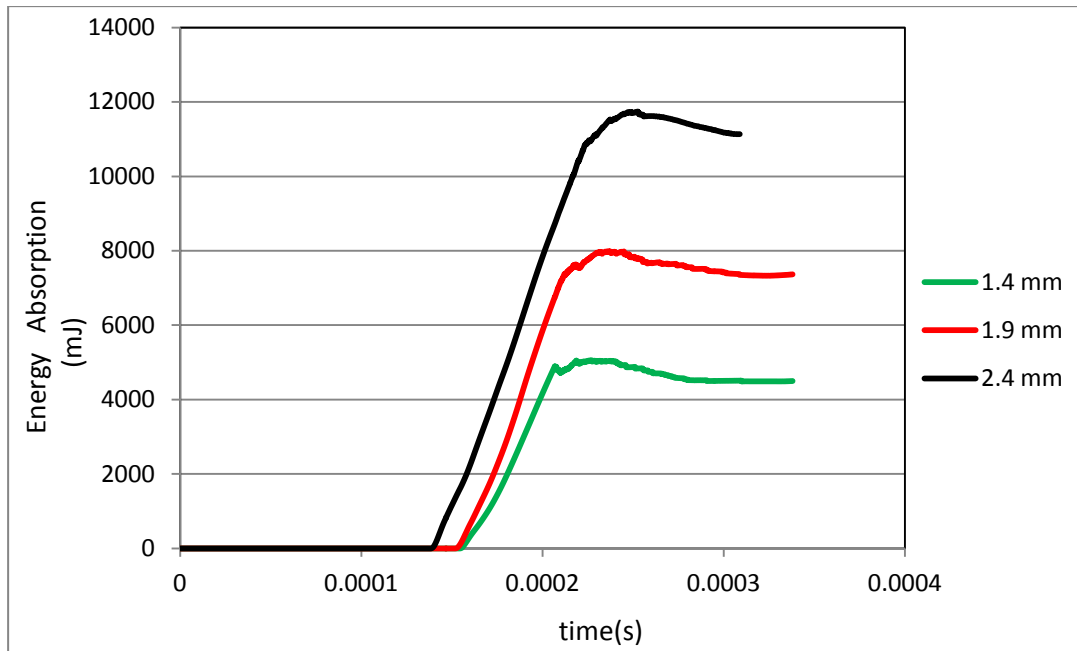


Figure 5.20: Energy absorption distribution at 40 mm distance.

5.4 Behavior of PMMA plates during impact

It was occurred that fragmentation all analyses for PMMA plates at any thickness of plate and any impact points. It was seen that von Mises stress values increased when thickness of PMMA plates are increased. Also, von Mises stresses increased toward clamped edge at all thickness in table 5.8.

Table 5.8: Maximum von Mises stress values.

	1.4 mm thickness	1.9 mm thickness	2.4 mm thickness
Plate Center (MPa)	53.1	56.8	57.6
At 20 mm (MPa)	56.6	58.7	58.9
At 40 mm (MPa)	59.4	61.6	60.9

It is shown that von Mises stress at middle of PMMA plates and different thickness. Maximum Stress is seen at 2.4 mm thickness in Fig. 5.21 below.

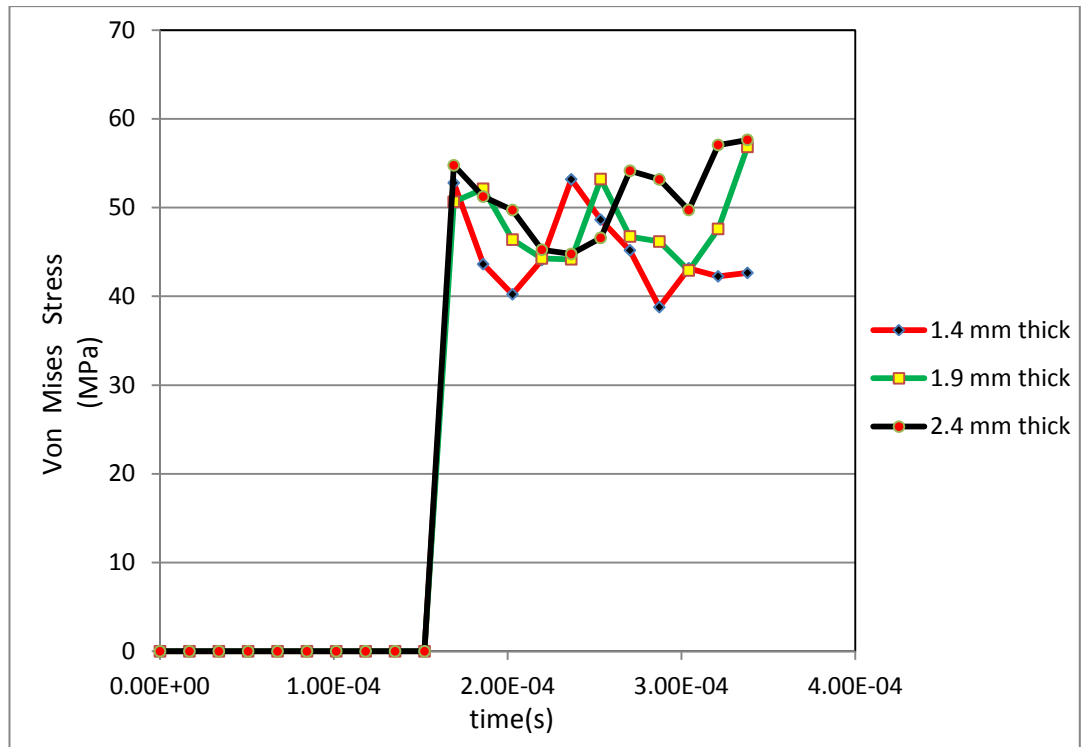


Figure 5.21: Von Mises stress distribution at plate center.

It is shown that maximum shear stress increased towards fixed edge when thickness of plate increased. Furthermore, maximum shear stress increased toward clamped edge at same thickness of PMMA plate in Table 5.9.

Table 5.9: Maximum shear stress values for PMMA plates.

	1.4 mm thickness	1.9 mm thickness	2.4 mm thickness
Plate Center (MPa)	30.5	32.6	33.2
At 20 mm (MPa)	32.6	33.9	34.1
At 40 mm (MPa)	34.2	35.6	35.2

It is seen that maximum shear stress simulations at plate center and 1.4 m thickness of plate in Fig. 5.22 and 5.23.

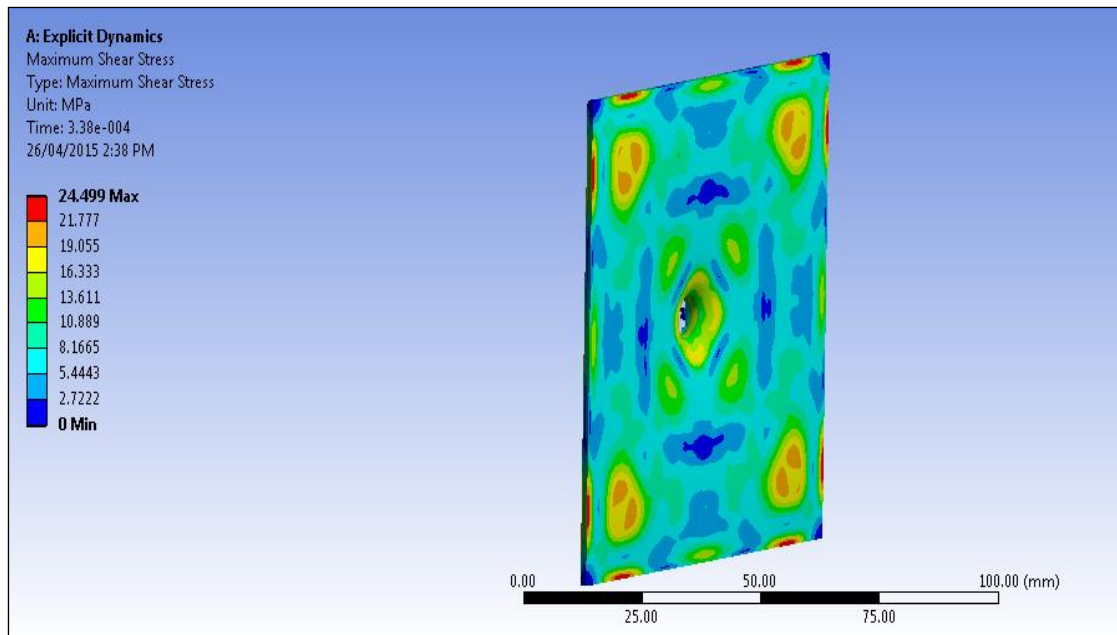


Figure 5.22: Maximum shear stress in front of plate.

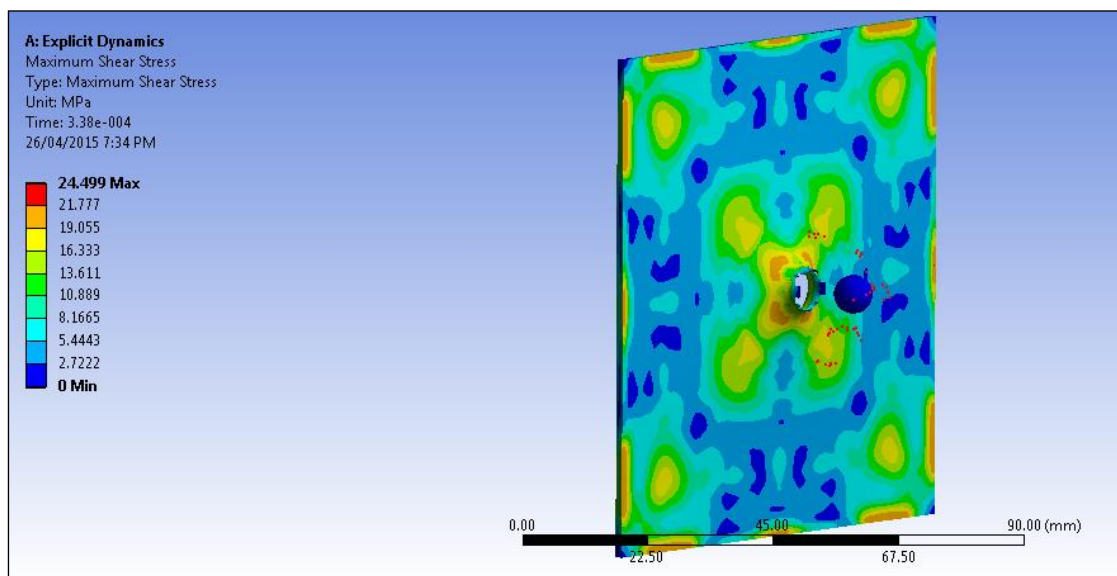


Figure 5.23: Maximum shear stress at back of plate.

It is given that maximum shear stress graph at plate center and different thickness of plates in Fig. 5.24. Maximum shear stress increased from 1.4 mm thickness to 2.4 mm thickness.

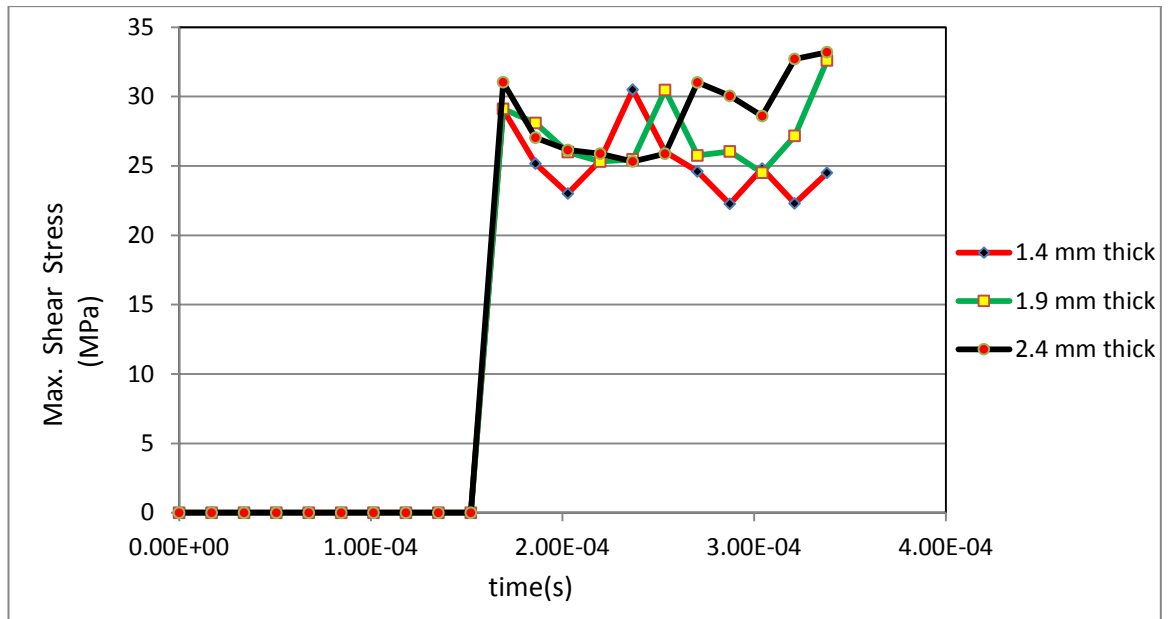


Figure 5.24: Maximum shear stress graph at plate center.

It is shown that maximum shear stress simulation at 40 mm distance and 1.9 mm thickness in Fig. 5.25.

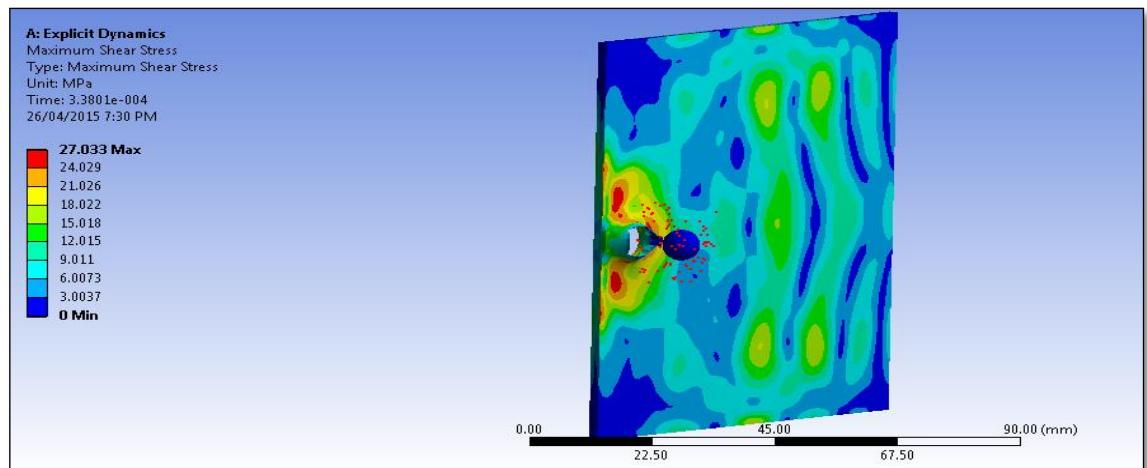


Figure 5.25: Maximum shear stress simulation at 40 mm distance and 1.9 mm thickness of plate.

It is given that maximum deformation values for PMMA plates in table 5.10.

Table 5.10: Maximum deformation values.

	1.4 mm thickness	1.9 mm thickness	2.4 mm thickness
Plate Center (mm)	8.9	8.9	10.2
At 20 mm (mm)	8.8	9.3	10.1
At 40 mm (mm)	7.8	8.2	8.6

Maximum deformation was shown at 20 distance and 1.9 mm thickness of plate for PMMA plate in Fig. 5.26.

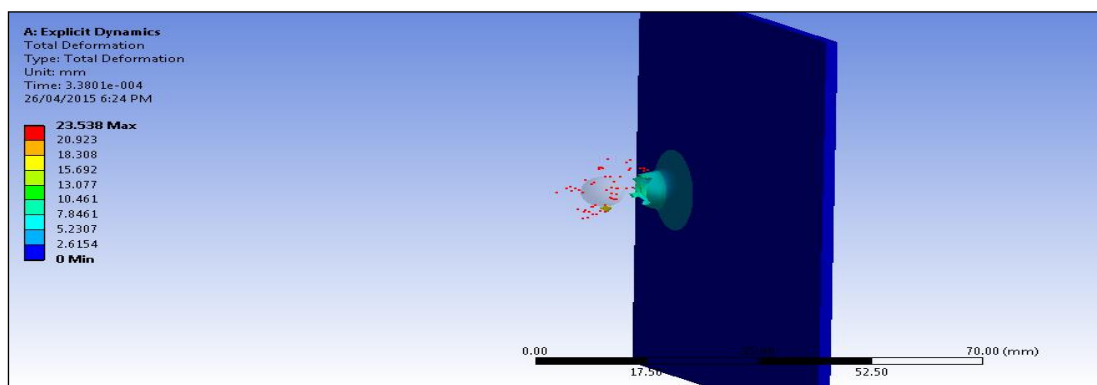


Figure 5.26: Maximum deformation simulation at 20 distance and 1.9 mm thickness.

It is given that maximum plastic strain values at different thicknesses and different impact locations in table. All values were close to each other as shown in table 5.11 below.

Table 5.11: Maximum plastic strain values for PMMA plates.

	1.4 mm thickness	1.9 mm thickness	2.4 mm thickness
Plate Center	1.49	1.48	1.49
At 20 mm	1.49	1.42	1.48
At 40 mm	1.48	1.48	1.49

It is given that maximum plastic strain values for 1.4 mm thickness in Fig. 5.27.

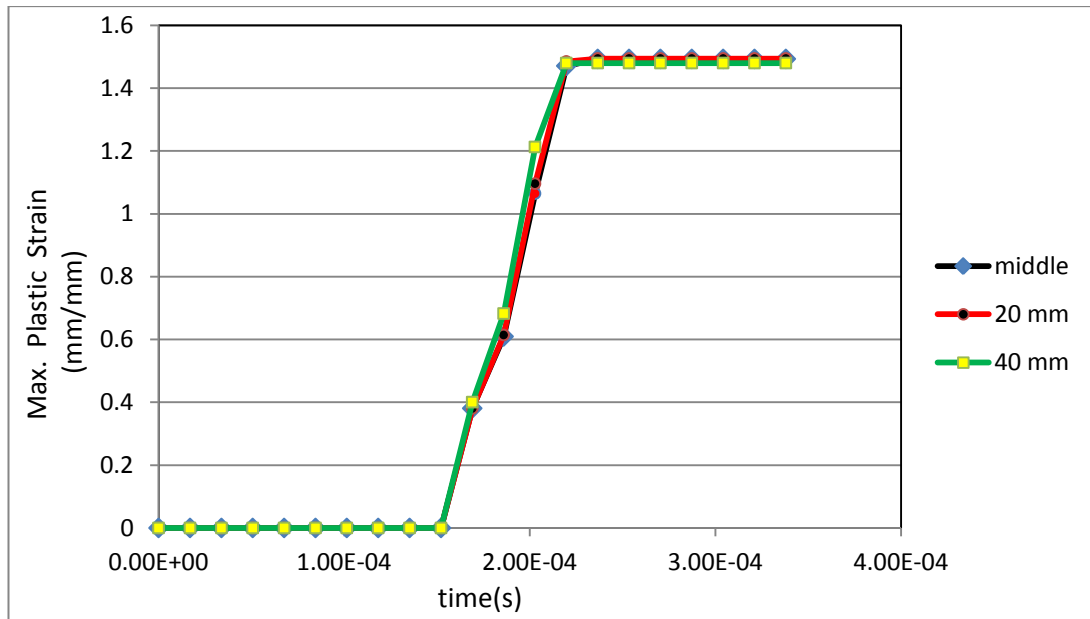


Figure 5.27: Maximum plastic strain values for 1.4 mm thickness of plate.

It is seen that maximum plastic strain simulation for 40 mm distance and 1.4 mm thickness in Fig. 5.28.

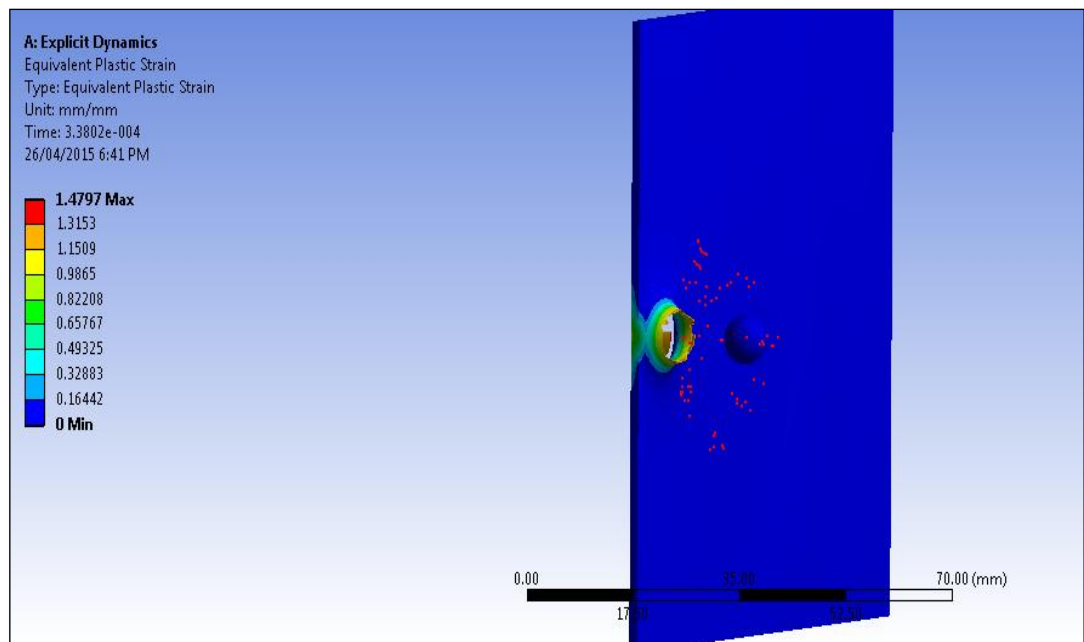


Figure 5.28: Maximum plastic strain simulation at 40 mm distance and 1.4 mm thickness of plate.

It is given that maximum energy absorption values at different thicknesses and different impact points in table 5.12. The energy absorption increased from 1.4 mm thickness to 2.4 mm thickness.

Table 5.12: Maximum energy absorption values for PMMA plates.

	1.4 mm thickness	1.9 mm thickness	2.4 mm thickness
Plate Center (J)	3.2	5.1	7.6
At 20 mm (J)	3.1	5.2	7.9
At 40 mm (J)	3.3	5.2	7.6

It is given that energy absorption distribution for 2.4 mm thickness of plate in Fig. 5.29. It was found that all results regarding energy absorption for PMMA plates at different thicknesses of plate were close to each other.

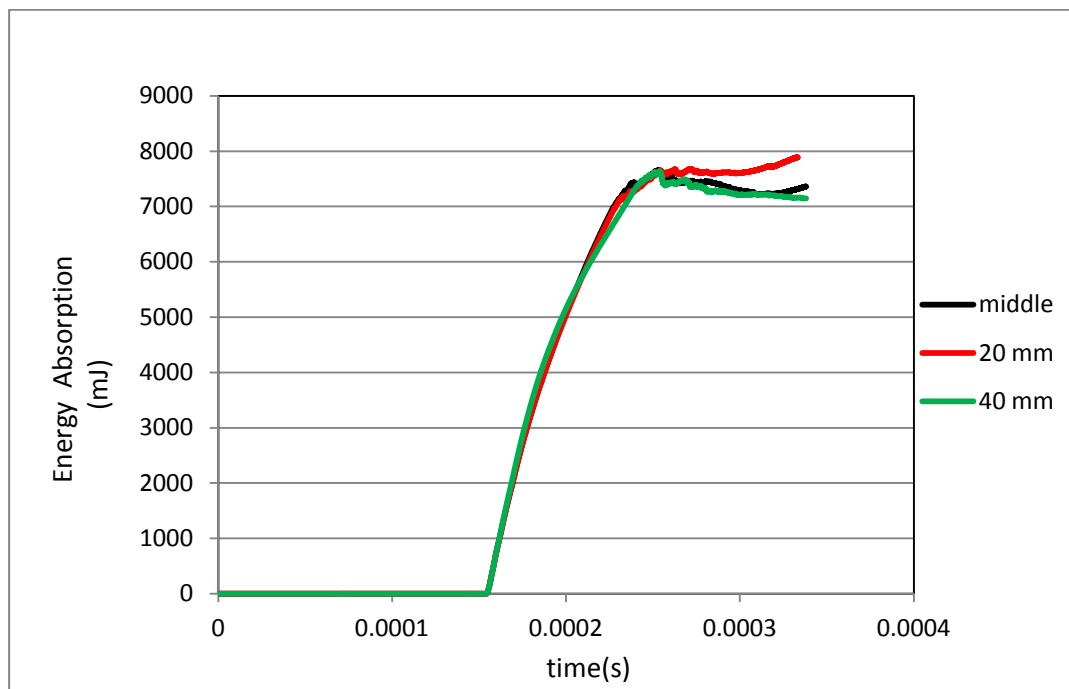


Figure 5.29: Energy absorption distribution for 2.4 mm thickness.

It can be seen that energy absorption distribution at different thicknesses and at plate center for PMMA plates in Fig. 5.30. The energy absorption increased from 1.4 mm thickness to 2.4 mm thickness.

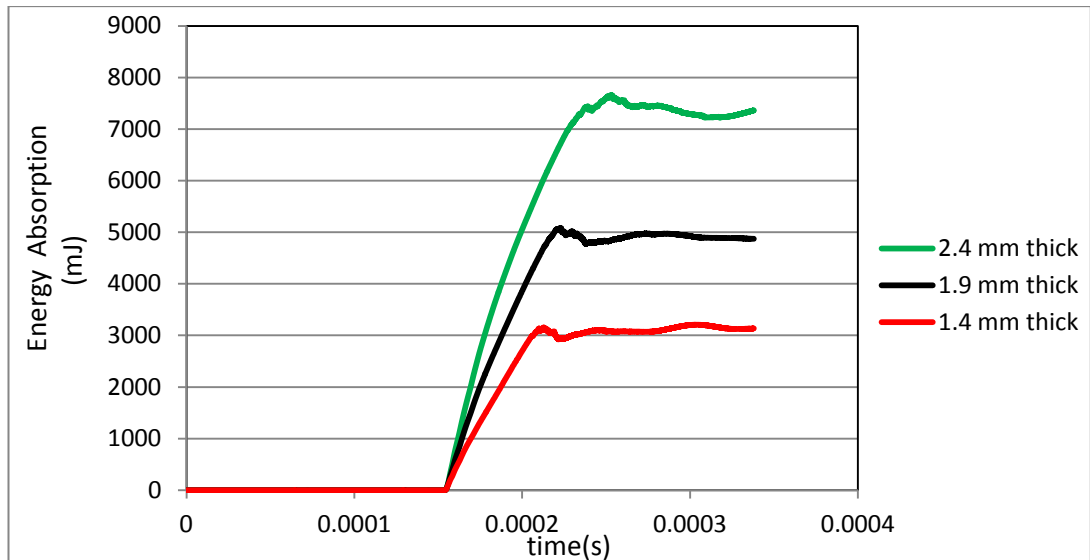


Figure 5.30: Energy absorption distribution at plate center.

5.5 Comparison of Behavior of Polycarbonate and PMMA Plates Under Impact

The polycarbonate and PMMA plates were modeled as 1.4 mm, 1.9 mm and 2.4 mm thickness. Additionally, impacts were made at the center, 20 and 40 mm of the plate. Some results are shown in Fig. 5.31 below.

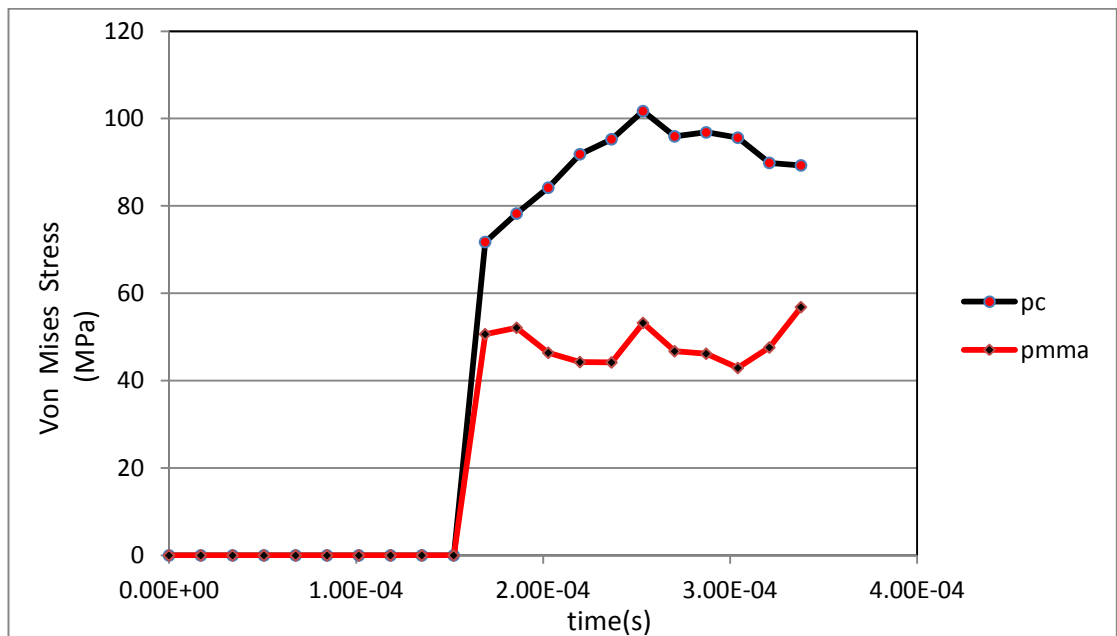


Figure 5.31: At plate center and 1.9 mm thickness.

Maximum von Mises stress of polycarbonate plate was 104.07 MPa and maximum von Mises stress of PMMA plate was 56.836 MPa for 1.9 mm thickness of plate in Fig. 5.31. Also, all values of maximum von Mises stress of polycarbonate plates were greater than the values of PMMA plates at any thickness of plates as shown in table 5.13.

Table 5.13: Von Mises Stress for PC and PMMA plates.

	Thickness	Plate Center	20 mm	40 mm
PC (MPa)	1.4 mm	100.5	100.7	97.9
	1.9 mm	101.7	99.1	102.7
	2.4 mm	88.8	46.1	102.7
PMMA (MPa)	1.4 mm	53.2	56.7	59.4
	1.9 mm	56.8	58.7	61.6
	2.4 mm	57.6	58.9	60.9

The values of maximum shear stress of polycarbonate plates were greater than the values of PMMA plates at any thickness and any points as shown table 5.14 below.

Table 5.14: Maximum shear stress for PC and PMMA plates.

	Thickness	Plate Center	20 mm	40 mm
PC (MPa)	1.4 mm	57.1	57.4	55.1
	1.9 mm	56.8	56.1	58.3
	2.4 mm	45.5	46.1	57.9
PMMA (MPa)	1.4 mm	30.5	32.6	34.3
	1.9 mm	32.6	33.9	35.5
	2.4 mm	33.2	34.1	35.2

The value of maximum shear stress at middle of plate and 1.4 mm thickness for polycarbonate and PMMA plates are shown in Fig. 5.32.

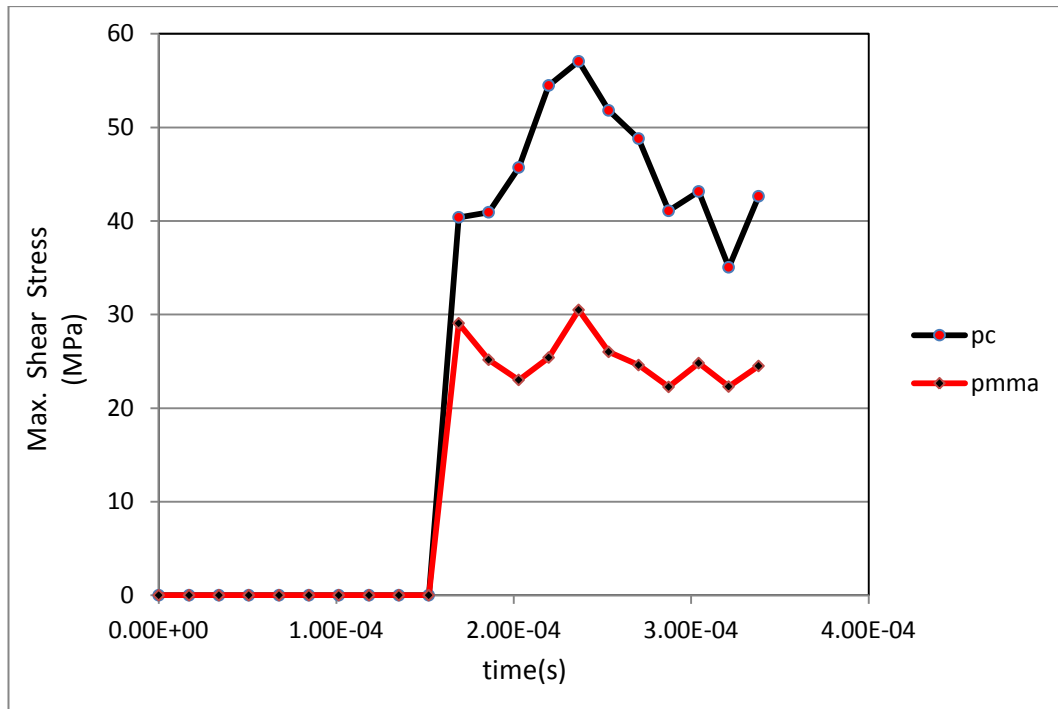


Figure 5.32: Maximum shear stress for PC and PMMA at middle of plate and 1.4 mm thickness.

The values of deformation for polycarbonate and PMMA plates are shown in table 5.15.

Table 5.15: Maximum Deformation of PC and PMMA plates.

	Thickness	Plate Center	20 mm	40 mm
PC (mm)	1.4 mm	8.6	8.6	7.3
	1.9 mm	10.5	10.6	7.1
	2.4 mm	9.1	9.2	9.1
PMMA (mm)	1.4 mm	8.8	8.8	7.8
	1.9 mm	8.9	9.3	8.2
	2.4 mm	10.1	10.1	8.6

The values of maximum plastic strain for PMMA were greater than the values of maximum plastic strain for polycarbonate as shown table 5.16 below . As shown in table 5.16, maximum values of plastic stain for PMMA plates were greater than maximum values of plastic stain for polycarbonate plates.

Table 5.16: Maximum plastic strain for PC and PMMA plates.

	Thickness	Plate Center	20 mm	40 mm
PC	1.4 mm	1.3	1.3	1.3
	1.9 mm	1.2	1.1	1.3
	2.4 mm	0.8	0.9	1.2
PMMA	1.4 mm	1.5	1.5	1.4
	1.9 mm	1.4	1.4	1.4
	2.4 mm	1.5	1.4	1.5

Maximum plastic strain curves were drawn at the center of plate for 1.4 mm thickness of plate in Fig. 5.33.

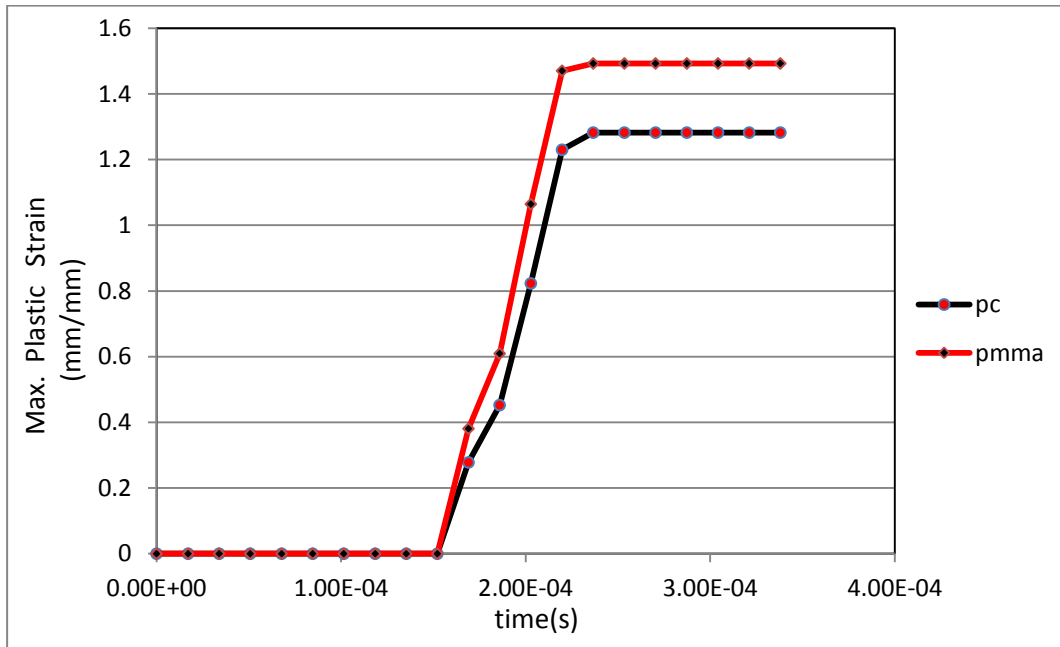


Figure 5.33: Maximum plastic strain for PC and PMMA plates.

The maximum energy absorption values for polycarbonate plates were found greater than the values of PMMA plates at all thickness and impact points as shown in table 5.17.

Table 5.17: The maximum energy absorption for PC and PMMA plates.

	Thickness	Plate Center	20 mm	40 mm
PC (J)	1.4 mm	5.2	5.2	5.1
	1.9 mm	8.8	9.7	7.9
	2.4 mm	9.5	10.2	11.7
PMMA (J)	1.4 mm	3.2	3.2	3.2
	1.9 mm	5.1	5.2	5.2
	2.4 mm	7.6	7.9	7.6

Energy absorption curves are given for polycarbonate and PMMA plates at 40 mm distance from center of plate and for 1.4 mm thickness of plate in Fig. 5.34.

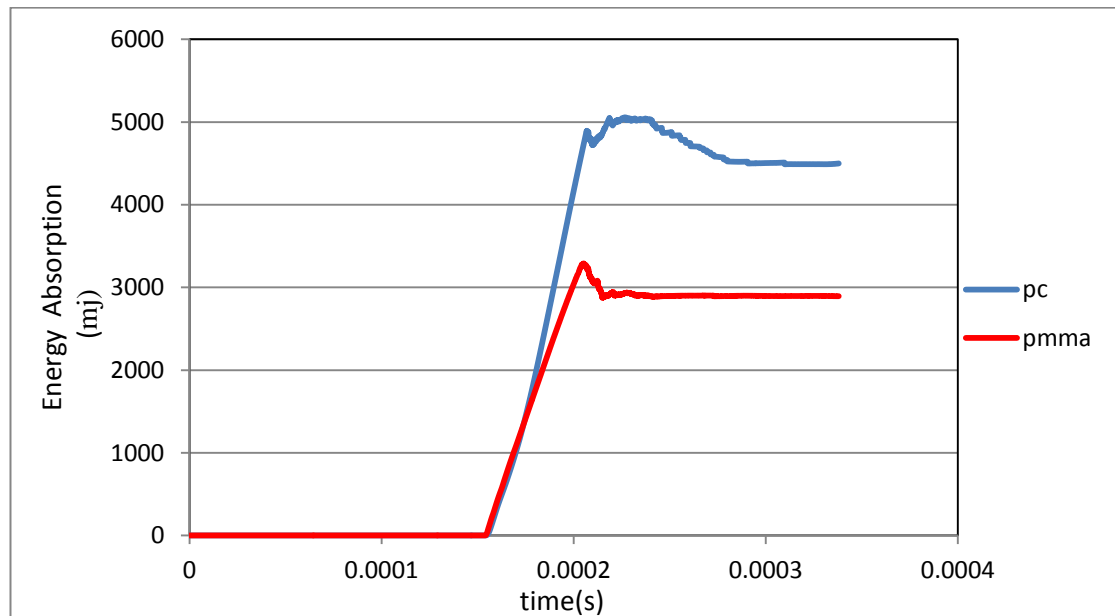


Figure 5.34: Energy absorption for PC and PMMA plates at 1.4 mm thickness.

Energy absorption curves are given for polycarbonate and PMMA plates at the center of plate and 2.4 mm thickness of plate in Fig. 5.35 below.

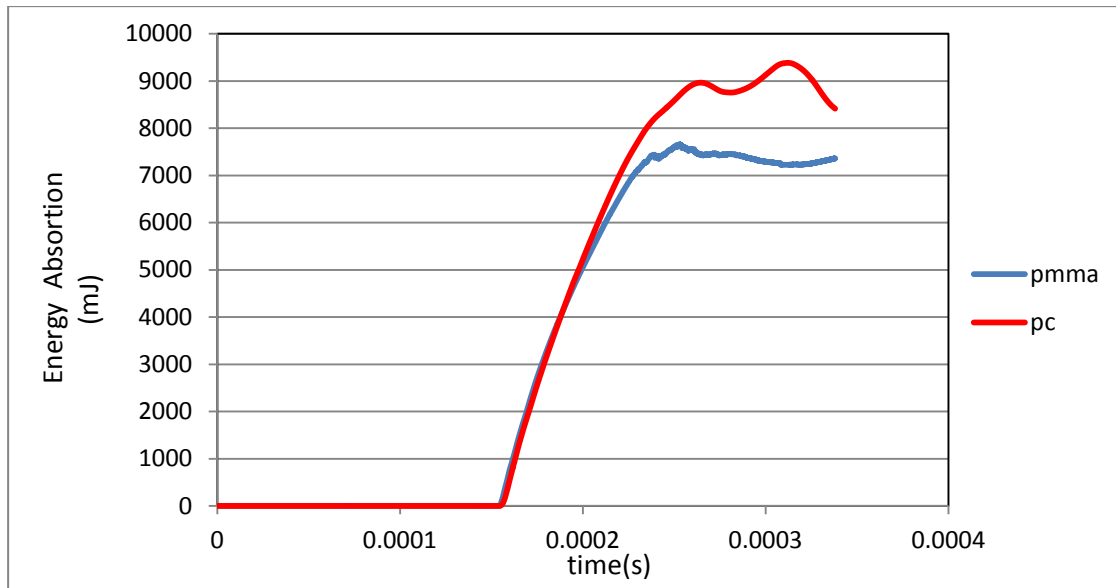


Figure 5.35: Energy absorption for PC and PMMA plates for 2.4 mm thickness and at center of plate.

Energy absorption curves are shown for polycarbonate and PMMA plates at 40 mm distance from center of plate and for 2.4 mm thickness of plate in Fig. 5.36.

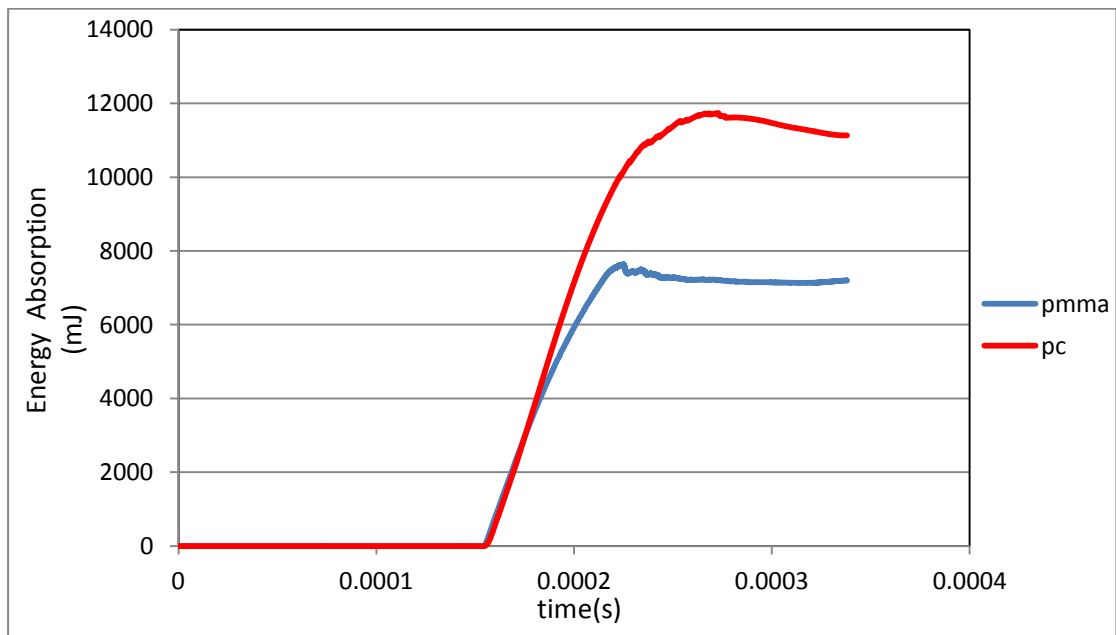


Figure 5.36: Energy absorption for PC and PMMA plates for 2.4 mm thickness of plate and 40 mm distance from center of plate.

5.6 Determine Strain Rates of Polycarbonate Plates For 1.9 mm Thickness At Plate Center

This study was implemented to determine strain rates at different velocity for PC. It is shown that strain rates at plate center in 1.9 mm thickness in table 5.18.

Table 5.18: Strain Rates at Different Velocity.

Velocity (m/s)	Strain Rates (s^{-1})
90	3448.008
140	6587.875
180	21626.35

5.7 Determine Strain Rates of PMMA Plates For 1.9 mm Thickness At Plate Center

This study was implemented to determine strain rates at different velocity for PMMA similarly. It is given that strain rates at plate center in 1.9 mm thickness in table 5.19.

Table 5.19: Strain Rates at Different Velocity.

Velocity (m/s)	Strain Rates (s^{-1})
90	4702.524
140	17209.302
180	21988.157

5.8 Comparison of Polycarbonate Plates For Shell and Solid Elements

It is given some results about polycarbonate plates for 1.9 mm thickness of plate using shell elements during impact loading. Shell element placement is only used polycarbonate modeling on finite element analysis such as LSDYNA, Abaqus, AUTODYN etc.

It is shown that von Mises stress simulations for shell elements at plate center in Fig. 5.37.

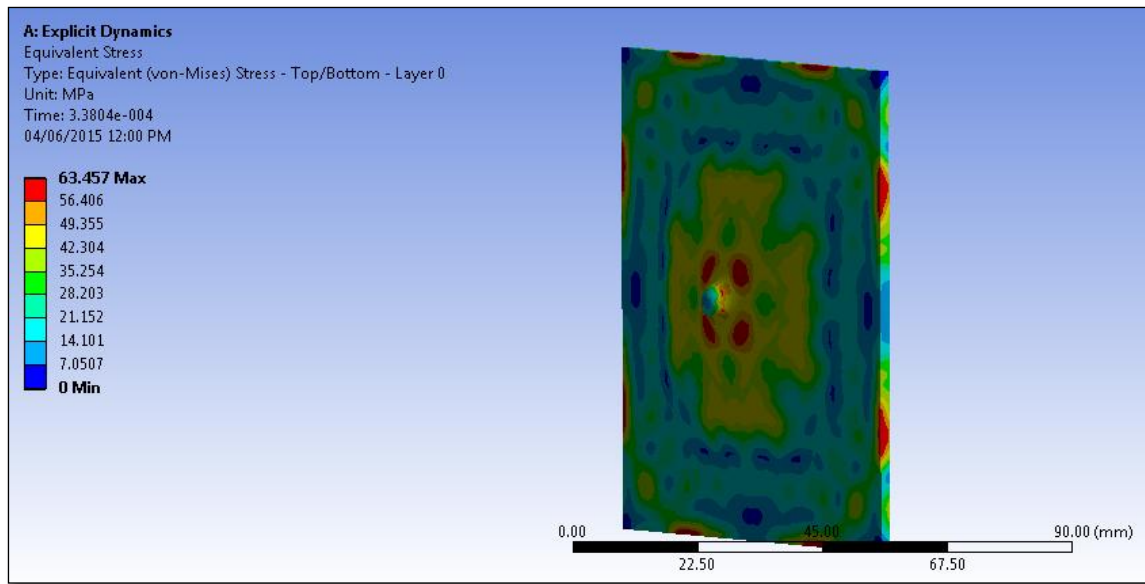


Figure 5.37: Von Mises stress simulation at plate center and 1.9 mm thickness of plate for shell element.

It is also given that von Mises stress simulations for shell element at plate center as other perspective in Fig. 5.38.

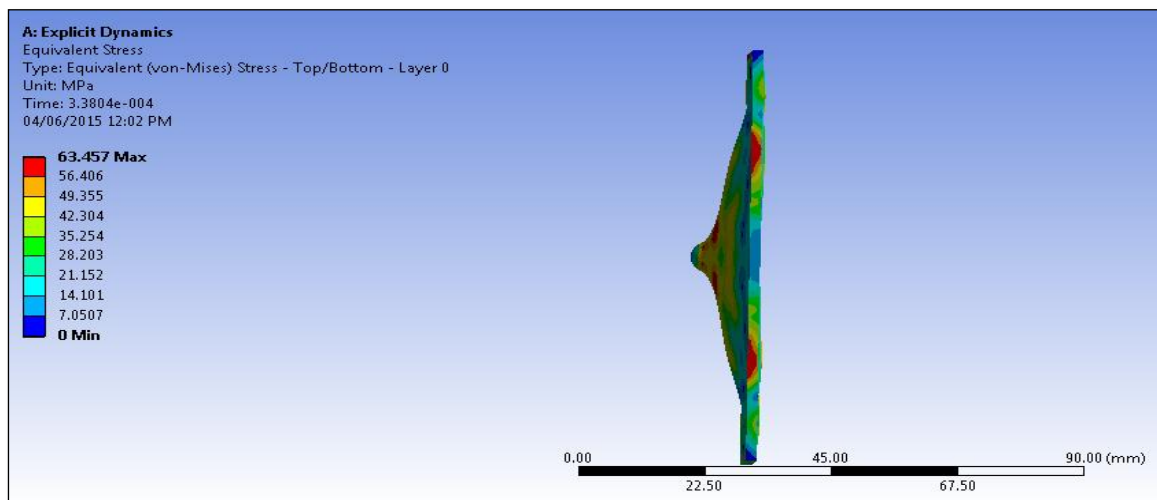


Figure 5.38: Von Mises stress simulation at side profile of plate and 1.9 mm thickness for shell element.

It is shown that von Mises stress simulations for solid elements at plate center in Fig. 5.39.

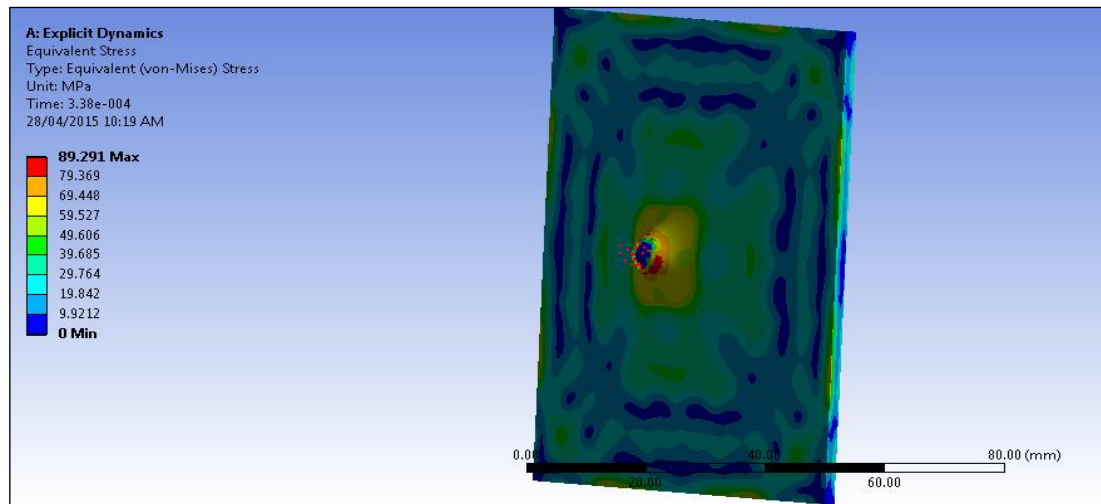


Figure 5.39: Von Mises stress simulation at plate center and 1.9 mm thickness of plate for solid element.

It is given that von Mises stress comparison for shell and solid elements at 40 mm distance from plate center and 1.9 mm thickness of plate in Fig. 5.40.

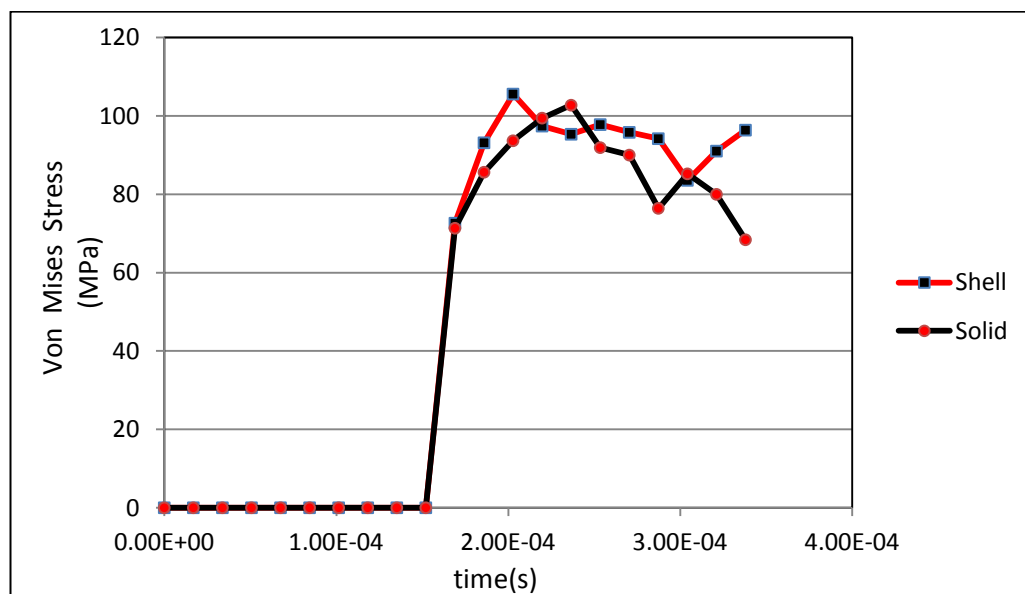


Figure 5.40: Von Mises stress at 40 mm distance and 1.9 mm thickness for solid and shell element.

It is shown that maximum shear stress simulations for shell elements at plate center in Fig. 5.41 below.

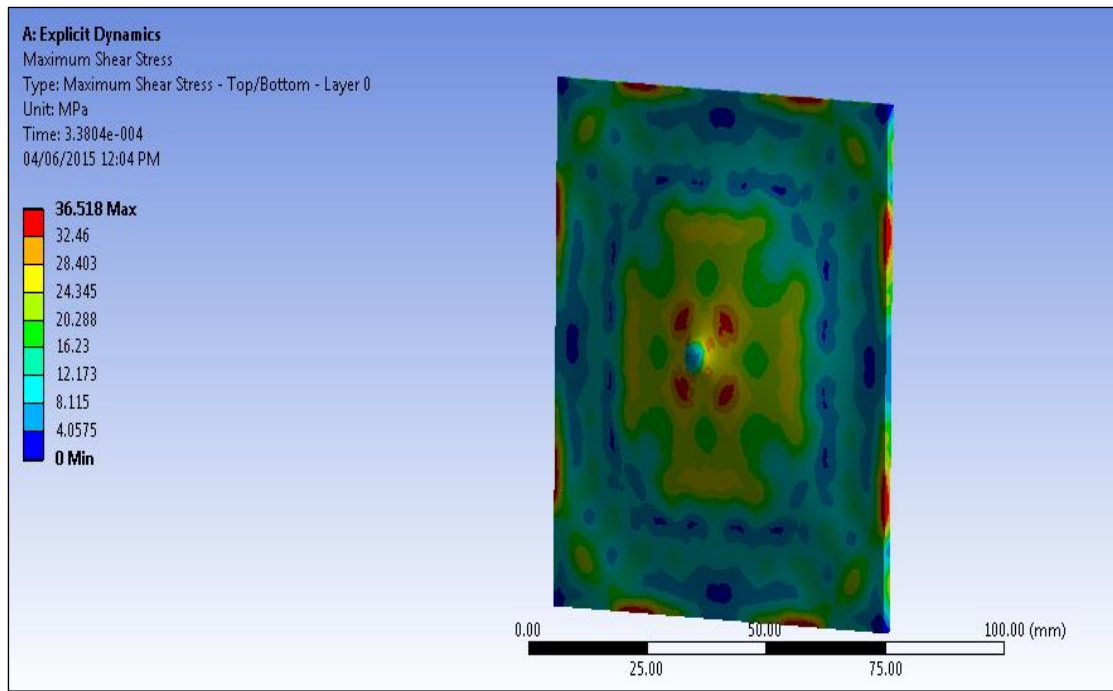


Figure 5.41: Maximum shear stress simulation at plate center and 1.9 mm thickness of plate for shell element.

It is shown that maximum shear stress comparison for shell and solid elements at middle of plate and 1.9 mm thickness in Fig. 5.42.

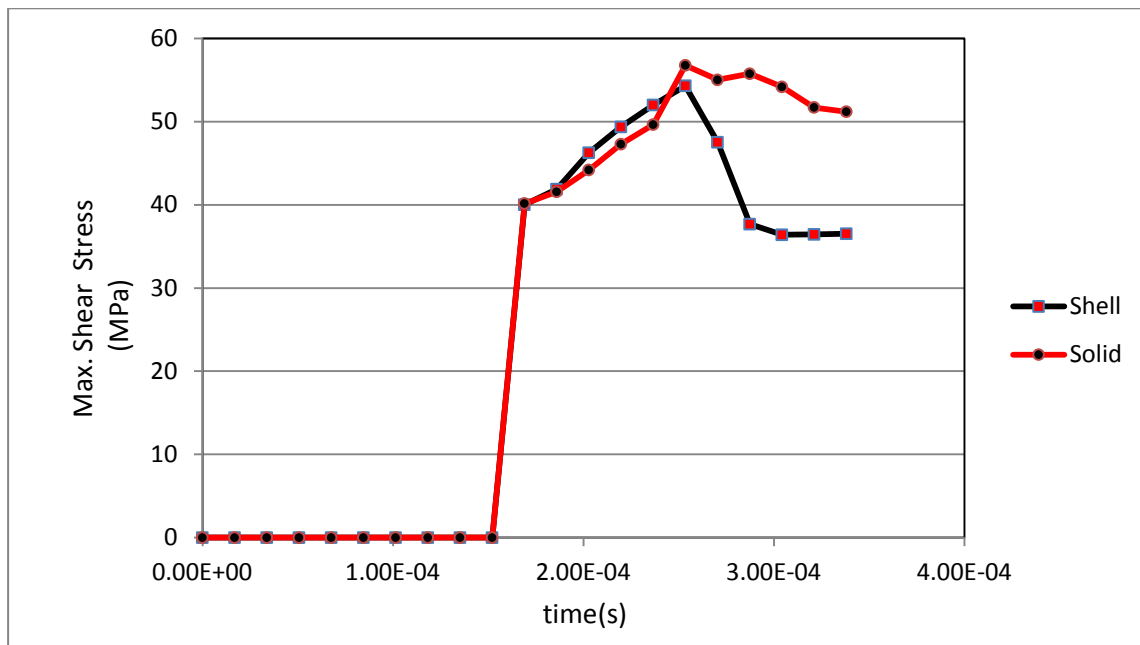


Figure 5.42: Maximum shear stress at plate center and 1.9 mm thickness for solid and shell element.

It is shown that deformation simulation for shell elements at plate center in Fig. 5.43.

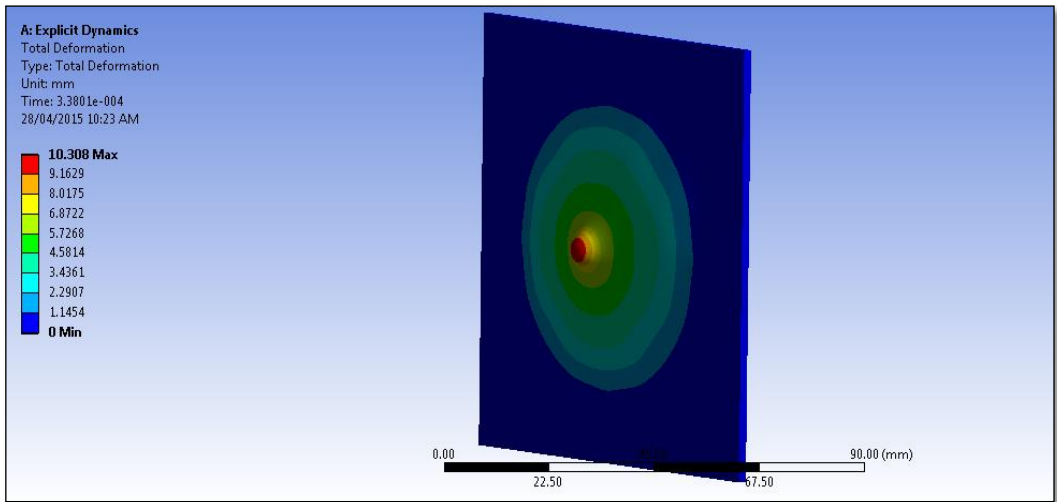


Figure 5.43: Deformation simulation at plate center and 1.9 mm thickness for shell element.

It is given that plastic strain simulation for shell elements at plate center in Fig. 5.44.

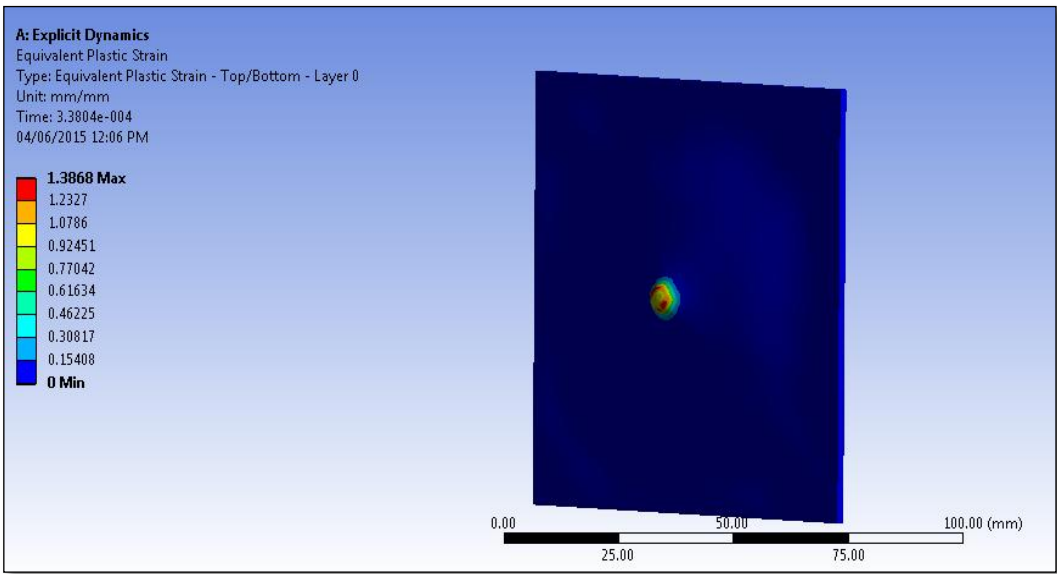


Figure 5.44: Plastic strain simulation at plate center and 1.9 mm thickness for shell element.

It is shown that plastic strain comparison for shell and solid elements at middle of plate and 1.9 mm thickness in Fig. 5.45.

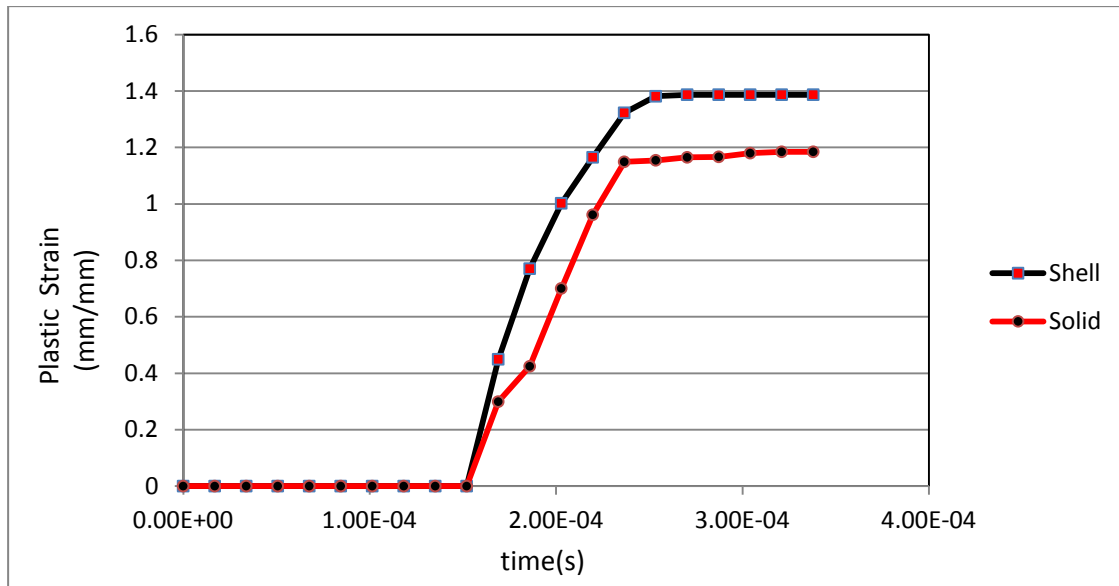


Figure 5.45: Plastic strain at plate center and 1.9 mm thickness for solid and shell element.

It is shown that energy absorption comparison for shell and solid elements at plate center and 1.9 mm thickness in Fig. 5.46.

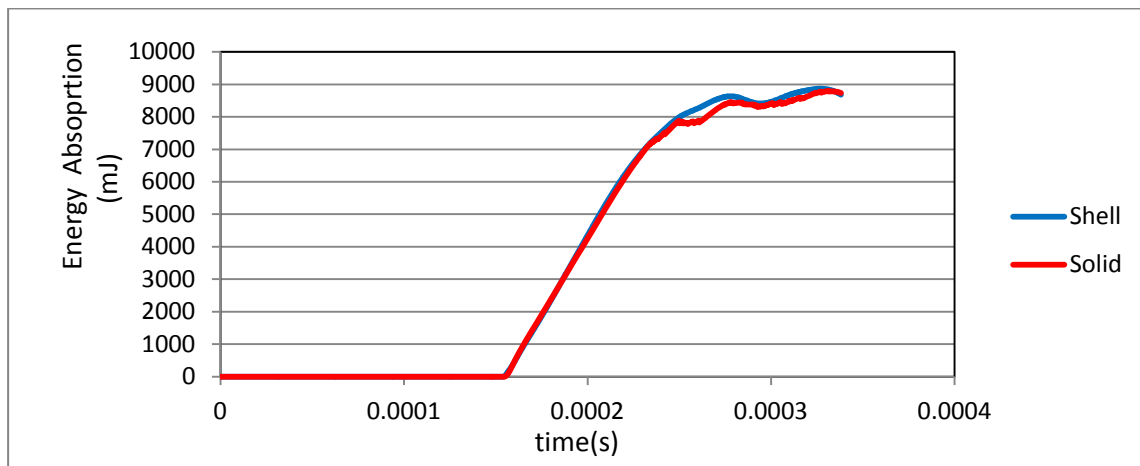


Figure 5.46: Energy absorption distribution at plate center for solid and shell element

All results about shell and solid elements for polycarbonate plate at plate center, 20 and 40 mm distance from center of plate are shown in table 5.20.

Table 5.20: All conclusions for shell and solid elements.

		Plate Center	20 mm	40 mm
PC Shell	Maximum von Mises Stress (MPa)	100.8	97.6	105.6
	Maximum Shear Stress (MPa)	54.3	53.3	59.7
	Maximum Deformation mm	10.4	10.1	12.4
	Maximum Plastic Strain (mm/mm)	1.4	0.7	1.9
	Maximum Energy Absorption (J)	8.9	9.7	7.1
PC Solid	Maximum von Mises Stress (MPa)	101.7	99.1	102.8
	Maximum Shear Stress (MPa)	56.8	56.1	58.3
	Max. Deformation (mm)	14.1	15.2	19.1
	Maximum Plastic Strain (mm/mm)	1.2	1.2	1.3
	Maximum Energy Absorption (J)	8.8	9.7	7.9

In this study, it was performed that difference using shell and solid elements for 1.9 mm thickness polycarbonate plates toward clamped edge on ANSYS/Autodyn. It is predicted to understand with only experimental work with respect to accuracy of which it was used element type in this present work. Thus, it was given some results for shell elements without commentary.

6. CONCLUSIONS

Thin square polycarbonate and PMMA plates were subjected to a spherical projectile impact at a velocity of 140 m/s. Successive impacts under similar conditions were conducted at locations of plate center, 20 and 40 mm distances. For polycarbonate plates, it was shown that maximum stress increased when thickness of plate was increased. Similarly, when thickness of plate is increased, maximum shear stress decreased. Furthermore, maximum shear stress values increased towards clamped edge. Since square plate edges were constrained, it was observed that higher stress at close to fixed edge than other impact locations as expected. For 1.4 mm thickness of pc plates, it was observed that fragmentation at all impact locations. That is, kinetic energy was not completely transformed into internal energy and therefore it was observed that perforated event. Maximum plastic strain values decreased while thickness of plate was increased. This situation was expected as well because resistance of plate increased when the plate thickness was higher. Further, maximum plastic strain increased toward clamped edge. It was seen that maximum plastic strain value was 1.3487 at 40 mm distance from plate center and 1.4 mm thickness. For 1.9 mm thickness for polycarbonate plates, it was shown that partially perforated at plate center and 20 mm distance. At 40 mm distance, it was seen that completely perforated. It was observed that large deformation at all impact points. At close to clamped edge, stress and strain values caused perforated event. Therefore, it was possible to be perforated at near the fixed edge. It was already observed that perforated event at 40 mm distance and all thickness of polycarbonate plates. For polycarbonate plates at all impact locations, maximum energy absorption values increased from 1.4 mm thickness to 2.4 mm thickness. This phenomenon was also expected due to the thicker plates have more resistance. Maximum energy absorption was seen that as 11.743 J at 40 mm distance and 2.4 mm thickness. At plate center, there was no perforation at 1.9 mm and 2.4 mm thickness. The reason for no perforation at the plate midpoints is due to the fact that the plate can deflect freely to a large lateral distance therefore absorbing more energy in plate failure mechanism.

For a certain projectile velocity which cause only an acceptable plastic deformation at the plate midpoints the deformation near the firmly clamped edge was significantly higher for a impact event. Also, it was observed that for the impact at 40 mm distance from plate center that is in the vicinity of the constrained edge, the localized deformation was very high as compared to the plate midpoint impact case. This is because due to rigid constraint the transverse plate deflection was minimized and all the projectile energy was consumed in local material deformation that results in a deep dent near to the plate edge.

For PMMA plates during impact loading, maximum shear stress values increased at any thickness of plates toward clamped edge. Likewise, maximum shear stress values increased from 1.4 mm thickness to 2.4 mm thickness. Maximum shear stress is found that as 35.214 MPa at 40 mm distance from plate center and 2.4 mm thickness. Furthermore, von Mises stress values increased when thickness of plate was increased for PMMA plates. Similarly, it was shown that von Mises stress values increased towards fixed edge. It was occurred that fragmentation event at all plate thickness and impact points for PMMA plates. It was found that maximum plastic strain results were close to each other and these results were higher than polycarbonate results. The higher deformation, the higher plastic strain. PMMA is a brittle material at room temperature. However, PMMA undergoes ductile deformation until it is fractured. Thus, two failure criteria were combined which ductile failure and tensile failure during numerical modeling. Additionally, energy absorption values for PMMA plates were close to each other. Energy absorption values for PMMA plates were found to be less than polycarbonate plate values regarding energy absorption values as expected. Because, polycarbonate material is more impact resistance than PMMA material.

As it is clear from the above mentioned discussion that the impact points near the fixed straight edge is the crucial locations for the possible earlier failure, it was decided to investigate the plate midpoint, 20 mm and especially 40 mm distance from plate center. When designing the rectangular or square armor plates made up of a ductile polymer like polycarbonate, special care must be taken for the protection against the projectile striking near the clamped straight should be provided near the clamped edges. Some impact points were occurred that penetration and perforation

for pc and PMMA plates. In fact, it was seen that perforated event all impact locations for PMMA target plates. In addition, it was shown that perforated for 1.4 mm thickness and all impact points for pc plates. Further, for 2.4 mm thickness and 40 mm distance, it was seemed to be perforated. In order to prevent such failure especially close to clamped edge it is suggested to incorporate an additional plate to cover the near edge zone. In addition to these results, it is understand that polycarbonate plates are much more useful than PMMA plates with respect to designing more firm material such as canopy, bullet proof etc.

There might be conducted two future works. First study is comparison of the results by using different software program. Further, it can be used solver targets such as LS-DYNA. The second one is an experimental study of the comparison of polycarbonate and PMMA materials.

REFERENCES

- [1] **Mikko, K., Marcin, G., Paavo, R., Rantala, J.T.** (2004). Synthesis and characterization of optical sol–gel adhesive for military protective polycarbonate resin. *J Sol–Gel Sci Technol.* 31:369–72.
- [2] **Hsieh, A.J., DeSchepper, D., Moy, P., Dehmer, P.G., Song, J.W.** (2004). The effects of PMMA on ballistic impact performance of hybrid hard/ductile all-plastic-and glass-plastic-based composites. US Army Research Laboratory ARL-TR-3155, Report no. A878024, February.
- [3] **Jones, N.** (1994). Low velocity perforation of metal plates: shock and impact on structure, Computational Mechanics Publications; 53–71.
- [4] **Shah, Q.H., Abakr, YA.** (2008). Effect of distance from the support on the penetration mechanism of clamped circular polycarbonate armor plates. *International Journal of Impact Engineering*, 35:1244–50.
- [5] **de Rosset William, S.** (2003). Patterned armor performance evaluation for multiple impacts. ARL-TR3038; August.
- [6] **Paul, J.J., Galea, S.C., Jones, R.** (1994). Residual strength of composites with multiple impact damage. AR-008-383. DSTO Australia.
- [7] **Gearing, B.P., Anand, L.** (2004). On modeling the deformation and fracture response of glassy polymers due to shear-yielding and crazing. *Int J Solids Struct*, 41:3125–50.
- [8] **Fountzoulas, C.G., Cheeseman, B.A., Sands, J.M.** (2005). A study of numerical simulation capabilities in the impact analysis of laminate transparent armor. In: The third international conference on structural stability and dynamics, Kissimmee, Florida (US Army Research Laboratory, Aberdeen Proving Ground), June 19–22.
- [9] **Van der Giessen E, Estevez R, Pijnenburg KGW, Tijssens MGA.** (1999). Computational modeling of failure processes in polymers. In: European conference on computational mechanics (ECCM '99) August 31–September 3, München, Germany.
- [10] **Du Bois, P.A., Kolling, S., Koesters, M., Frank, T.** (2006). Material behaviour of polymers under impact loading. *Int J Impact Eng*; 32:725–40.
- [11] **Hassan, M., Yuehui, Z., Anwarul, H., Abdelmoniem, A., Uday, V., Jeelani, S.** (2000). Investigation of high-velocity impact on integral armor using finite element method. *Int J Impact Eng*; 24:203–17.
- [12] **Shinji, O., Tomoyuki, I., Akira, K.** (1998). Study on impact perforation fracture mechanism in PMMA. *J Mater Sci Lett*; 17:691–2.

- [13] **Frank, H., Stefan, H., Marika, N.** (2005). Material models for polymers under crash loads: existing LSDYNA models and perspective, vol. 4. Bamberg: LSDYNA Anwenderforum; 1–12.
- [14] **Chung Kim Yuen, S., Nurick, G.N.** (2005). Experimental and numerical studies on the response of quadrangular stiffened plates subjected to uniform blast load. *Int J Impact Eng*; 31:55–83.
- [15] **Langdon, G.S., Chung Kim Yuen, S., Nurick, G.N.** (2005). Experimental and numerical studies on the response of quadrangular stiffened plates. Part II: localized blast loading. *Int J Impact Eng*; 31: 85–111.
- [16] **Neuberger, Peles, S., Rittel, D.** (2007). Scaling the response of circular plates subjected to large and close-range spherical explosions. Part I: air blast loading. *Int J Impact Eng*; 34:859–73.
- [17] **Teeling-Smith, R.G., Nurick, G.N.** (1991). The deformation and tearing of thin circular plates subjected to impulsive loads. *Int J Impact Eng*; 11(1):77–91.
- [18] **Gupta, N.K., Nagesh, S.** (2007). Deformation and tearing of circular plates with varying support conditions under uniform impulsive loads. *Int J Impact Eng*; 34:42–59.
- [19] **Qian L, Qu M, Feng, G.** (2005). Study on terminal effects of dense fragment cluster impact on armor plate. Part I: analytical model. *Int J Impact Eng*; 31:755–67.
- [20] **Qian, L., Qu, M.** (2005). Study on terminal effects of dense fragment cluster impact on armor plate. Part II: numerical simulations. *Int J Impact Eng*; 31:769–80.
- [21] **Qasim, H.S., Yousif, A.A.** (2008). Effect of distance from the support on the penetration mechanism of clamped circular polycarbonate armor plates. *Int J Impact Eng*; 35(11):1244e50.
- [22] **Qasim, H.S.** (2009). Impact resistance of a rectangular polycarbonate armor plate subjected to single and multiple impacts. *Int J Impact Eng*; 36(9):1128e35.
- [23] **Rosenberg, Z., Surujon, Z., Yeshurun, Y., Ashuach, Y., Dekel, E.** (2005). Ricochet of 0.3" AP projectile from inclined polymeric plates. *Int J Impact Eng*; 31:221e33.
- [24] **Dorogoy, A., Rittel, D., Brill, A.** (2010). A study of inclined impact in polymethylmethacrylate plates. *Int J Impact Eng*; 37:285e94.
- [25] **D. Rittel, A.** (2013). Dorogoy Impact of thick PMMA plates by long projectiles at low velocities. Part I: Effect of head's shape. *Mechanics of Materials* 2013
- [26] **Satapathy, S., Bless, S.** (2000). Deep punching PMMA. *Exp. Mech* 40, 31–37.
- [27] **Rittel, D., Brill, A.** (2008). Dynamic flow and failure of confined polymethylmethacrylate. *J. Mech. Phys. Solids* 56, 1401–1416.
- [28] **Rosenberg, Z., Surujon, Z., Yeshurun, Y., Ashuach, Y., Dekel, E.** (2005). Ricochet of 0.3 '' AP projectile from inclined polymeric plates. *Int. J. Impact Eng.* 31, 221–233.

- [29] **Dorogoy, A., Rittel, D., Brill, A.** (2011). Experimentation and modeling of inclined ballistic impact in thick polycarbonate plates. *Int. J. Impact Eng.* 38, 804–814.
- [30] **Powell, P.C., Ingen Housz, A.J.** (1998). *Engineering with polymers*, Stanley Thornes.
- [31] **Tadmor, Z., Gogos, C.G.** (2006). *Principles of polymer processing* (2nd edition), Wiley Interscience.
- [32] **Vlug, M.** (2004). In: *Proceedings medical plastics*. Hexagon Holding APs.
- [33] **Crawford, R. J.** (1998). *Plastics engineering*. Butterworth Heinemann.
- [34] **Van Krevelen, D.W.** (2003). *Properties of polymers*, ELSEVIER.
- [35] **Harper, Charles, A., Edward, M.** (2003). *Petrie. Plastics Materials and Processes* John Wiley & Sons
- [36] **Mehlmann, F.** (2008). *Proceedings medical grade polymers*. AMI Plastics, Philadelphia, Pennsylvania.
- [37] **Järvelä P. et al., Ruiskuvalu, Plastdata.** (2000).
- [38] **Brebbia, C.A., ed.** (1982). *Finite Element Systems. A Handbook*, Springer-Verlag, Berlin.
- [39] **Zienkiewicz, O.C., Taylor, R.L.** (1989). *The Finite Element Method*, McGraw Hill Co., London.
- [40] **Chandmpatla, T., Belegundu, A.** (1991). *Introduction to Finite Elements in Engineering*, Englewood Cliffs, N. J., Prentice Hall.
- [41] **ANSYS User's Manual: Procedures**, Vol. I, Swanson Analysis Systems, Inc.
- [42] **Wilkins, M.L.** (1973). *Calculation of elastic-plastic flow*. Lawrence Livermore Laboratory Report UCRL-7322, revision 1.
- [43] **Hancock, S., PISCES 3DELK** (1985) *Theoretical Manual*, Physics International
- [44] **Gingold, R.A., Monaghan, J.J.** (1977). Smoothed particle hydrodynamics: Theory and application to non-spherical stars. *Monthly Notices of the Royal Astronomical Society*, vol. 181, 375-389.
- [45] **Ziegler, H.** (1959). A Modification of Prager's Hardening Rule, *Quart. Appl.Math.*, Vol.17, No.1, pp.55.
- [46] **Raghava, R.S., Caddell, R.M.** (1973). A Macroscopic Yield Criterion for Crystalline Polymers, *int. J. Mech. Sci.*, Pergamon Press, Vol.15, 967-974.
- [47] **Ottosen, N.S., Ristinmaa, M.** (2005). *The Mechanics of Constitutive Modelling*, Elsevier.
- [48] **Meyers and Chawla** (1999). *Mechanical Behavior of Materials*, 98-103.
- [49] **McCrum, N.G., Buckley, C.P, Bucknall, C.B.** (1997). *Principles of Polymer Engineering*, Oxford Science Publications. Chapter 5 "Yield and fracture".

- [50] **Powell, P.C., A Jan Ingen Housz, A.** (1998). Engineering with polymers, Stanley Thornes (Publishers) Ltd. Chapter 6 “Strength of polymer products”.
- [51] **Raghava, R.S., Caddell, R.M., Yeh, G.S.Y.** (1973). J. Mat. Sci. 8, 225.
- [52] **Ansys help menu**
- [53] **Tjong, S.C., Jiang, Wei.** (1999). Mechanical Performance of Ternary In Situ Polycarbonate/Poly(acrylonitrile-butadiene-styrene)/Liquid Crystalline Polymer Composites, Journal of Applied Polymer Science 74, 2274–2282.
- [54] **Drucker, D.C., Prager, W.** (1952). Soil mechanics and plastic analysis for limit design. Quarterly of Applied Mathematics, vol. 10, no. 2, pp. 157–165.
- [55] **Shaha, Q.H., Abakrb, Y.A.** (2007). Effect of distance from the support on the penetration mechanism of clamped circular polycarbonate armor plates. Int J Impact Eng., 35:11 p 1244-1250.
- [56] **Rittel, D., Maigre, H.** (1996). An investigation of dynamic crack initiation in PMMA. Mech Mater; 23(3):229–39.
- [57] **Ansys library**
- [58] **Buchar, J., Rolc, S, Voldrich, J., Lazar, M., Starek, M.** (2001). The development of glass laminates resistant to the small arms fire. In: 19th international symposium of ballistics, Interlaken, Switzerland, p. 1439–45.
- [59] **Zhouhua, L., John, L.** (2001). Strain rate effect on the thermomechanical behavior of polymers. Int J Solids Struct; 38:3549–62.
- [60] **Gailly, B.A, Espinosa, H.D.** (2002). Modelling of failure mode transition in ballistic penetration with a continuum model describing microcracking and of pulverized media. Int J Numer Methods Eng., 54:365–98.
- [61] **Qian, L., Qu, M.** (2005). Study on terminal effects of dense fragment cluster impact on armor plate. Part II: numerical simulations. Int J Impact Eng., 31:769–80.
- [62] **Abaqus/explicit version 6.7-1.** (2007). Abaqus documentation, Dassaults Systemes. New York: Springer.
- [63] **Molodets, A.M., Dremin, A.N.** (1980). Subcritical stage of cleavage fracture. Combust Explos Shock Wave., 16:545–8.
- Url-1**<<http://en.wikipedia.org/wiki/Polycarbonate>>, received date: 15.04.2015
- Url-2**<<http://www.bpf.co.uk/Plastipedia/Polymers/Polycarbonate.aspx>>, received date: 13.04.2015
- Url-3**<<http://www.bpf.co.uk/Plastipedia/Polymers/Polycarbonate.aspx>>, received date: 14.04.2015
- Url-4**<<http://www.azom.com/article.aspx?ArticleID=788>>, received date: 11.04.2015

- Url5**<https://www.google.com.tr/search?biw=1600&bih=799&tbm=isch&sa=1&q=Rear+lights+Polymethyl+methacrylate++&oq=Rear+lights+Polymethyl+methacrylate++&gs_l=img.3...10271.10841.0.11462.2.2.0.0.0.278.378.0j1j1.2.0.msedr...0...1c.1.64.img..1.1.99.9G_o2xlYus#imgrc=ScyRgwoiXOKPjM%253A%3BubToV7pZZ22N1M%3Bhttp%253A%252F%252Fimages.wisegeek.com%252Ffred-car-tail-light.jpg%3Bhttp%253A%252F%252Fwww.wisegeek.org%252Fwhat-is-acrylic-resin.htm%3B1000%3B618>, received date: 18.04.2015
- Url6**<https://www.google.com.tr/search?biw=1600&bih=799&tbm=isch&sa=1&q=Lamp+covers++Polymethyl+methacrylate&oq=Lamp+covers++Polymethyl+methacrylate&gs_l=img.3...46499.46499.0.47150.1.1.0.0.0.108.108.0j1.1.0.msedr...0...1c.1.64.img..1.0.0.LBHdcdhY0Rc>, received date: 18.04.2015
- Url-7**<<http://www.greycoproducts.com/polycarbonate-lexan/>>, received date: 18.04.2015
- Url-8**<<http://www.greycoproducts.com/polycarbonatelexan/>>, received date: 18.04.2015
- Url9**<http://en.wikiversity.org/wiki/Nonlinear_finite_elements/Lagrangian_and_Eulerian_descriptions>, received date: 16.04.2015.
- Url10**<http://homepages.engineering.auckland.ac.nz/~pkel015/SolidMechanicsBooks/Part_II/08_Plasticity/08_Plasticity_01_Introduction.pdf>, received date: 16.04.2015.
- Url11**<https://www.google.com.tr/url?sa=t&rct=j&q=&esrc=s&source=web&cd=1&ved=0CBwQFjAA&url=http%3A%2F%2Fwww.researchgate.net%2Fpublictopics.PublicPostFileLoader.html%3Fid%3D54395b1cd3df3e4b7e8b466c%26key%3Dd207f0e8-0839-4be2-a00be42cc60013bc&ei=EzFBVfiAMNXvaMKcgagJ&usg=AFQjCNERJaUd1P7gAS_a1BT5iHzPuG9R1w>, received date: 16.04.2015.
- Url-12**<<http://www.open.edu/openlearn/science-maths/technology/science/chemistry/introduction-polymers/content-section-5.2.1>>, received date: 09.04.2015

CURRICULUM VITAE

Name Surname: Fehmi Mullaoglu

Place and Date of Birth: Hatay / 25.09.1990

E-Mail: fehmi@mullaoglu.com

EDUCATION:

B.Sc.: 2012, MKU, Faculty of Mechanical Engineering, Mechanical Engineering

M.Sc.: 2015, ITU, Department of Aeronautics and Astronautics Engineering, Aeronautical Engineering

